A Novel Iron-NHC Catalyst Supported on Expanded Starch: Synthesis, Characterization and Application

BADRIYA AL MONTHERY

MSc by Research

University of York
Chemistry

December 2016

Abstract

The synthesis and characterization of a novel iron-*N*-heterocyclic carbene (iron-NHC) supported on expanded high amylose corn starch (HACS), using a convergent strategy, and its application as efficient catalyst for fructose to HMF conversion is reported. The NHC ligand was prepared via a multi-step approach and tethered on to suitably derivatized (succinimidyl carbonate, DS = 0.33±0.11) expanded HACS in good yield (61.5%). The synthesis was carried out using *green(er)* solvents such as propylene carbonate and CPME in preference of DMF and CH_2Cl_2 where appropriate. An iron-loading of 0.26 mmol/g was achieved. Present of iron was confirmed qualitatively by colour change and quantitatively by ICP in addition to complementary XPS, TGA, STA and TEM analysis. However, it is assumed that all iron detected is complexed to the NHC ligand and not trapped within the mesoporous structure of the starch support.

After modification, BET surface area and pore volume dropped from 186.65 m^2/g and 0.91 cm^3/g for expanded starch to 135.49 m^2/g and 0.60 cm^3/g for the final Fe-NHC catalyst. The drop in pore volume may be due to possible blocking and filling of the porous structure by the ligand and iron.

The Fe-NHC was proved to be heterogeneous as no discernible iron leaching was observed and it showed good performance for the dehydration of fructose to 5-hydroxymethyl furfural (HMF) when the reaction was explored at 100 °C and varying time (0.5 h, 1 h, 3 h and 6 h). Best yield (63.54%) was achieved at t=1 h with a fructose to HMF conversion of 75.83% and HMF selectivity of 83.79%. Interestingly, under nitrogen flow, poor conversion was reported.

Catalyst re-usability investigation showed that it can be re-used for up to 4 times without significant loss in performance. Comparison of catalytic activity to other heterogeneous catalysts, e.g. Amberlyst-15, Montmorillonite K-10 and ZSM-30 reported relatively similar behaviour.

Contents

List of Tables

List of Figures

List of Schemes

Acknowledgements

No single act, no matter how significant it may seem or not; should go without something as simple and sincere as a thank you. First of all, I thank Allah for giving me the ability to complete this work. Before I go any further I would like to dedicate these few words to those whom have contributed to my work; even in the slightest of ways. I owe a superb part of my work to my supervisor Dr. Avtar Matharu, without whom my academic and social knowledge would be far less. I credit the level of my Maste's degree to his incite and dedication. I just could not wish for a better supervisor. I want to give my sincere gratefulness to Dr Duncan Macquarrie for his appreciated and valuable suggestions as IPM. Suleiman Ahmed deserves my humble of thank you and respect for his cooperation as well. He supported me impressively and was always willing to help me. Special thanks go to the Ministry of Education in Sultanate of Oman for their financial assistance.

I gratefully acknowledge the GCCE technical team for all of their assistance in my experimental work. The members of the green chemistry group have added a lot to my personal and professional experience during my time at the university of York. The group has been a source of a good guidance and collaboration. Friends who encouraged and supported me in my days at the University of York and in Oman deserve my thanks and appreciation also. Thank you to James Shannon, Roxana Milescu, Karima Al Bulushi, Andrea Muñoz and Eduardo Melo.

Throughout my life my father Sulaiman Al Monthery, has been the one I would turn to in times of need, and for that I thank him graciously. Words cannot help me expressing how beholden I am to my mother Fatima and my grandmother Moza for their prayer for me was what sustained me thus far. My wonderful husband, my soul mate and my best friend ever Monther Al Monthery and my beautiful children (Reem, Laura and Hamed), have witnessed me at my best and worst and have gone through this journey with me, without them I would not dream to be who I am. Thank you to all those who have allowed me to prosper, thrive and discover my own self.

Declaration of Authorship

I declare that this thesis is a presentation of original work and I am the sole author. This work has not previously been presented for an award at this, or any other, University. All sources are acknowledged as References. This thesis is based on work done by myself and some of the results introduced were gained with the assistance of:

- SEM and TEM images were obtained by Dr. Meg Stark and Dr. Anna Simon, Department of Biology, University of York.
- Some solid state ^{13}C NMR analysis were carried out by Dr. Pedro M.Aguiar and Ms Julia Walton, Department of Chemistry, University of York.
- ^{13}C NMR and ^{1}H NMR analysis for the NMR study were carried out by Ms. Heather Fish, Department of Chemistry, University of York.
- Some FIR results were attained with the assistance of Mr Suleiman Ahmed, Green Chemistry Centre of Excellence.
- Some HPLC results were gained by Dr. Amanda Dixon, Department of Chemistry, University of York and some by Suleiman Ahmed, Green Chemistry Centre of Excellence.
- ICP-MS results were done by Ms Andrea Muñoz and Ms Maria Garcia Gallarreta, Green Chemistry Centre of Excellence.
- XPS was carried out by Dr. Billy Murdoch, NEXUS, Newcastle University.
- MS was done by Mr Karl Heaton, Department of Chemistry, University of York.

Chapter 1

Introduction

Chemistry has a direct impact on the world, some good and some bad. Thus, all chemical processes must be managed carefully so that more good is done than harm. For example, mis-use, abuse and over-production of chemicals and their articles all have a detrimental effect on climate change, environment and health. To this effect, on 25^{th} of September 2015, 193 member countries of the United Nations (UN) approved the importance of achieving global sustainability via adoption of 17 Sustainable Development Goals (SDGs) (Figure 1.1) designed to protect the planet and its inhabitants. [1]

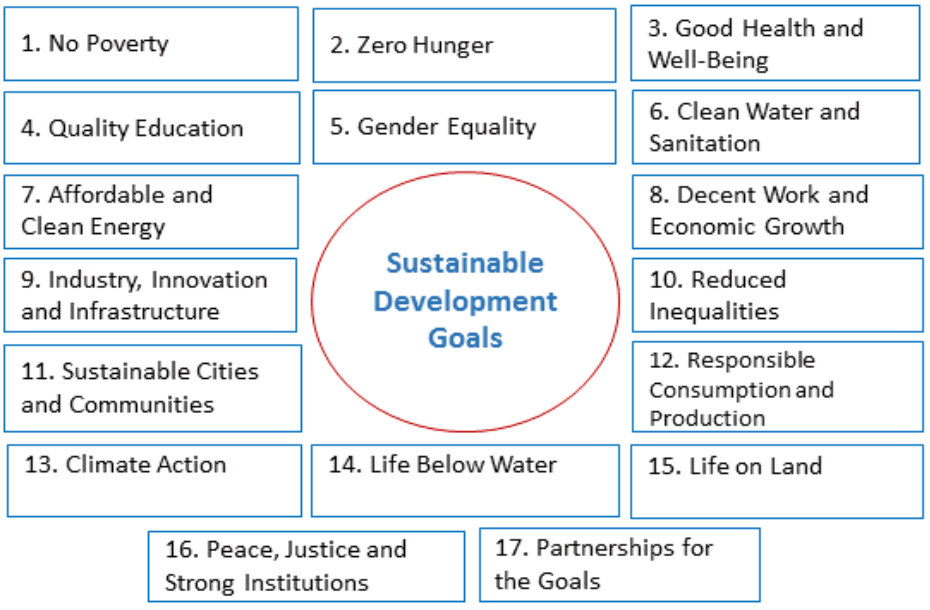

FIGURE 1.1: Sustainable Development Goals (SDGs).

In particular, SDG 12 strives to control the environmental impact of wastes through responsible consumption and production, resource efficiency and circular- rather than linear-thinking, i.e., *doing more with less*. Interestingly, pioneered over 25 years ago by Anastas and Warner, the 12 guiding principles (Figure 1.2) of green chemistry are commensurate with today's UN sustainable development goals. Green chemistry is an attitude that affords policy to improve chemical products and processes for the purpose of reducing their damage on human health as well as on the environment completely. [2]

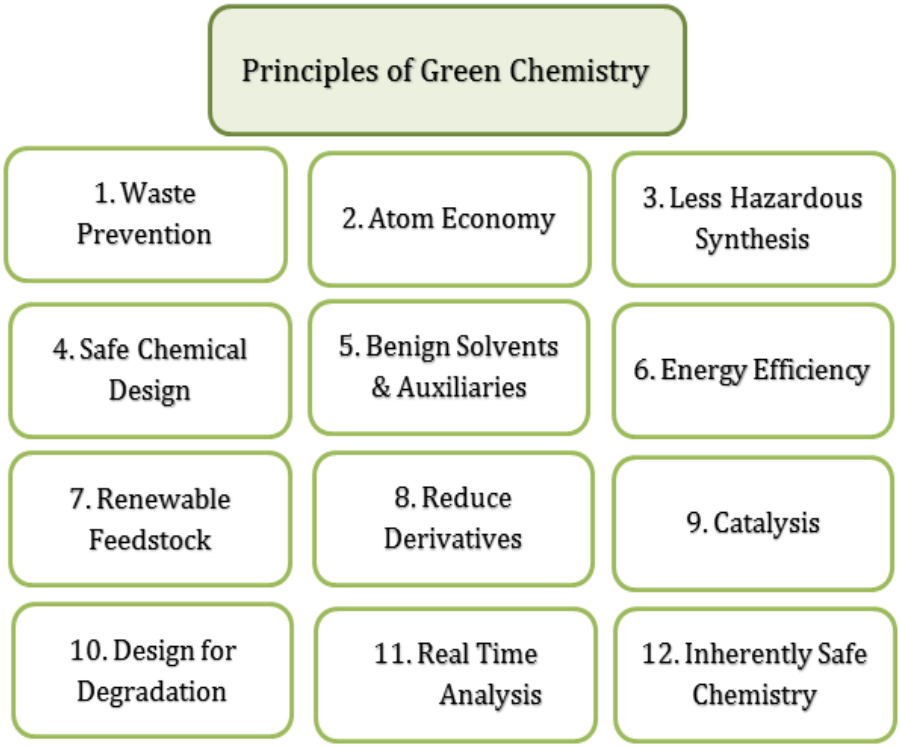

FIGURE 1.2: Principles of green chemistry.

According to principle 7, where possible, petroleum resources should be avoided and replaced by renewable feedstocks. Our reliance on crude oil, a finite source, as a feedstock for our continual and future energy, chemical and materials needs is incommensurate for a sustainable 21^{st} Century. However, the planet is not short of under-utilised or waste biomass, both land and marine. In particular, primary and secondary agricultural residues, forestry wastes, food supply chain wastes are a rich source of cellulose, lignin, proteins, lipids, carbohydrates, sugars, *etc*, all of which are examples of renewable materials. [2] Starch is considered one of the most abundant biopolymer types in the world and it has some important industrial applications. For example, chemically modified corn starch is used as a

filler and structural component in many (bio)composites, as a separation medium in chromatography and as a catalytic support. [3]

Catalysis is an important facet of green chemistry. Principle 9 states, *"Catalytic reagents (as selective as possible) are superior to stoichiometric reagents."* [2] Catalysis minimizes the energy of the reaction and achieves selectivity which hence reduces waste. [2], [4] and [5] In industry, more than 90% of chemical reactions are accomplished using catalysts. [6] Catalysts are generally divided into two categories, homogeneous and heterogeneous. Heterogeneous catalysts are usually solids (and powders) which can be easily recovered from a reaction mixture thus affording recyclability. [7] Carbonaceous materials make good catalyst supports because of their robustness to harsh chemical environments, high porosity, high surface area, good electron conductivity, low reactivity and the fact they may be produced from residual biomass. [8]

1.1 Overview of Aims and Rationale

The overall aim of this research (summarized in Figure 1.3) was to investigate the synthesis of a novel iron-nitrogen heterocyclic carbene (Fe-NHC) supported on expanded starch (**1**) as a potential catalyst for the dehydration of fructose (**2**) to 5-hydroxymethyl furfural (HMF) (**3**), an important platform molecule i.e., chemical building block derived from biomass. HMF is considered a renewable material and an excellent platform molecule because it can be acquired from biomass through chemical dehydration using homogeneous and/or heterogeneous acid catalysts. [9] and [10] However, the chemical transformation of biomass to platform molecules can be extremely challenging due to complex chemistries and/or is tediously slow. Thus, new materials, e.g., catalysts, need to be explored so that efficient and selective transformations can take place.

The synthesis of Fe-NHC (**1**) using a convergent strategy, from expanded high amylose corn starch (HACS) (**4**) and *N*-(3-aminopropyl)imidazole (**7**), is depicted in Scheme 1.1.

The detailed aims and objectives were:
i. to adopt existing synthetic procedures (see Scheme 1.1) but where possible look to replace non-green solvents, for example, DMF with *green(er)* solvents such as propylene carbonate and CPME;

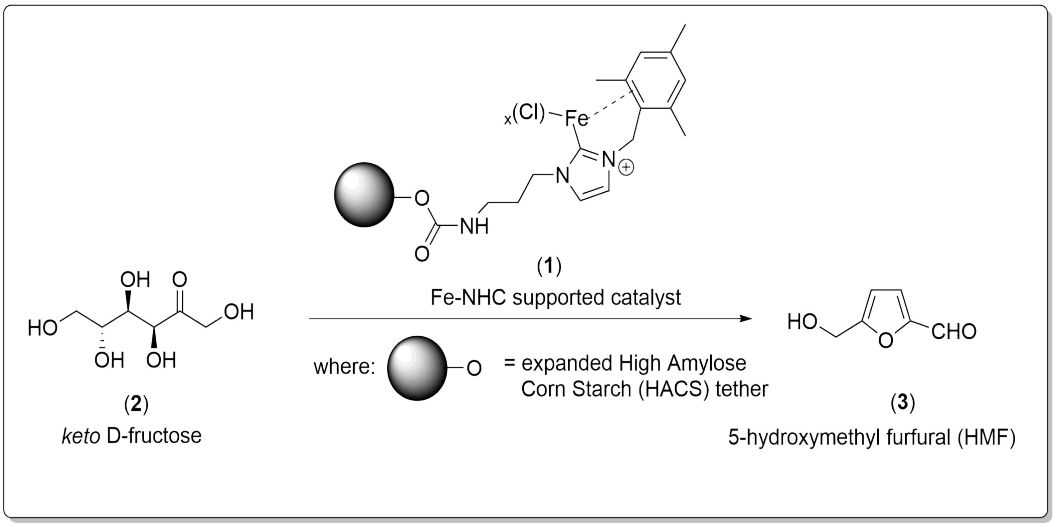

FIGURE 1.3: Overview of fructose (**2**) to 5-hydroxymethyl furfural (**3**) reaction using Fe-NHC (**1**) .

ii. to investigate the extent of iron-loading on the NHC, with an assumption that it is related to the degree of substitution (DS) of starch, i.e. greater the DS the greater the extent of iron-loading;

iii. to explore the catalytic potential of (**1**) for the conversion of fructose (**2**) to HMF (**3**) at fixed temperature (100 °C) and varying time (0.5 h, 1 h, 3 h and 6 h);

iv. to explore catalyst re-usability and compare catalytic activity with respect to other heterogeneous catalysts, e.g. Amberlyst-15, Montmorillonite K-10 and ZSM-30, and ;

v. to investigate changes in porosity during chemical derivatization. Mesoporosity and high surface area of expanded HACS are significant factors in defining the final catalyst performance because it is important for the iron particles to be spread and stabilized in the mesoporous support so they can contact a large number of catalytically active atoms. [11]

1.1.1 Why carbenes?

Carbenes are an interesting group of carbon containing compounds comprising a divalent carbon atom with two unshared valence electrons. [12] *N*-Heterocyclic carbenes (also called Arduengo carbenes) [13] are defined as *"heterocyclic species containing a carbene carbon and at least one nitrogen atom*

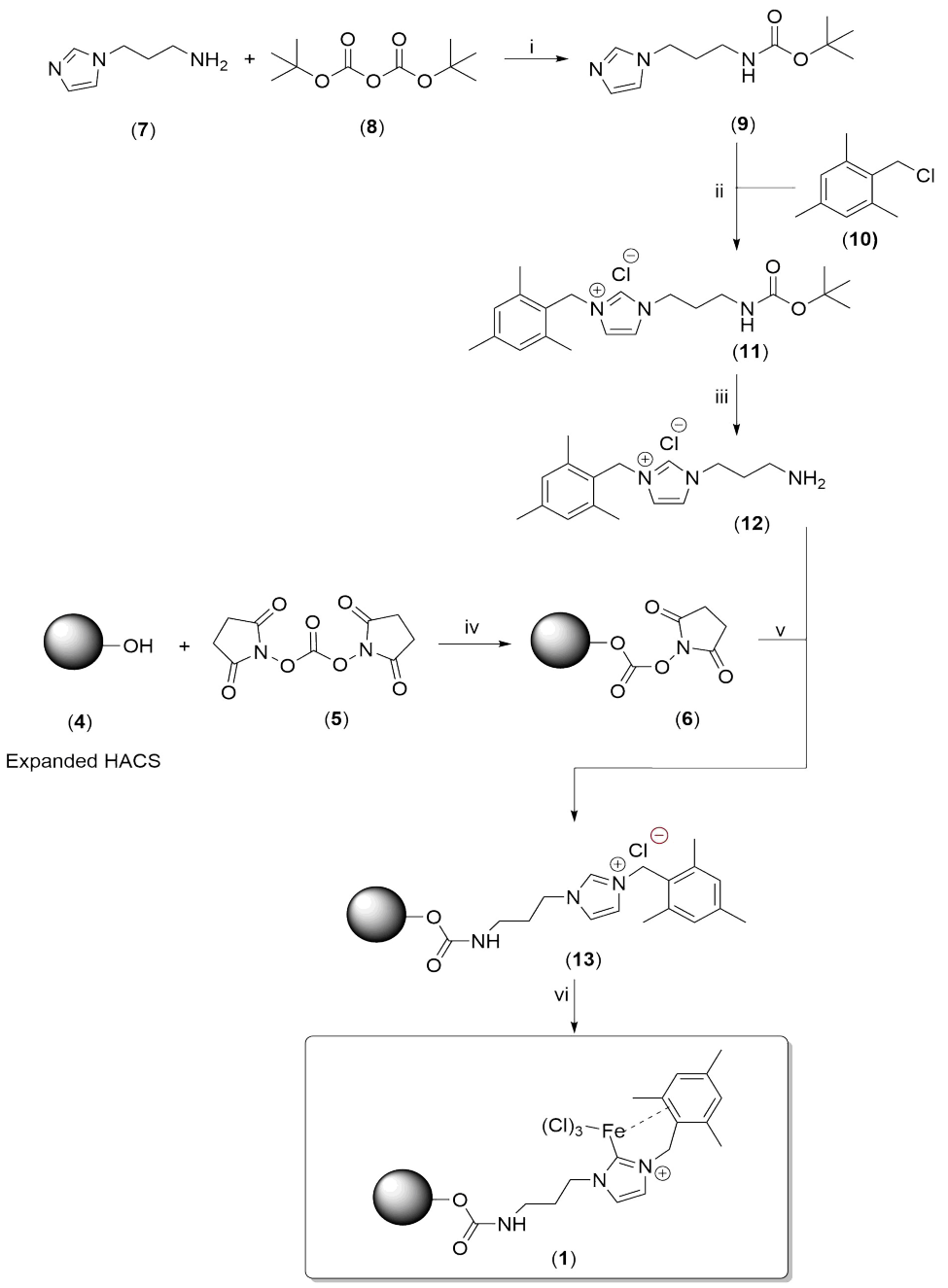

Reagents and conditions: i. $NaHCO_3$, CPME, 4 h, rt; ii. CPME, 80 °C,18 h; iii. TFA, CPME, 50 °C, 6 h; iv. DMAP, propylene carbonate, 80 °C,18 h; v. TEA, propylene carbonate, 80 °C,18 h; vi. K^{t}OBu, $FeCl_3$, propylene carbonate, 80 °C, 18 h

SCHEME 1.1: Synthesis of iron-NHC catalyst (**1**).

within the ring structure." [14] NHCs are special among other carbenes because they are stable, directly synthesized, can attach to metals with different oxidation states and can form organometallic complexes that are stable as catalysts (see Figure 1.4). The stability of NHCs can be explained by their ability to form a σ-bond using their sp^2 hybridized lone pair with a σ-accepting

orbital of the transition metal. [12] and [14]

The general design of a supported NHC catalyst is shown in Figure 1.5. The NHC is usually tethered on to a polymer support via a short linker or spacer.

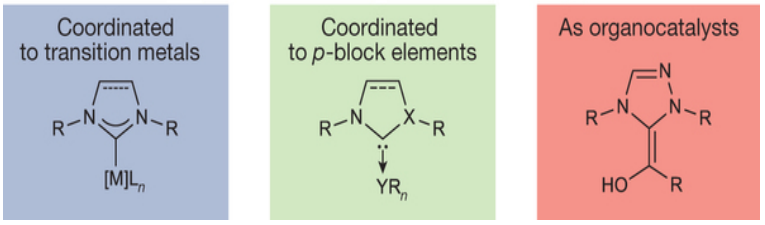

FIGURE 1.4: Examples of different types of NHCs. [14]

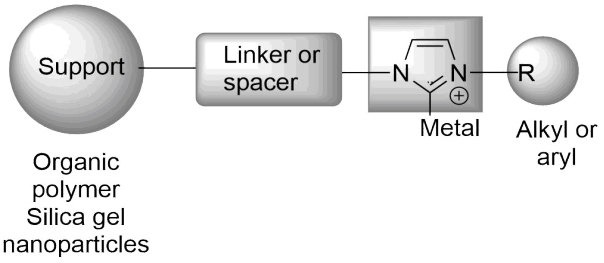

FIGURE 1.5: General design of a heterogeneous NHC-metal complex catalysts. [15]

NHC catalysts for fructose to HMF conversion have been reported in the literature. For example, G. Yang *et al* used a NHC-Cr/ionic liquid system to convert fructose and glucose in to HMF in good yield and high re-usuability [16] whilst Y. Kim *et al* showed Fe-NHCs tethered on to polysterene resins as good catalysts for HMF production (73% selectivity; 97% conversion). [17] Although, these are relevant examples, they are slightly flawed due to the use of toxic chromium in the first example and a non-renewable support (polystyrene) in the second case.

1.1.2 Why expanded starch as a support?

In this research, expanded high amylose corn starch (**4**) was used as a support because it is (bio)renewable, and readily available from a variety of waste biomass types. Importantly, to the best of our knowledge the tethering of a Fe-NHC on to starch has not been reported before.

Starch consists of two polymers of glucose; amylose and amylopectin (Figure 1.6 and 1.7). Corn starch for instance contains 28% amylose and 72% amylopectin [18] whereas high amylose corn starch, e.g. HYLON VII, consists of 71% amylose. [19] Amylose is a linear molecule of (1→4) linked α-D-glucopyranosyl units. Amylopectin on the other hand is the highly branched component of starch that is composed of chains of α-D-glucopyranosyl attached with each other generally by (1→4) linkages and at the branch points of (1→6) bonds. [20] Within the anhydroglucose unit of starch, there are three hydroxyl groups: C_2; C_3; and; C_6, which are available for chemical modification. Thus the theoretical maximum degree of substitution (DS) is 3. The C_6-OH has the highest probability for substitution due to least steric hindrance. [21]

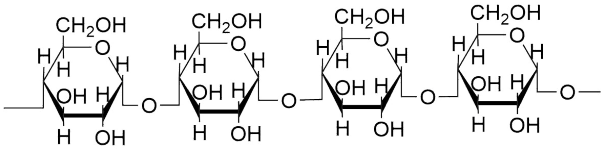

FIGURE 1.6: Structure of amylose.
[22]

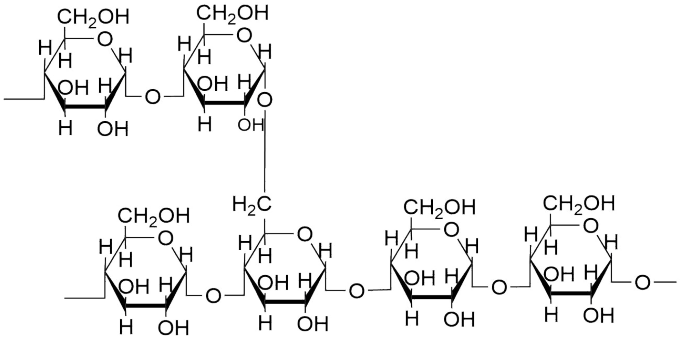

FIGURE 1.7: Structure of amylopectin.
[22]

1.1.3 Why iron?

Depletion of elements without their recovery and reuse makes the periodic table unsustainable. Elemental sustainability is of global concern. [23]

All elements within the earth's crust are available in limited quantities. Aluminium, iron and silicon, are highly abundant compared to platinum, silver and selenium for instance. As shown in Figure 1.8, plentiful elements are among those which have present known reserves (known weights of metals that can be

economically and legally extracted using existing techniques) that are considered to be expended in less than 50 years if their extraction levels remain unchanged. [24]

NHC complexes have been prepared using different metals such as palladium [25] and gold [26]. According to Figure 1.8, the remaining years for gold are 5-50 years whereas for palladium 50-100 years. Compared to these elements, iron is abundant, of low toxicity and benign, widely recycled and, thus, conforms to elemental sustainability. In addition, the chemistry of iron compounds shows a wide-range of geometric and electronic possibilities. For example, its oxidation states range from low valent (Fe(0) and Fe(I)) to high-valent (Fe(II) , Fe(III) Fe(IV) and Fe(V)) (Figure 1.9 shows NHC complexes of Fe(0), Fe(II), Fe(III), and Fe(IV)). The coordination at the iron center affords different geometries, for example, tetrahedral, octahedral trigonal bipyramidal, square planar or three-coordinate iron complexes. [27]

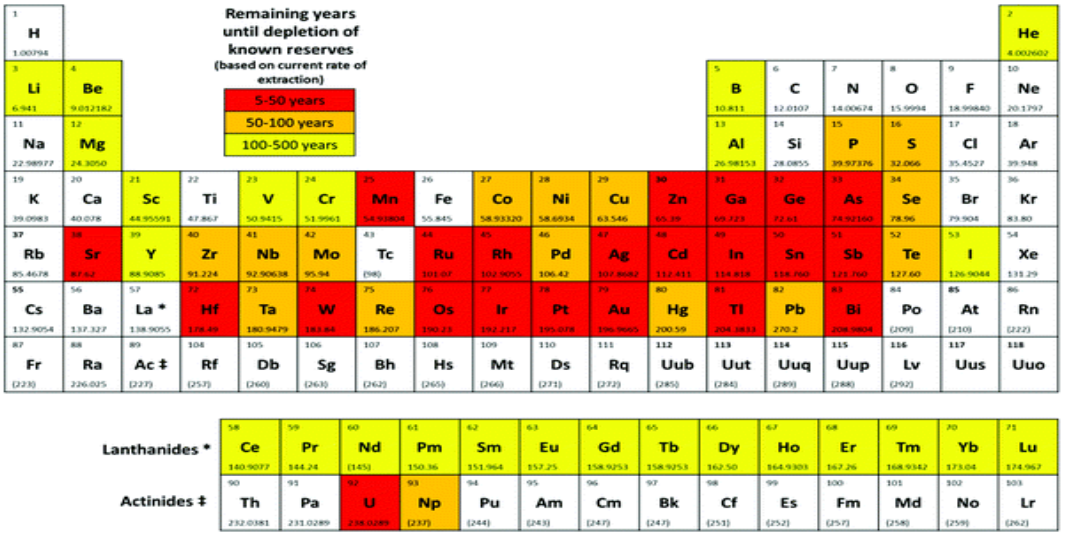

FIGURE 1.8: Remaining years until depletion of known reserves of elements. [23]

W. Fehlhammer *et al* reported the synthesis of Fe-NHC compounds via base-induced deprotonation of a particular imidazolium salts (Figure 1.10, route D). [27], [28] and [29] Butyllithium, metal alkoxides or sodium hydride are usually used as bases whereas Fe(II) and Fe(III) salts of bromide and chloride are used as the metal precursors. [27]

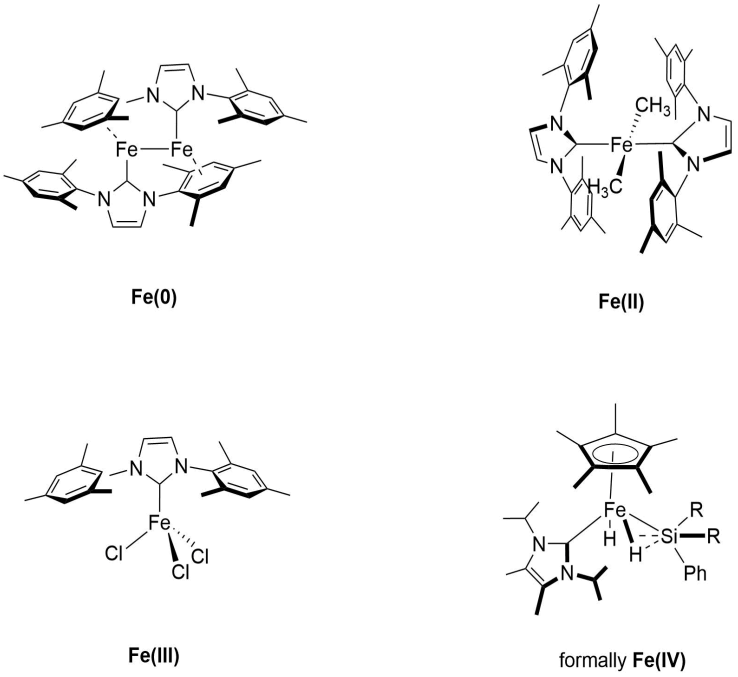

FIGURE 1.9: NHC complexes of Fe(0), Fe(II), Fe(III), and Fe(IV). [30]

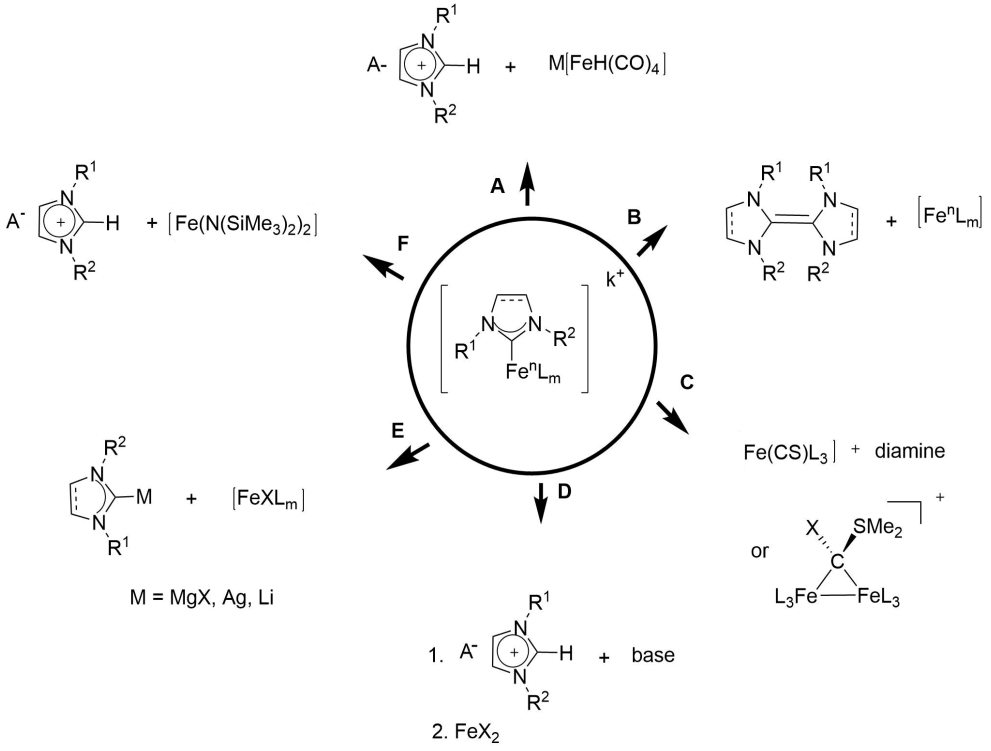

FIGURE 1.10: Common synthetic routes toward Fe-NHC complexes. [27]

1.1.4 Why fructose to HMF conversion?

In 2004, the US department of energy (DoE) identified 12 platform molecules or building blocks derived from biomass that could replace their existing synthetic, petroleum-derived counterparts. [31] HMF (**3**) is a listed platform molecule [32] and the presence of both hydroxymethyl (-CH_2OH) and aldehyde (-CHO) groups in its structure makes it a reactive molecule affording further products (see Figure 1.11). HMF (**3**) is a precursor for 2,5-dimethylfuran (DMF), a biofuel and in the production of downstream products such as levulinic acid, 2,5-diformylfuran (DFF), 5-hydroxy-4-keto-2-pentenoic acid, 2,5-furandicarboxylic acid (FDA) and 2,5-dihydroxymethylfuran. [33] and [34]

However, the conversion of carbohydrates to HMF (**3**) alone is not easy since many side reactions and byproducts are formed. Traditionally, dehydration of hexoses such as D-fructose in the presence of either homogeneous and/or heterogeneous acid catalysts produces HMF (**3**). [35] and [36] For example, J. Zhao *et al* reported sulfonated carbon spheres as solid acid catalysts for the dehydration of fructose to HMF (90% yield, 160 °C, 1.5 h) in DMSO as solvent. [37] J. Chen *et al* reported recyclable sulfonic acid-functionalized metal-organic frameworks (MOF-SO_3H) for 100% fructose conversion affording 90% HMF yield (120 °C, 1 h) in DMSO as solvent. [38]

Z. Xue *et al* reported Nb-containing catalysts (Nb-NNTMPA) synthesized from the reaction of niobium chloride and methylenephosphonic acid (NTMPA) in pseudo-ionic liquid comprising *N,N′*-dimethylacetamide (DMA) and NaBr to furnish HMF in excellent yield (85.6%). [39] A. Dibenedetto *et al* successfully used cerium(IV) phosphates for the dehydration of fructose to HMF in aqueous media both in batch and flow conditions; when in batch mode selectivity was high (93%) but yield moderate (52%) whilst flow conditions (170 °C single pass) gave equally high selectivity (95%) but very poor yield (24%) because the phosphate group was thought to leach from cerium(IV) phosphate as phosphoric acid causing catalyst de-activation. [40]

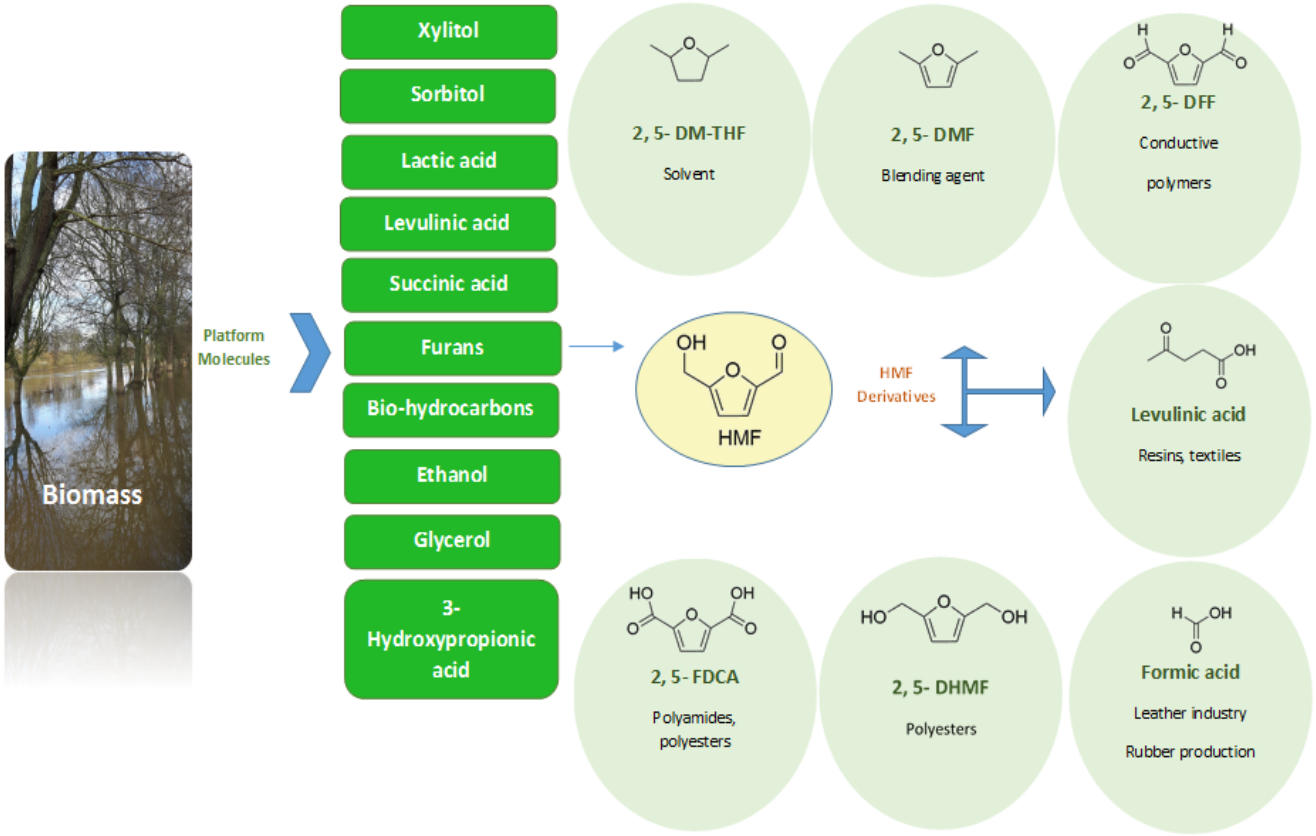

FIGURE 1.11: Summary of platform molecules as stated by Bozell and Petersen and 5-HMF directly derived molecules. [41] and [42]

T. Wang *et al* have shown a variety of metal- and mixed-metal oxides coupled with microwave irradiation capable of successfully dehydrating fructose to HMF, e.g., ZrO_2, WO_x/ZrO_2, MoO_x/ZrO_2, $SO_4^{2-}/$ WO_x^- ZrO_2 and SO_4^{2-}/MoO_x ZrO_2, in dimethyl sulfoxide. The $SO_4^{2-}/WO_x^-ZrO_2$ catalyst showed the best activity with 83.90% 5-HMF yield and 95.80% fructose conversion which was achieved within 5 minutes at 150 °C. [43] X. Tong *et al* reported Ge(IV) catalysts for production of HMF from both fructose and sucrose. At 150 °C for 100 min, fructose and sucrose dehydration to HMF gave 62% and 37% yield, respectively in the presence of a dual GeO_2/Ge_3N_4 catalyst. In addition, using sulfated GeO_2 (SO_4^{2-}/GeO_2) catalyst and fructose as a starting material, 68% HMF yield was gained in DMSO. [44]

The reaction pathway of acid catalysed dehydration of fructose is summarized in Figure 1.12. According to literature there are two possible pathways for the mechanism of the fructose dehydration to HMF. The first involves a series of reactions that start with fructofuranose ring while the second supports a sequence of reactions taking place via open-chain intermediates. [45] Partially dehydrated intermediates are produced as a result of elimination of one or two water molecules from fructose as a start of HMF formation. A further third dehydration affords the product (HMF). However, inter-molecule condensation side reactions of these intermediates lead to formation of side products such as insoluble humins and soluble polymers. [45]

In comparison to aldohexoses, ketohexoses form HMF with higher selectivity and efficiency due to the higher degree of enolisation which is a rate determining step in the formation of fructose. [46] This can be explained by the higher abundance of acyclic fructose and hence it can form less stable ring structure. Another reason is that difructose and dianhydrides are formed by fructose which can reduce the production of by-products due to the blockage of the reactive groups. [33]

In the high temperature dehydration of hexoses in aqueous acidic solution, formic acid and levulinic acid are formed accompanied with HMF in a rehydration reaction. [46]

A full mechanistic understanding of the fructose to HMF dehydration reaction is further complicated because fructose has three types of structural isomers (Figure 1.13): *keto*-D-fructose; D-fructofuranose, and; D-fructopyranose. The latter two have two diastereoiomers, so the difficulty is in finding out which isomers are

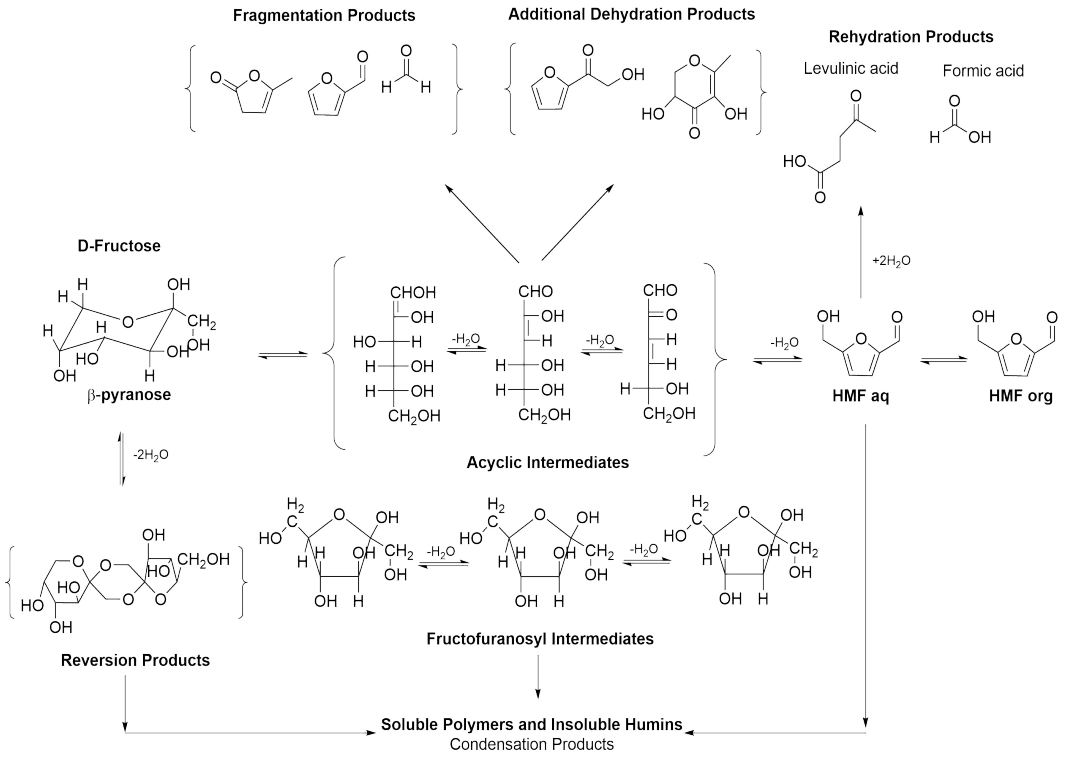

FIGURE 1.12: Reaction pathways of acid catalysed dehydration of fructose. [47]

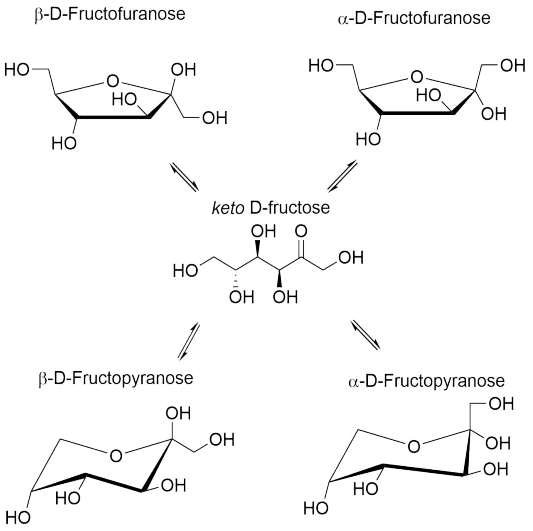

FIGURE 1.13: Tautomeric forms of D-fructose in solution. [48]

responsible for the production of HMF. [49] Due to the existence of five tautomers in solution, fructose has a complex ^{1}H NMR spectrum.

Fructose dehydration reaction in water is a nonselective reaction because it leads to the formation of many by-products other than HMF. Using non-aqueous solvent such as DMSO can help to reduce the formation of these side products. [46] However recent studies showed better results with respect to the use of acetonitrile and acetone with low concentration of fructose, yet this still leads to low HMF yield. [47] K. Shimizu *et al* investigated removal of water (0.97 x10^5 Pa) from the reaction to afford near quantitative yield of HMF in the presence of solid acid catalysts. [50]

Certain ionic liquids, e.g., 1-butyl-3-methylimidazolium tosylate ([BMIM] [TSO], have been used successfully to yield HMF (96%, 0.5 h, 80 °C). [51] J. Chheda *et al* reported the use of biphasic systems (organic extracting phase containing dichloromethane or a 7:3 (w/w) MIBK:2-butanol mixture and reactive aqueous phase adjusted with DMSO) affording 89% selectivity for HMF from fructose. Continual separation of HMF prevented further side reactions. [52] However, due to the high solubility of HMF in water as well as in the organic phase, the use biphasic system requires large volumes of solvent which is considered as a disadvantage. [53]

1.1.5 Summary

The importance of platform molecules as a cornerstone for our energy, chemicals and materials requirements for a future sustainable 21^{st} century is critical as crude oil reserves decline. The development of new catalysts that offer high yield and high selectivity of platform molecules such as HMF is a growing area of research. However, production of HMF from biomass is straightforward but dependent on a multitude of variables as depicted in Figure 1.14. [54]

Thus, in order to add new knowledge to this important but complicated reaction, herein, the synthesis, characterization and application of a novel Fe-NHC supported on to expanded starch (**1**), as a catalyst, for the dehydration to fructose (**2**) to HMF (**3**) is now discussed. Chapter 2 reports experimental procedures whilst Chapter 3 gives an in-depth discussion of the synthetic

procedures and catalytic potential of the Fe-NHC. Conclusions and further perspectives are offered in Chapter 4.

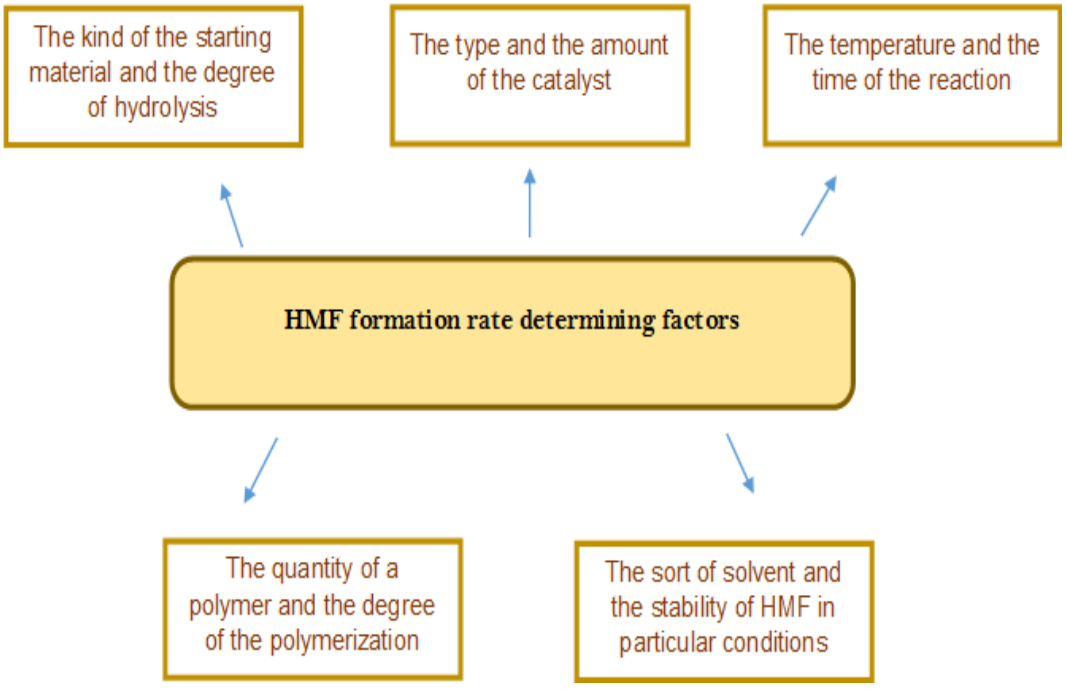

FIGURE 1.14: HMF formation rate determining factors.

Chapter 2

Experimental

2.1 Materials and Reagents

Expanded high amylose corn starch (HACS) (**4**) was provided by the Green Chemistry Centre of Excellence, University of York. Propylene carbonate (purity 99.7%), iron(III) chloride (purity 97%), potassium-*tert*-butoxide (K^tOBu) (purity 98%), triethyl amine (purity $\geq$ 99%), D-(-)-fructose **(2)** (purity $\geq$ 99%), Di-*tert*-butyl dicarbonate (**8**), *N*-(3-aminopropyl)imidazole (purity $\geq$ 97%), 2,4,6-trimethylbenzyl chloride (**10**) (purity 98%), trifluoroacetic acid (TFA) (purity 99%), dimethyl sulfoxide-d_6 (DMSO-d_6) (99% atom D), Chloroform-*d* ($CDCl_3$) (99.8% atom D), Amberlyst-15 and Montmorillonite K-10 were purchased from Sigma-Aldrich. *N,N′*-Disuccinimidyl carbonate (DSC) (**5**) (purity $\geq$ 95.0%) was obtained from Fluka and 4-dimethylaminopyridine (DMAP) (purity 99%) from Acros chemicals Ltd. Cyclopentyl methyl ether (CPME) was obtained from ZEON corporation, Japan whilst ZSM-30 was acquired from RS Minerals, UK. All materials were used without further purification.

2.2 Instrumentation

2.2.1 Attenuated Total Reflection Infrared Spectroscopy (ATR-IR)

The Attenuated Total Reflection Infrared (ATR-IR) was performed on a Bruker Vertex 70 ATR controlled using OPUS software. 128 background scans 64 sample scans were recorded for each sample. Where appropriate, Far infrared (FIR) was performed on a Burker Tensor 37 with platinum ATR with 4 cm^{-1} resolution, 24 background scans and 24 sample scans.

2.2.2 Porosimetry

BET surface area measurements (nitrogen adsorption/desorption measurements) of expanded HACS (**4**) and its modified compounds were determined using a Micromeritics ASAP 2020 surface area and porosity analyzer. The sample (about 20 mg) was degassed at 120 °C for 240 min using a flow of N_2. The mass was corrected after the degassing. The data was processed using ASAP software. Specific surface areas were calculated using the Brunauer, Emmett and Teller (BET) equation. [55]

$$\frac{p}{v(p^o - p)} = \frac{1}{v_m c} + c - \frac{1p}{v_m c p^o} \tag{2.1}$$

where p= equilibrium pressure, p°= saturation pressure, v= volume of gas adsorbed, v_m= volume of gas adsorbed in one unimolecular layer, c= BET constant which equals

$$e^{\frac{E_1 - E_L}{RT}} \tag{2.2}$$

where E_1 is the heat adsorption of the first layer and E_T is the heat of liquification.

2.2.3 Scanning Electron Microscopy (SEM) and Transmittance Electron Microscopy (TEM)

Scanning electron microscopy images were obtained with the assistance of Dr Meg Stark, Department of Biology, University of York, UK and transmittance

electron microscopy images were taken with the help of Dr Meg Stark and Dr Anna Simon, Bioscience Technology Facility, Biology Department, University of York. Scanning electron microscopy micrographs were recorded using a JEOL JSM-6490 LV with 5 Kv scanning electron microscope. Samples were put on SEM stubs and coated with gold and palladium before analysis. Resolutions used were x1000, x2000, x5000 and x10000. TEM imaging was performed using a Tecnai 12 BioTWIN from FEI that is operated at 120 kV with a SIS Megaview 3 camera. A 200 Mesh copper grids with pioloform coating were used.

2.2.4 Solid State ^{13}C NMR

Solid state ^{13}C-MAS NMR analysis was carried out with the support of Dr. Pedro M. Aguiar and Julia Walton, Department of Chemistry, University of York, UK. ^{13}C ^{1}H CPMAS spectra were attained using a 400 MHz Bruker Avance III HD spectrometer fitted out with a Bruker 4 mm H(F)/X/Y triple-resonance probe and 9.4 T Ascend superconducting magnet. The CP experiments were carried out a 1.5 ms linearly-ramped contact pulse, optimized recycle delays of 3 seconds, spinning rates of 12000 $\pm$ 2 Hz (or 9000 Hz), spinal-64 heteronuclear decoupling (at rf =85 kHz) and are a sum of 512 co-added transients. Chemical shifts are stated with respect to TMS, and adamantane (29.5 ppm) was used as an external secondary reference.

2.2.5 Simultaneous Thermal Analysis (STA)

Simultaneous Thermal Analysis (STA) was carried out using Stanton Redcroft STA 625. About 0.01 g of the sample was weighed in an aluminum crucible. The system was purged with nitrogen and then with air at a flow rate of 50 ml/min to 600 °C with a heating rate of 20 °C/min.

2.2.6 Inductively Coupled Plasma-Mass Spectroscopy (ICP-MS)

Inductively Coupled Plasma Mass Spectroscopy (ICP) was obtained with the help of Andrea Muñoz, Green Chemistry Centre of Excellence, Chemistry Department,

University of York, using an Agilent 7700x fitted with standard Ni sample and skimmer cones and coupled to a Mass Spectrometer (MS). The samples were run in He mode. The sample introduction line was rinsed for 60 sec between samples using 5% HCl and 2% HNO_3 (30 sec with each compound). Samples were prepared by acid digestion ((5 ml) 75% HCl:25% HNO_3), Fe-NHC (50 mg, 80 °C, 4 h). The resultant digest was filtered and diluted with ultra-pure deionized water to 100 ml and further dilution to 10 ml.

2.2.7 Nuclear Magnetic Resonance (NMR)

Liquid ^{1} H NMR (64 scans) and ^{13}C NMR (1024 scans) spectra were obtained using a Jeol ECS 400 A NMR operating at 400 MHz and 100 MHz, respectively. Spectral referencing was with respect to tetramethylsilane.

2.2.8 High Performance Liquid Chromatography (HPLC)

High performance liquid chromatography was carried out by Amanda Dixon, Department of Chemistry, University of York using Shimadzu Dominance RP-HPLC with CNW Athena C18-WP (250 x 4.6 mm, 5 μm) column maintained at 35 °C with 0.8 ml/min flow rate and eluting with 75% H_2O:25% acetonitrile.

2.2.9 Mass Spectrometry (MS)

Mass Spectrometry analysis was carried out by Karl Heaton, Department of Chemistry, University of York, using Bruker micrOTOF time of flight mass spectrometer. Data were acquired in the mass range 100 m/z to 480 m/z and using positive mode electrospray ionisation. A 4500 V capillary voltage, 1.5 bar nebuliser pressure, 8 L/min drying gas flow and 160 °C drying gas temperature were used. Spectra were calibrated using mass values obtained from a sodium formate internal standard and mass measurement errors were calculated using Bruker Data Analysis software.

2.2.10 X-ray Photoelectron Spectroscopy (XPS)

X-ray Photoelectron Spectroscopy (XPS) was carried out by Dr. Billy Murdoch, National EPSRC XPS Users Service (NEXUS), Newcastle University.

2.3 Determination of Degree of Substitution (DS)

Degree of substitution was determined according to the literature method as following [56] and [57]: the appropriate DSC activated expanded HACS (**6**) (0.5 g) and 75% ethanol in distilled water (25 ml) were mixed and stirred at 50 °C for 30 min. The mixture was then allowed to cool to room temperature. An aqueous solution of potassium hydroxide (0.5 N, 20 ml) was then added to the mixture and stirred at room temperature for 72 h followed by addition of phenolphthalein (2 drops) indicator. The solution was titrated with hydrochloric acid (0.5 N). Expanded HACS (**4**) sample (unmodified) was treated the same way. These processes were repeated 3 times and the average was recorded. The % of DSC was found according to the following equation:

$$\%DSC = \frac{[(V_o - V_n) \times N \times 0.1421 \times 100]}{M} \tag{2.3}$$

Where, 142.1 is the molar mass of the DSC group. V_o is the used volume of HCl for titration of unmodified expanded HACS, V_n is the used volume of HCl for titration of DSC activated expanded HACS, N is the normality of HCl used and M is the weight of the sample used.

DS was found using the following equation:

$$DS = \frac{162 \times \%DSC}{[14210 - (142.1 \times \%DSC)]} \tag{2.4}$$

Where, 162 is repeat unit starch molar mass and 14210 is the molar mas of DSC group multiplied by 100. The percentage of DSC groups and D.S for compounds ($\mathbf{6}_a$) and ($\mathbf{6}_b$) is reported in the Chapter 3 and the raw data are provided in AppendexA.

2.4 Conversion Study

2.4.1 Nuclear Magnetic Resonance (NMR)

^{1}H and ^{13}C NMR spectra were gained using Bruker Avance III HD 500. For the ^{1}H the acquisition time is 4.1 sec and 8000 Hz spectral width, prescan delay of 6.5 μ sec and 16 scans. For the ^{13}C the acquisition time is 1.0 sec and 31250 Hz spectral width, prescan delay of 6.5 μ sec and 16 scans.

2.5 Synthesis of NHC ligand (12)

2.5.1 1-[(*N*-*Tert*-butoxycarbonyl)aminopropyl]imidazole (9)

Under a nitrogen purge, a solution of di-*tert*-butyl dicarbonate (**8**) (50.0 g, 230.8 mmol) in CPME (25 ml) was added dropwise to a stirred mixture of *N*-(3-aminopropyl)imidazole (**7**) (23.0 g, 191.7 mmol), $NaHCO_3$ (38.0 g, 456.0 mmol) and CPME (50 ml). The reaction was stirred for 4 h at room temperature, filtered to remove solid $NaHCO_3$ and the solution was transferred to a separating funnel containing deionized water (200 ml). The organic layer was isolated whilst the aqueous layer was extracted with ethyl acetate (3 x 150 ml). The combined organic fractions were dried ($MgSO_4$) and the solvent was removed *in vacuo* to afford the desired 1-[(*N*-*tert*-butoxycarbonyl)aminopropyl]imidazole (**9**), 30.8 g (74.4%), a clear orange oil. ^{1}H NMR (400 MHz, $CDCl_3$, TMS) (δ ppm): 7.5 (s, 1H), 7.0 (s, 1H), 6.9 (s, 1H), 4.7 (s, 1H), 4.0 (t, 2H), 3.1 (q, 2H), 1.9 (quint, 2H), 1.4 (s, 9H, 3 x CH_3); ^{13}C NMR (101 MHz, $CDCl_3$, TMS) (δ ppm): 156.2 (-NH-**C**O_2-R), 137.2, 129.7, 118.9, 83.0, 56.4, 44.4, 31.7, 28.3, 23.6; IR (cm^{-1}): 3343, 2931, 2866, 1700 (-C=O str), 1489, 1366 (CH_3), 1250 (C-O-C); MS m/z (225.29 for $C_{11}H_{19}N_3O_2$, [M + H]$^{+}$, found 226.1554).

2.5.2 1-[*N*-*Tert*-butoxycarbonyl)-3-aminopropyl]-3-(2,4,6-trimethyl benzyl) imidazolium chloride (11)

1-[(*N*-*Tert*-butoxycarbonyl)aminopropyl]imidazole (**9**) (30.8 g, 154.1 mmol), 2,4,6-trimethylbenzyl chloride (**10**) (28.6 g, 151.3 mmol) in CPME (90 ml) were stirred at 80 °C for 18 h. Thereafter, the product was washed with CPME (5 x 50 ml) and dried (*in vacuo*) to afford the desired 1-[*N*-*tert*-butoxycarbonyl)-3-aminopropyl]-3-(2,4,6-trimethylbenzyl)imidazolium chloride (**11**), 48.1 g (79%), a clear yellow oil. ^{1}H NMR (400 MHz, $CDCl_3$, TMS) (δ ppm): 10.8 (s, 1H), 7.5 (s, 1H), 6.9 (s, 2H), 6.7 (s, 2H), 6.0 (s, 1H), 5.5 (s, 2H), 4.4 (t, 2H), 3.2 (q, 2H), 2.2 (s, 9H, CH_3 mesityl), 2.1 (quint, 2H), 1.4 (s, 9H, 3 x CH_3); ^{13}C NMR (400 MHz, $CDCl_3$, TMS) (δ ppm): 156.2, 139.9, 138.1 , 137.7, 130.0, 129.2, 83.0, 79.2, 56.4, 47.8, 47.4, 31.9, 30.8, 28.5, 23.6, 21.1, 19.8, 19.2; IR (cm^{-1}), 3386 (N-H), 2866, 2956 (C-H), 1698 (-C=O str), 1612 (C=C aromatic), 1516 (C-N (imidazole ring)), 1365 (CH_3), 1251 (C-O-C); MS m/z (358.5 for $C_{21}H_{32}N_3O_2$, [M^+], found 358.2487).

2.5.3 1-[Aminopropyl]-3-(2,4,6-trimethylbenzyl) imidazolium chloride (12)

A mixture of 1-[*N*-*tert*-butoxycarbonyl)-3-aminopropyl]-3-(2,4,6-trimethylbenzyl)imidazolium chloride (**11**) (48.05 g, 121.95 mmol), trifluoroacetic acid (243.9 ml) and methanol (300 ml) was heated at 50 °C for 18 h. Thereafter, the mixture was evaporated (rotary) to remove methanol and trifluoroacetic acid. The resultant crude residue was washed with CPME (5 x 50 ml) and dried (*in vacuo*) to afford the desired 1-[aminopropyl]-3-(2,4,6-trimethylbenzyl)imidazolium chloride (**12**), 34.00 g (95%), a clear, brown, viscous oil. ^{1}H NMR (400 MHz, $CDCl_3$, TMS) (δ ppm): 9.4 (s, 1H), 8.6 (s, 3H), 7.6 (s, 1H), 6.9 (s, 2H), 6.8 (s, 1H), 5.3 (s, 2H), 4.4 (s, 2H), 3.0 (s, 2H), 2.3 (s, 2H), 2.2 (s, 9H); ^{13}C NMR (400 MHz, $CDCl_3$, TMS) (δ ppm): 138.2, 130.0, 129.0, 118.0, 114.3, 47.8, 47.4, 31.2, 30.5, 28.3, 21.0, 19.5, 19.4 ; IR (cm^{-1}), 3400 (N-H), 3136 (NH_2), 2975, 1616 (C=C aromatic), 1508 (C-N (imidazole ring)), 718 (NH_2 wagging); MS m/z (258.38 for $C_{16}H_{24}N_3$, [M^+], found 258.1973).

2.6 Synthesis of Fe-NHC (1)

2.6.1 Succinimidyl carbonate expanded starch ($\mathbf{6}_{a-b}$)

The general procedure for making succinimidyl carbonate expanded starch ($\mathbf{6}_{a-b}$) is described below and the exact reagent quantities are listed in Table 2.1.

TABLE 2.1: Summary of the amount of reactants used in preparing succinimidyl carbonate expanded starch ($\mathbf{6}_{a-b}$)

	DSC **(5)**		DMAP		PC	**(4)**		Reaction	Yield
	(g)	(mmol)	(g)	(mmol)	(ml)	(g)	(mmol)	time (h)	%
($\mathbf{6}_a$)	15	58.55	6	49.1	50	3	18.5	18	60.0
($\mathbf{6}_b$)	30	117.11	12	98.2	150	3	18.5	18	68.6

The approprate amounts of *N,N′*-disuccinimidyl carbonate (**5**) and DMAP were added to a stirred mixture of expanded HACS (**4**) (3 g, 18.5 mmol) in propylene carbonate. The mixture was heated to 80 °C for 18 h, cooled and centrifuged (3000 rpm, 4 mins). The supernatant was removed and the pellet was washed with propylene carbonate (5 x 25 ml) and acetonitrile (3 x 40 ml). Each wash was centrifuged (3000 rpm, 4 mins) to remove solvent. After the final wash, the product was dried under vacuum at 80 °C for 3 h to yield the desired succinimidyl carbonate expanded starch (**6**), as a white solid. The yields are reported in Table A.2. ^{13}C NMR (400 MHz, TMS, admantane) (δ ppm): 173.4 (N-**C**=O), 156.4 (C-**C**=O), 101.2 (O-**C**-O), 82.1, 72.9, 62.3 (**C**-O-C=O), 39.1; IR (cm^{-1}), 3356 (OH str), 2950, 1735 (-O-CO-O-), 1654 (-CO-NR-CO-), 1250, 1151, 1079, 1021, (931, 861, 764) (anhydroglucose stretching vibration).

.

2.6.2 Expanded starch immobilized ligand (13)

Disuccinimidyl carbonate activated expanded HACS (**6a**) (2.5 g), NHC ligand (**12**) (26.7 g, 8.0 mmol) and triethyl amine (6.7 ml, 46.9 mmol) in propylene carbonate (50 ml) were allowed to react in a round bottom flask at 80 °C for 18 h with stirring. Thereafter, the resultant mixture was cooled and centrifuged

(3000 rpm, 4 mins). The supernatant was discarded and the pellet was washed with propylene carbonate (3 x 50 ml) and acetonitrile (3 x 40 ml). Each wash was centrifuged (3000 rpm, 4 mins) to remove solvent. After the final wash, the product was dried under vacuum at 80 °C for 3 h to yield the desired expanded starch immobilized ligand (**13**), 41.8%, as a white solid. ^{13}C NMR (400 MHz, TMS, admantane) (δ ppm): 156.4 (O-**C**=O-NH-), 139.2 (aromatic carbons), 130.1 (**C**H_2 imidazole), 101.2 (O-**C**-O), 82.1, 72.9, 62.3 (**C**-O-C=O), 40.0 (**C**H_2 aminopropyl), 20.2 (**C**H_3 mesityl); IR (cm^{-1}), 3356 (OH str), 2950, 1726 (-O-CO-NH-), 1649 (-CO-NR-CO-), 1256, 1152, 1078, 1021, (932, 856, 767) (anhydroglucose stretching vibration).

2.6.3 Fe-NHC catalyst (1)

In an inert atmosphere of nitrogen, a solution of iron(III) chloride (0.6 g, 4.0 mmol) in propylene carbonate (10 ml) was added to a stirred mixture of starch immobilized ligand (**13**) (2.0 g), potassium-*tert*-butoxide (0.5 g, 4.4 mmol) and propylene carbonate (50 ml). The reaction mixture was heated at 80 °C for 18 h, cooled and centrifuged (3000 rpm, 4 mins). The supernatant was discarded and the pellet was washed with propylene carbonate (3 x 50 ml), brine solution (50 ml), deionized water (2 x 50 ml) and methanol (3 x 40 ml). Each wash was centrifuged to remove solvent. After the final wash, the product was dried under vacuum at 80 °C for 3 h to yield the desired Fe-NHC catalyst (**1**), 61.5%, a light brown solid . ^{13}C NMR (400 MHz, TMS, admantane) (δ ppm): 156.4 (O-**C**=O-NH-), 139.2 (aromatic carbons), 130.1 (**C**H_2 imidazole), 101.2 (O-**C**-O), 82.1, 72.9, 62.3 (**C**-O-C=O), 40.0 (**C**H_2 aminopropyl), 20.2 (**C**H_3 mesityl); IR (cm^{-1}), 3355 (OH str), 2950, 1728 (-O-CO-NH-), 1654 (-CO-NR-CO-), 1258, 1152, 1079, 1021, (932, 858, 764) (anhydroglucose stretching vibration).

2.7 Fructose (2) conversion to HMF (3)

The general procedure for making 5-(hydroxymethyl)furfural **(3)** is described below:

Four screw-top vials (45 mm length, 20 mm diameter), equipped with a magnetic stirrer, containing fructose (**2**) (91.5 mg, 0.5 mmol), DMSO-d_6 (2 ml)

and Fe-NHC catalyst (**1**) (10.0 mg) were heated to 100 °C in a specially constructed multipoint hotplate. After 0.5 h, the first vial was removed, cooled, filtered (pipette plugged with cotton wool) and stored in a freezer (-20 °C) to minimize further reaction. The second, third and fourth vials were removed from heat after 1 h, 3 h and 6 h, respectively and treated in the same way. All solutions were analyzed by ^{1}H NMR, ^{13}C NMR and HPLC as described in the discussion section (see later).
The above procedure was also used with other heterogeneous catalysts (Amberlyst-15, Montmorillonite K-10 and ZSM-30) comparison test experiments.

2.7.1 Sample preparation for conversion study

A solution of D-fructose (**2**) (91.5 mg) and Fe-NHC catalyst (**1**) (10 mg) in DMSO-d_6 (2 ml) was mixed in a small vial. It was put in a sonication path for 3 minutes to allow mixing up the reactant. Some of the sample was then transferred to an NORELL S400 NMR tube (4 cm sample depth) for the study.The spectra were recorded starting from 25 °C with 5 °C increase each time until 100 °C. At 100 °C, the spectra were then taken immediately (0 h) and after 0.5 h, 1 h, 3 h and 6 h.

2.7.2 Catalyst recycling study

Appropriate amounts of fructose (**2**), DMSO-d_6 and the Fe-NHC catalyst (**1**) (as given in Table 2.2) were heated in a screw-top vial (85 mm length, 25 mm diameter) in a specially constructed multipoint equipped with a magnetic stirrer hotplate to 100 °C. After 6 h, the vial was removed, cooled and the solution was centrifuged (3000 rpm , 4 mins) to separate the catalyst. The supernatant was kept in the freezer (-20 °C) to minimize further reaction prior to analysis by ^{1}H NMR, ^{13}C NMR and HPLC. The separated catalyst was washed with ethanol (3 x 30 ml). Each wash was centrifuged (3000 rpm, 4 mins) to remove solvent.

After the final wash, the product was dried under vacuum at 80 °C for 3 h.

TABLE 2.2: Amounts of reactants used in the Fe-NHC catalyst (**1**) recycling experiments

Experiment	Fructose (**2**) (mg)	Fe-NHC catalyst (**1**) (mg)	DMSO-d_6 (ml)
1 st	640.5	70.0	14.0
2 nd	502.9	50.5	11.0
3 rd	371.5	40.6	8.1
4 th	266.3	29.1	5.8
5 th	219.6	24.0	4.8

Chapter 3

Results and Discussion

This chapter is divided in to three parts, namely:i. synthetic overview and characterization of expanded starch supported Fe-NHC catalysts (**1**), which discusses the synthetic strategy employed, mechanisms where appropriate, and associated characterization studies to confirm the identity of intermediates and final product(s);ii. characterisation of Fe-NHC bio-based catalyst (**1**), which discusses results from different analytical techniques employed to determine presence and concentration of iron (FIR, TEM, CPMAS, ICP-MS, XPS), and assesses changes in porosity (surface area and pore volume) and surface texture (SEM), and;iii. fructose (**2**) to HMF (**3**) conversion, which discusses the application of Fe-NHC (**1**) as a catalyst for fructose dehydration to HMF in the presence of DMSO as solvent. The progress of the reaction is monitored by NMR spectroscopy and mechanisms for products observed are proposed where appropriate. Interestingly, the progress of the reaction differed based on the exernaal atmosphere, either air or nitrogen The effectiveness of (**1**) as a catalyst is compared with commercially available heterogeneous acid catalysts, e.g., Amberlyst-15, Montmorillonite K-10 and, ZSM-30.

3.1 Synthetic overview and characterization of expanded starch supported Fe-NHC catalysts (1)

The desired expanded starch supported Fe-NHC catalyst (**1**) was successfully synthesized using a convergent strategy, as outlined in Scheme 1.1 (Introduction, p. 23), from the appropriate NHC ligand (**12**) and succinimidyl carbonate activated expanded HACS (**6**) followed by complexation with iron(III) chloride. As discussion of the individual steps employed in the synthesis of (**1**) now follows.

3.1.1 Conversion of expanded HACS (4) to succinimidyl carbonate derivatives ($\mathbf{6}_{a-b}$)

Expanded HACS (**4**) suspended in propylene carbonate was successfully converted in to succinimidyl carbonate derivative (**6**), in the presence of *N,N′*-disuccinimidyl carbonate (**5**) and catalyzed by DMAP, in good yield (60%). The mechanism of this reaction is shown in Figure 3.1. DMAP can function either as a base in which case it may deprotonate hydroxyl moieties on starch or may act as nucleophile and react with *N,N′*-disuccinimidyl carbonate (**5**) to give the more reactive acyl pyridinium salt enabling facile reaction with the hydroxyl groups on starch. In both cases, DMAP is regenerated and thus functions as a catalyst.

In certain cases, this conversion has been carried in dimethyl formamide (DMF), [58] a toxic dipolar aprotic solvent, which is removed by washing with copious amounts of water post reaction resulting in considerable amounts of aqueous waste. The latter is usually incinerated but because DMF is a nitrogen containing solvent, NOx emissions are produced. On the other hand, propylene carbonate (used in this case and other conversions within Scheme 1.1) is a *green(er)* alternative produced from (waste) carbon dioxide and propylene oxide. Unlike DMF, incineration of propylene carbonate affords carbon dioxide and water only.

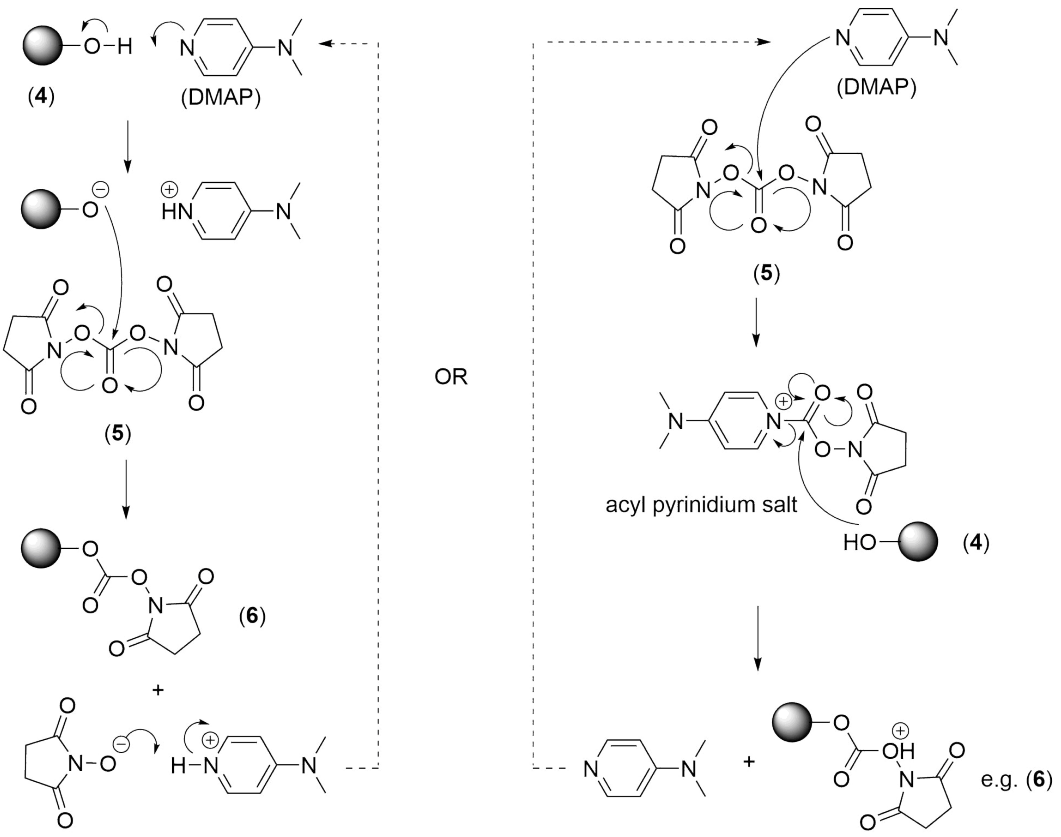

FIGURE 3.1: Suggested mechanism for the DSC activation of expanded HACS (**4**).

The theoretical degree of substitution (DS) of starch (**4**) is 3 because it comprises three hydroxyl moieties per each anhydroglucose unit, i.e., at C2, C3 and C6. As the stoichiometry of starch (**4**) with respect to *N,N′*-disuccimidyl carbonate (**5**) is 1:3, initially the conversion to its succinimidyl carbonate derivative (**6**) was performed using a slight excess of (**5**), i.e., 3.16 molar equivalents or 0.16 molar excess, to afford a DS of 0.33±0.11 corresponding to 20.92±4.88% of succinimidyl carbonate. The low DS may be due to inaccessibility of the hydroxyl moieties within starch despite using expanded HACS (**4**) and due to steric hindrance associated with the bulky succinimdyl carbonate group. It is envisaged that substitution has most likely taken place preferentially on the C6-OH because it is least hindered. In an extreme attempt to increase the DS, twice the concentration of *N,N′*-disuccinimidyl carbonate (**5**), (6.22 molar equivalents or 3.22 molar excess) was used for the conversion of (**4**) to (**6**). Surprisingly, the resulting DS was slightly lower 0.28±0.05 (18.70±1.72% succinimdyl carbonate) thus suggesting the difficulty converting (**4**) in to (**6**) with high DS even with an extreme excess of (**5**).

The ATR-IR spectrum of succinimidyl carbonate derivative (**6**) in comparison with expanded HACS (**4**) is shown in Figure 3.2. The appearance of two new absorption bands in the spectrum of (**6**) at 1735 cm^{-1} and 1654 cm^{-1} provide clear evidence for the inclusion of the succinimidyl carbonate moiety corresponding to the carbonyl stretching frequency of the starch-carbonate ester (starch-O-CO-O-) and imidyl (-CO-NR-CO-) moiety, respectively. Furthermore, the spectra indicate distinctive bands of starch such as the broad O-H stretching vibration at 3356 cm^{-1} and associated absorption bands at 1259 cm^{-1}, 1151 cm^{-1}, 1079 cm^{-1} and 1021 cm^{-1} characteristic of C-O bond stretching. The C-H stretch was evident at 2950 cm^{-1}. Weak absorption bands 931 cm^{-1}, 861 cm^{-1} and 764 cm^{-1} are related to the anhydroglucose ring stretching vibrations. [59]

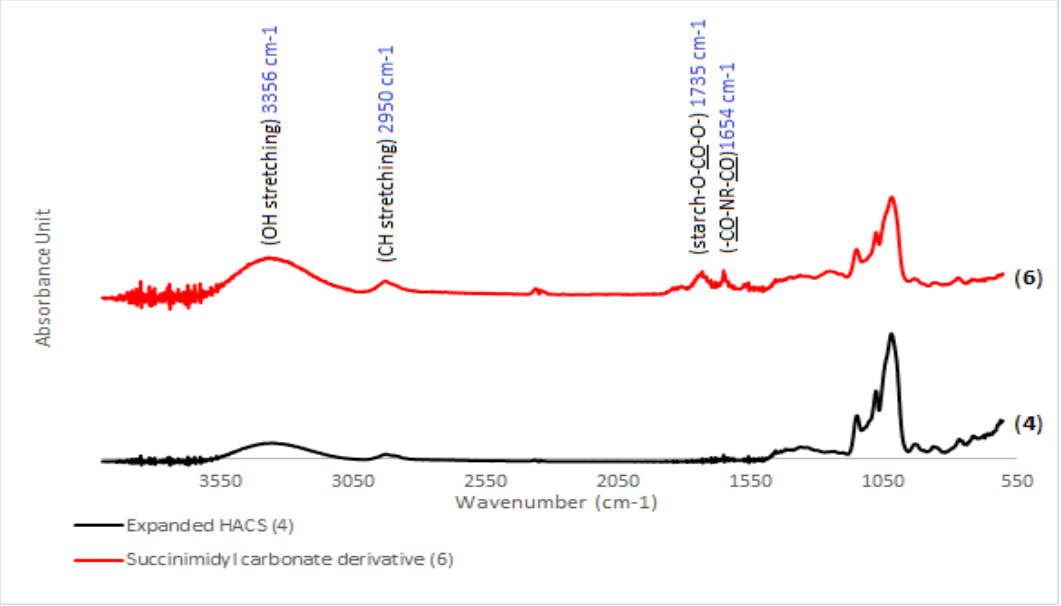

FIGURE 3.2: ATR-IR spectra of expanded HACS (**4**) and succinimidyl carbonate derivative (**6**).

Cross polarization magic angle spinning (CPMAS) ^{13}C NMR was also used to characterize (**6**) as shown in Figure 3.3 which also displays the spectrum for expanded HACS (**4**) for reference. Both spectra show characteristic signals for the anhydroglucose unit of starch: 101.2 ppm is attributed to C1; C2, C3 and C5 are centred at 72.9 ppm; 82.1 ppm corresponds to C4, and; 62.3 ppm represents C6. [60] On closer inspection of the intensity ratio of the C1 signal with respect to C6 signal for both expanded HACS **(4)**, C1(1):C6(1.33) and its succinimidyl carbonate derivative (**6**) reveals a decrease in upon derivatisation, C1(1):C6(1.08) thus indicating attachment at C6. Additionally, the chemical shift of the C6 signal moves upfield from 62.3 ppm to 61.9 ppm upon derivatisation. Similarly, a

comparison of the intensity ratio of the C1 signal with respect to the broad signal at centred at 72.9 ppm representing C2, C3 and C5 shows a decrease in this ratio post derivation from C1(1):C2,C3,C5(4.33) to C1(1):C2,C3,C5(3.75) suggesting substitution may also be occurring at OH groups of C2 and C3.

Importantly, the appearance of new signals in the spectrum of (**6**) at 173.4 ppm (peak numbered 8) and 156.4 ppm (peak numbered 7) provide conclusive evidence for derivatization because they correspond to the carbonyl of the imide (N-**C**=O) and the carbonyl of the carbonate (O-**C**=O) moieties, respectively. Furthermore the methylene carbons (-CH_2-, peak numbered 9) of the succinimdyl ring are observed at 39.1 ppm.

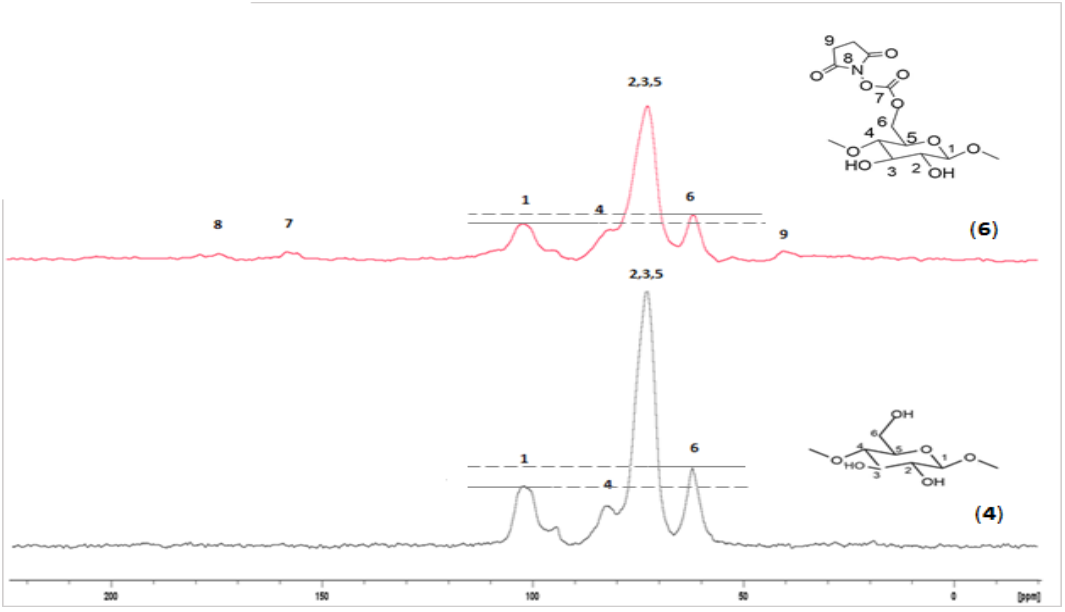

FIGURE 3.3: CPMAS ^{13}C NMR spectra of expanded HACS (**4**) and succinimidyl carbonate derivative (**6**).

3.1.2 NHC Ligand synthesis (12)

In order to synthesize the desired NHC ligand (**12**) a *t*-BOC protection-deprotection strategy was employed so as to ensure the correct regiochemistry of substituents on initial imidazole (**7**). The terminal NH_2 (aminopropyl moiety) was protected thus leaving the imidazole N available for *N*-alkylation with 2,4,6-trimethylbenzyl chloride to afford (**11**). Trifluoroacetic acid-mediated removal (deprotection) of *t*-BOC from (**11**) furnished the desired NHC ligand (**12**). A more detailed discussion of these steps is given as follows.

3.1.2.1 Conversion of *N*-(3-aminopropyl)imidazole (7) to 1-[(*N*-*tert*-butoxycarbonyl)aminopropyl]imidazole (9)

The *t*-BOC protection of *N*-(3-aminopropyl)imidazole (**7**) was successfully achieved in the presence of di-*tert*-butyl dicarbonate (**8**) to afford the desired 1-[(*N*-*tert*-butoxycarbonyl)aminopropyl]imidazole (**9**) in good yield (74.4%). *t*-BOC protection is commonly performed in CH_2Cl_2 [61] and $CHCl_3$ [62], but in this instance CPME was employed, a *green(er)* solvent. CPME is more akin to THF but is water immiscible and has been shown to be viable alternative to CH_2Cl_2 in the preparation of (**9**). Characteristic ^{1}H NMR (3 x $\underline{CH_3}$, 9 H, 1.40 ppm) and ^{13}C NMR (-NH-$\underline{C}O_2$-R, 156.2 ppm) and main IR absorption bands for the t-BOC moiety (-C=O str, 1700 cm^{-1}) were observed commensurate with literature values. [61] and [63] The mechanism of *t*-BOC protection is shown in Figure 3.4.

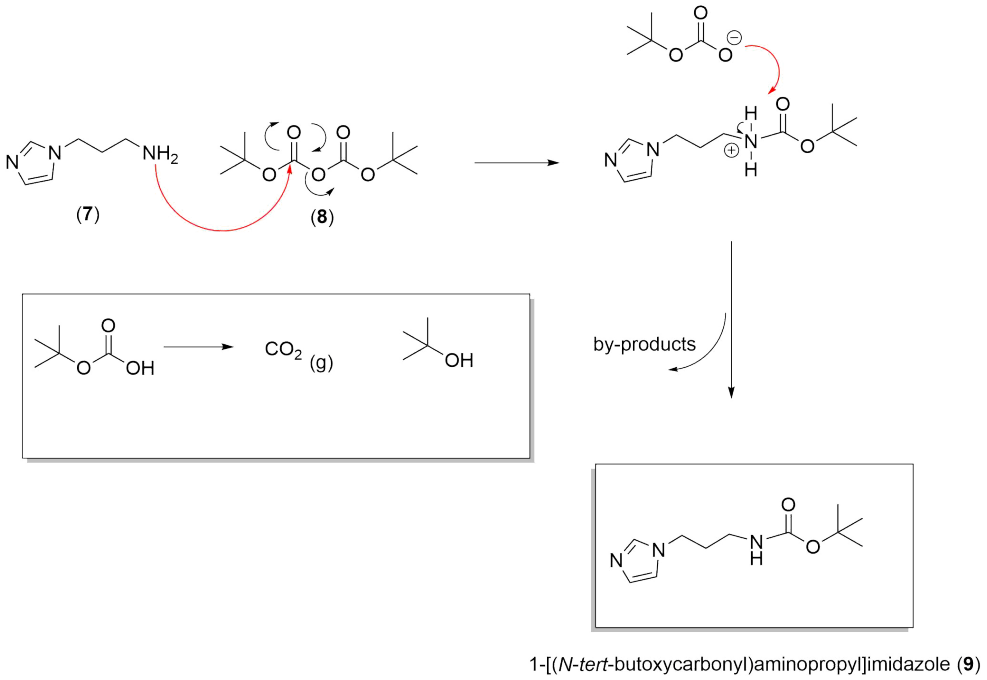

FIGURE 3.4: Mechanism of *t*-BOC protection (conversion of (**7**) to (**9**)).

3.1.2.2 Conversion of (9) to 1-[*N*-*tert*-butoxycarbonyl)-3-aminopropyl]-3-(2,4,6-trimethylbenzyl)imidazolium chloride (11)

Compound (**9**) was successfully reacted with 2,4,6-trimethylbenzyl chloride (**10**) in CPME instead of CH_2Cl_2 as solvent to furnish the desired

1-[*N*-*tert*-butoxycarbonyl)-3-aminopropyl]-3-(2,4,6-trimethylbenzyl)imidazolium chloride (**11**) in high yield (72%). 1-[*N*-Substituted]-3-azoles (e.g (**9**)) are quaternised easily with alkyl halides (e.g (**10**)) at the imine nitrogen (3-position) as the latter possesses a lone pair of electrons not involved in the aromatic sextet of the heterocycle and is thus amenable to nucleophilic substitution. As shown in Figure 3.5, the mechanism may be either S_N1 or S_N2 as resonance stabilization of the benzyl cation and steric considerations (favours S_N1) but the solvent, CPME, a dipolar aprotic solvent, favours S_N2 as it does not solvate the nucleophile but importantly will solvate the transition state as charge builds up.

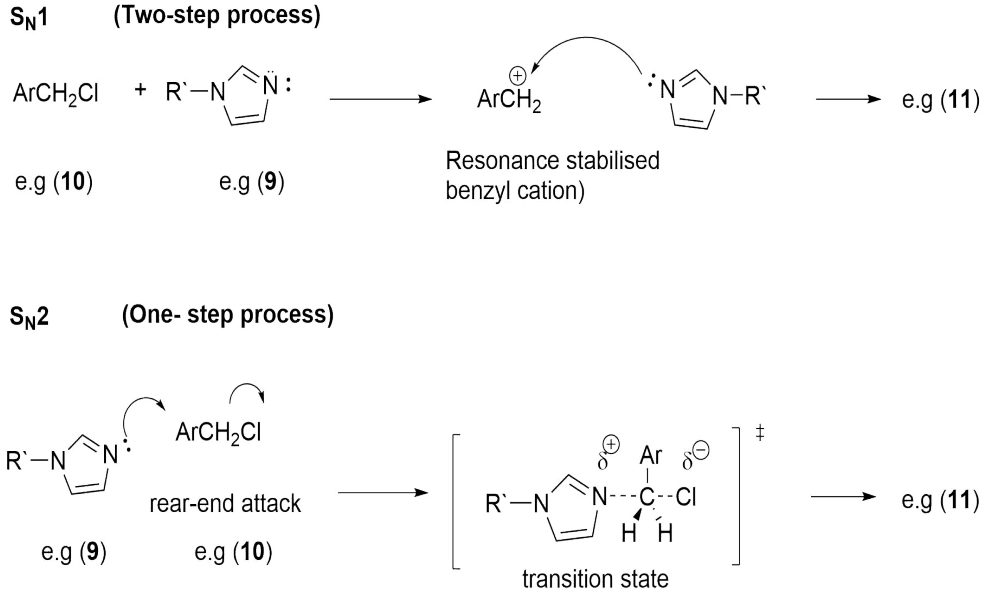

FIGURE 3.5: S_N1 and S_N2 mechanism for conversion of **(9)** to **(11)** .

The ATR-IR of (**11**) in comparison with its precursor (**9**) is shown in Figure 3.6. The intensity of absorption bands akin to the C-H stretch centred at approx. 3000 cm^{-1} increase in the spectrum of (**11**) coupled with perturbation of absorption bands between 1600 - 1000 cm^{-1} associated with the inclusion of the 2,4,6-trimethyl benzyl moiety.

The alkylation of the ligand is further proved by the presence of the ^1H NMR peak at 2.2 ppm (s, 9H) as well as the peak at 6.7 (s, 2H) that are related to 2,4,6-trimethylbenzyl chloride (**10**) (CH_3 groups and CH_2, respectively). ^{13}C NMR signals for these peaks were assigned at 19.8 and 21.1 ppm whereas the peaks at 129.2, 138.1 and 139.9 are assigned to CH_3-C=**C**-, CH_3-**C**=C-C-N- and CH_3-**C**-C-, respectively.

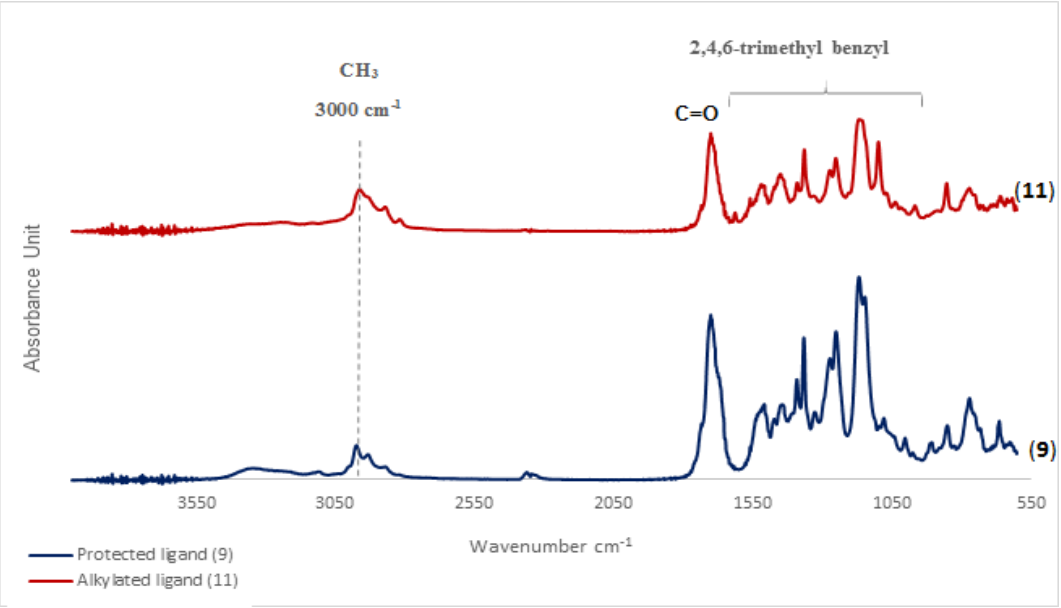

FIGURE 3.6: ATR-IR spectra of protected ligand (**9**) and alkylated ligand (**11**).

3.1.2.3 Conversion of 1-[*N*-*tert*-butoxycarbonyl)-3-aminopropyl]-3-(2,4,6-trimethylbenzyl)imidazolium chloride (11) to 1-[aminopropyl]-3-(2,4,6-trimethylbenzyl) imidazolium chloride (12)

Compound (**11**) was successfully deprotected in the presence of trifluoroacetic (TFA) in methanol to yield the desired 1-[aminopropyl]-3-(2,4,6-trimethylbenzyl) imidazolium chloride (**12**) in high yield (95%). The mechanism of *t*-BOC deprotection via TFA is shown in Figure 3.7.

Deprotection of (**11**) was evidenced by ATR-IR by the disappearance of the carbonyl absorption (1700 cm^{-1}) of the *t*-BOC moiety. Similarly, the corresponding carbon signal (156 ppm) in the ^{13}C NMR also disappeared on conversion of (**11**) to (**12**).

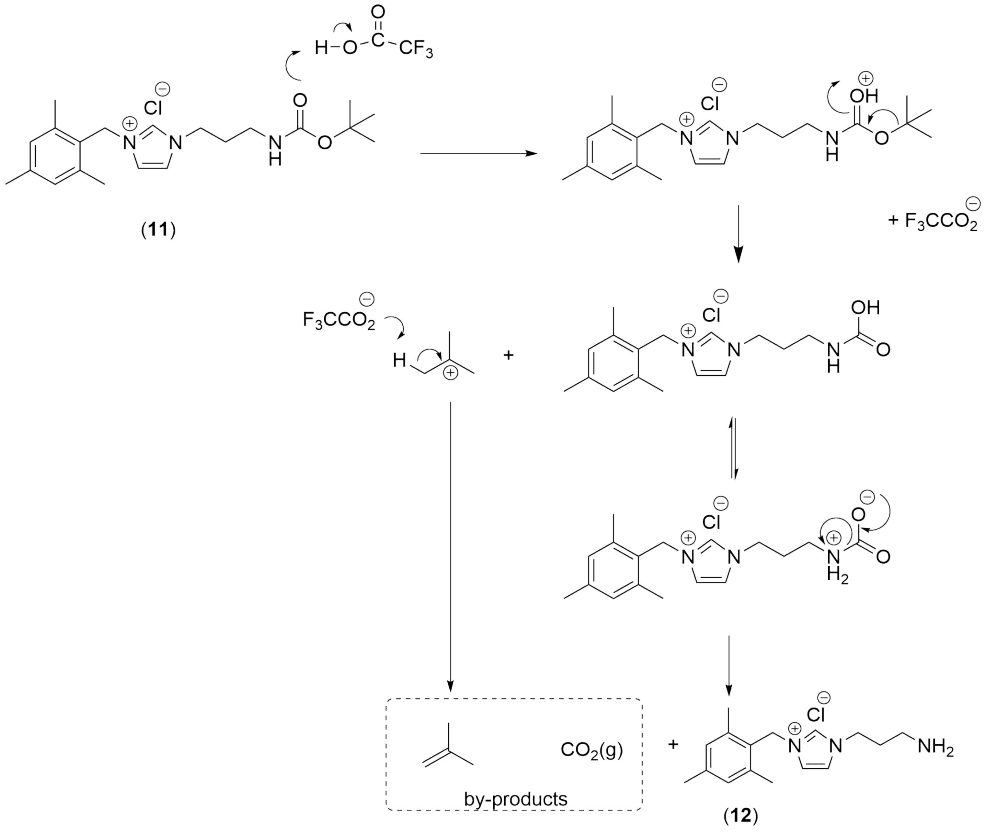

FIGURE 3.7: Mechanism of TFA deprotection (conversion of (**11**) to (**12**)).

3.1.3 Ligand immobilization on to succinimidyl carbonate expanded starch (6), i.e., preparation of (13)

Using our convergent strategy as outlined in Scheme 1.1, deprotected NHC ligand (**12**), in the presence of triethyl amine as base and propylene carbonate as solvent, was immobilized successfully on to succinimidyl carbonate activated expanded HACS (**6**) in moderate yield (41.8%). The mechanism for this conversion is shown in Figure 3.8 and for clarity substitution (attachment) is shown at the C6 hydroxyl moiety only.

A comparison of the stacked ATR-IR spectrum of (**6**) and the newly formed immobilized ligand (**13**) (Figure 3.9) shows the latter contains characteristic absorption band of its precursor, i.e., (**6**). Greatest perturbation is seen in the carbonyl region (1630-1740 cm^{-1}) where the absorbance band of carbonyl stretch associated with the imidyl (-CO-NR-CO-) moiety within (**6**) decreases in intensity on the formation of (**13**) coupled with an increase in intensity of a

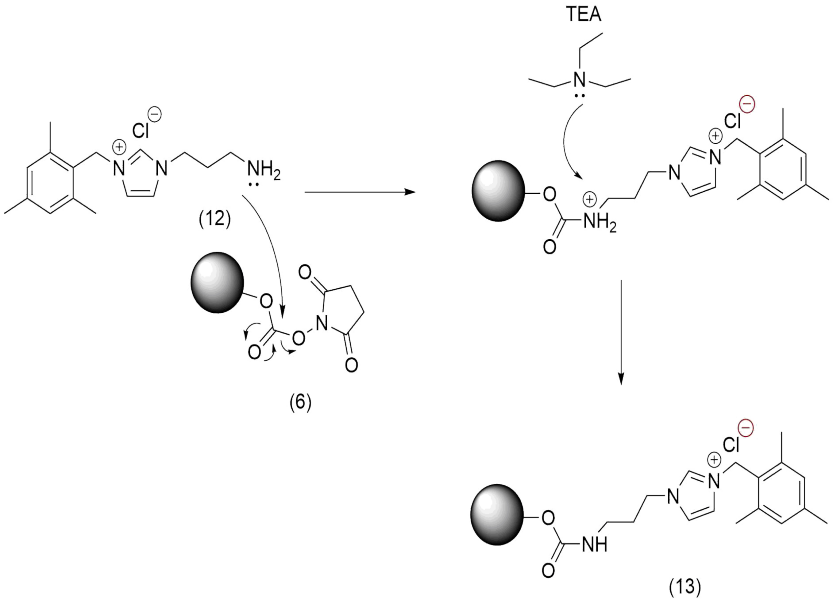

FIGURE 3.8: Mechanism of ligand immobilization on to succinimidyl carbonate expanded starch (**6**) (preparation of (**13**)).

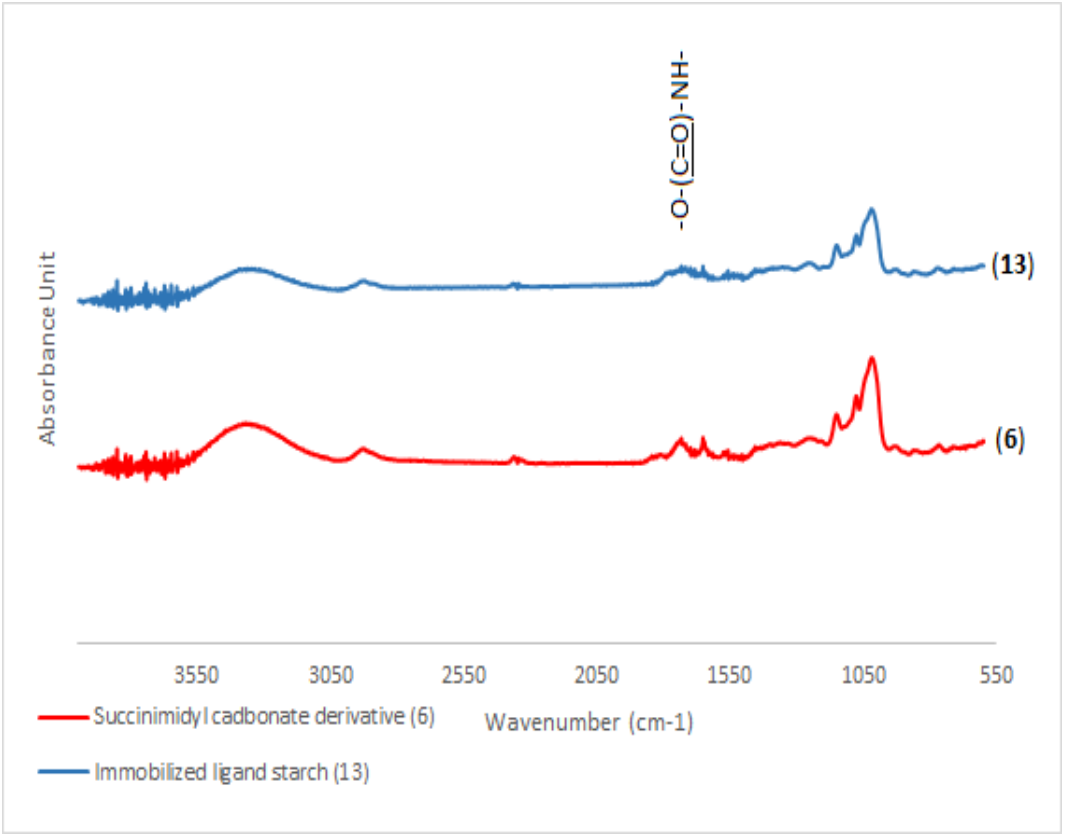

FIGURE 3.9: ATR-IR spectrum of succinimedyl carbonate derivative (**6**) and ligand immobilized starch (**13**).

broad carbonyl stretch centred at 1700 cm^{-1} most likely due to the new -O-(C=O)-NH- moiety.

Furthermore, the CPMAS ^{13}C spectrum of (**13**) in comparison with (**6**) as shown in Figure 3.10 reveals the appearance signals in the aliphatic region (10 - 60 ppm) corresponding to carbons associated with methyl groups (-CH_3) of the mesityl moiety and the methylene carbons (-CH_2-) of the aminopropyl group. The mesityl moiety is further evidenced with weak signals in the aromatic region (110 - 140 ppm) which also contains signals for the imidazoyl ring. A tentative assignment of the signals with respect to the carbons within (**13**) is shown in Figure 3.10 where we also assume that the signal at 47.3 ppm corresponds to N-C-mesityl. [60] The characteristic signals of expanded starch remain and interestingly the signal associated with succinimidyl carbon (approx. 173 ppm) in (**6**) disappears on conversion to (**13**). The remaining carbonyl signal (approx 165 ppm) is assumed to correspond to the newly formed O-(C=O)-NH- moiety which appears to have the same chemical shift as for O-(C=O)-O-.

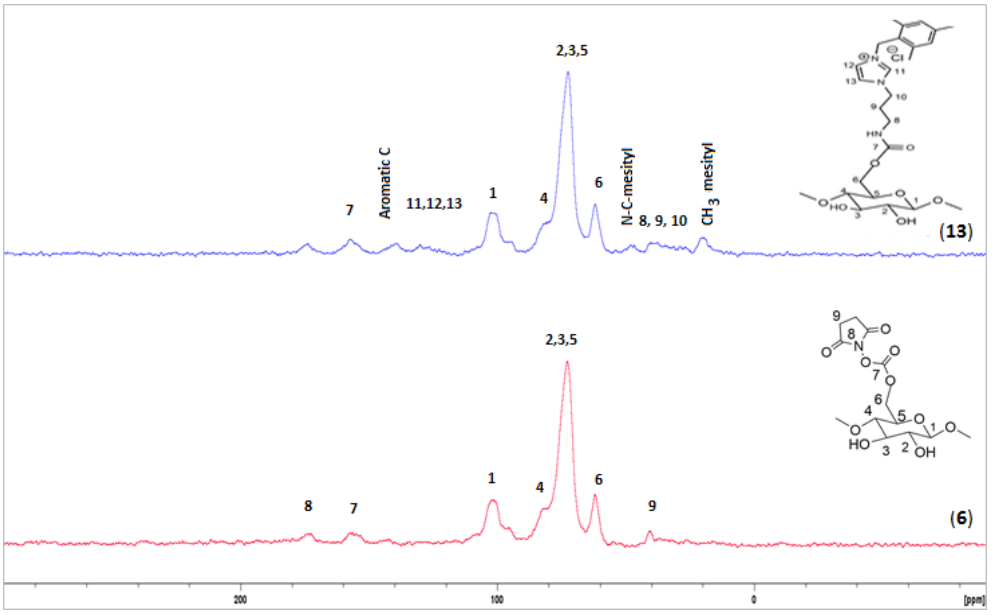

FIGURE 3.10: CPMAS ^{13}C NMR spectra of succinimidyl carbonate derivative **(6)** and ligand immobilized starch (**13**).

3.2 Characterization of Fe-NHC bio-based catalyst (1)

The desired Fe-NHC catalyst (**1**) was successfully acquired from the reaction between (**13**), in the presence of potassium *tert*-butoxide as base and propylene carbonate as solvent, and iron(III) chloride in good yield (61.5%). At a simplistic

level, iron was assumed to have been incorporated based on visual inspection of compound (**1**); a light brown appearance compared with respect to its precursor (**13**) as shown in Figure 3.11.

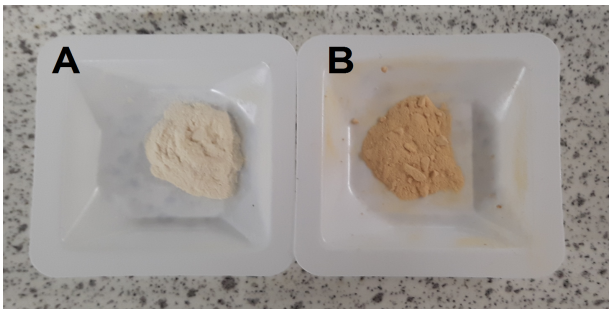

FIGURE 3.11: Photographic images of (A) immobilized ligand starch (**13**) (B) Fe-NHC catalyst (**1**).

Far Infrared (FIR) spectroscopy was undertaken to evidence Fe-Cl bond as its absorption band usually appears in the region 330 - 384 cm^{-1}. [64] However, as shown by Figure 3.12, a comparison of the FIR spectrum for expanded HACS (**4**), succinimidyl carbonate activated HACS (**6**), ligand grafted DSC activated HACS (**13**) and the desired Fe-NHC catalyst (**1**) provided inconclusive evidence. Minor perturbations are observed and it may be that the Fe-Cl absorption band is present but masked by the very percentage of carbon-hydrogen-nitrogen-oxygen skeletal vibrations.

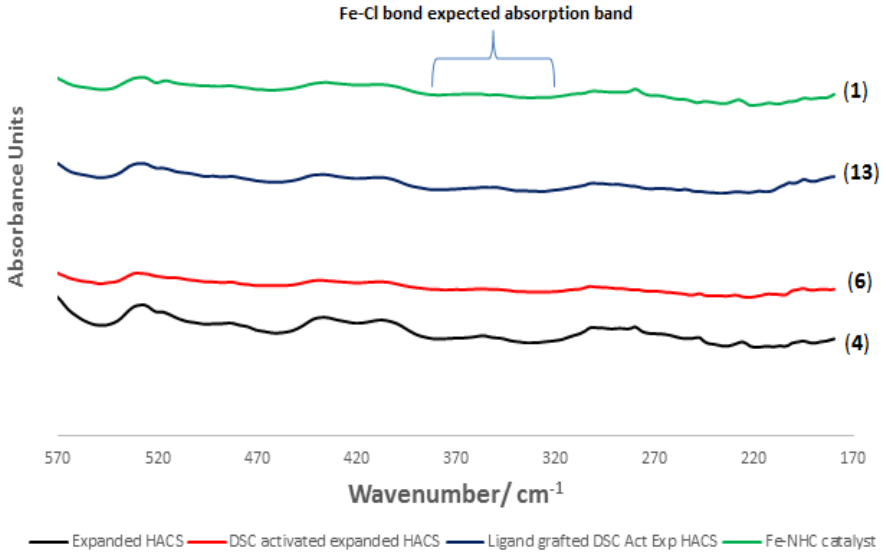

FIGURE 3.12: FIR spectrum for expanded HACS (**4**), succinimidyl carbonate activated HACS (**6**), ligand immobilized starch (**13**) and Fe-NHC catalyst (**1**).

Similarly, comparison of the CPMAS ^{13}C spectrum of (**13**) with respect to (**1**) showed no significant change in chemical shift value. Stronger perturbation was expected at the carbene centre (see Figure 3.13) but was not evident due to poor signal to noise ratio. The latter is common with iron containing sample as it may be that some (or all) of the iron atoms possess a *d*-configuration with a net non-zero spin. If so, then this will impede the ability to acquire good quality spectra. In particular, those signals arising from sites near the iron (within ca. 2-10 Angstroms) may not be observed at all, thus reducing signal intensity.

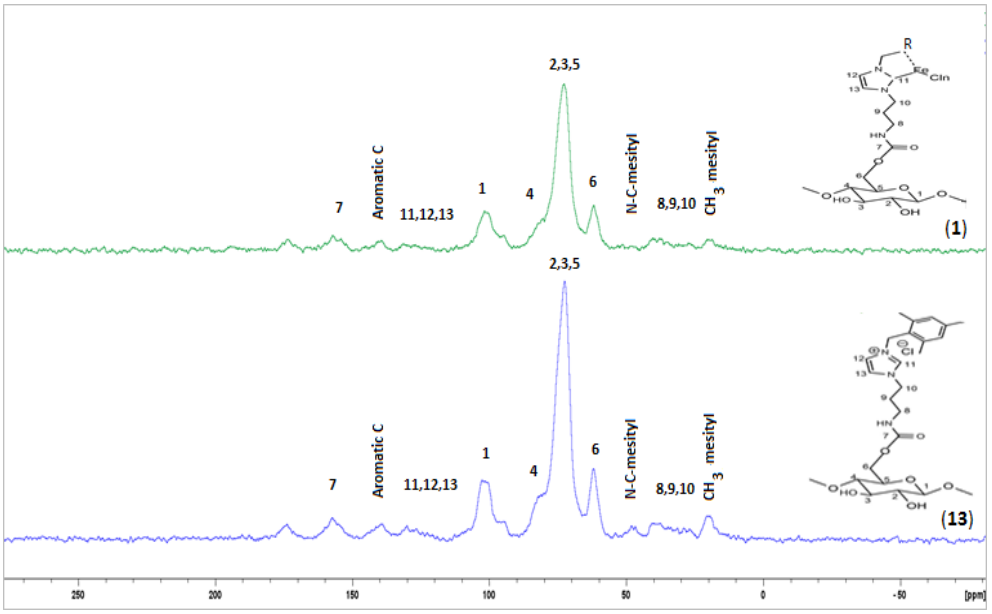

FIGURE 3.13: CPMAS ^{13}C NMR spectra of immobilized ligand (**13**) and Fe-NHC catalyst (**1**).

Thus, other analytical methods, direct and indirect, were used to evidence presence and concentration of iron, for example, ICP, TEM, TGA, XPS, and porosimetry. Direct iron loading was determined by ICP-MS which revealed 0.26 mmol/g Fe. The raw data and the corresponding conversion calculation are given in AppendixA. However, the iron loading is not strictly speaking all iron(III) chloride as it accounts for any species detected, for example, the sample may be contaminated with iron oxide or may still have an excess of (non-complexed) iron(III) chloride species. Transmission electron microscopy was used to image the sample to see the distribution of iron species.

3.2.1 Transmission Electron Microscopy (TEM)

TEM images are recorded as a result of strong elastic and inelastic scattering interaction between atoms (thin specimen) and a beam of transmitted electrons producing high resolution images. [65] TEM is perhaps the most significant method for the description of small supported particles morphology. [66] TEM supplies information about particle size, shape and web construction in addition to the chemical composition of discrete particles. [67] The TEM image of Fe-NHC catalyst (**1**) is shown in Figure 3.14, which reveals both *discrete* particles and large clusters or aggregates (50 nm diameter).

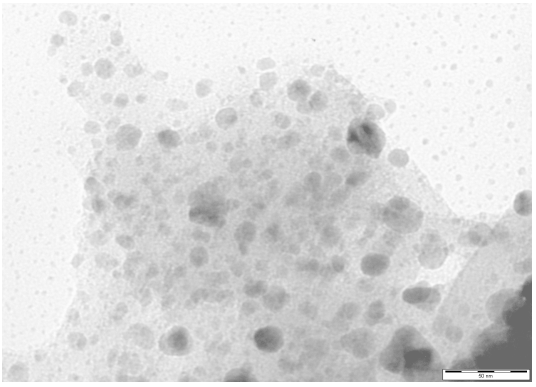

FIGURE 3.14: TEM micrograph of Fe-NHC catalyst (**1**).

3.2.2 Simultaneous Thermal Analysis (STA)

Simultaneous thermal analysis (STA) is a dual technique that monitors mass loss and the energy associated with a phase change with respect to temperature. [68] STA was used to examine the thermal decomposition of expanded HACS (**4**) and its modified compounds (**6**), (**13**) and (**1**) as shown in figure 3.15. The thermal decomposition of expanded starch (**4**) (corn starch) was as per literature [245-333 °C] [69]; Initial loss of moisture (approx. 9% water) both physi- and chemi-sorbed from 25 °C to 135°C is observed followed by main degradation and decomposition (T_d, 326 °C) of glycosidic bonds and the carbohydrate skeleton from 300-350 °C corresponding to approximately 70% mass loss. Further heating from 400-600 °C afforded a further much smaller mass loss of approximately 5%. Approximately, 18% of residue remained at the end of the analysis. The thermal decomposition of the subsequent compounds, i.e., succinimidyl carbonate starch (**6**) and ligand grafted starch (**13**) showed a similar decomposition profile to expanded starch

(**4**). Both show an initial mass (approx. 5%) from 25-135 °C again due to bound water within starch but a small and gradual mass loss is observed from 135-200 °C, which may be due to residual propylene carbonate solvent. Interestingly, conversion of (**4**) to (**6**), lowers the decomposition temperature from 326 °C (**4**) to 313 °C (**6**) indicating that the structure and packing within starch has been disrupted. In particular, the extensive inter- and intra-hydrogen bonding network associated with the hydroxyl groups of starch is disrupted as modification (DS, 0.33±0.11%) reduces the number of hydroxyl groups. Evidence for substitution may also be considered by the fact that approx. 24% of residue is left at the end of decomposition (600 °C) of (**6**) compared with approx. 18% residual mass for (**4**). The extra mass is from the additional elemental contribution (mainly carbon) from succinimidyl carbonate moiety.

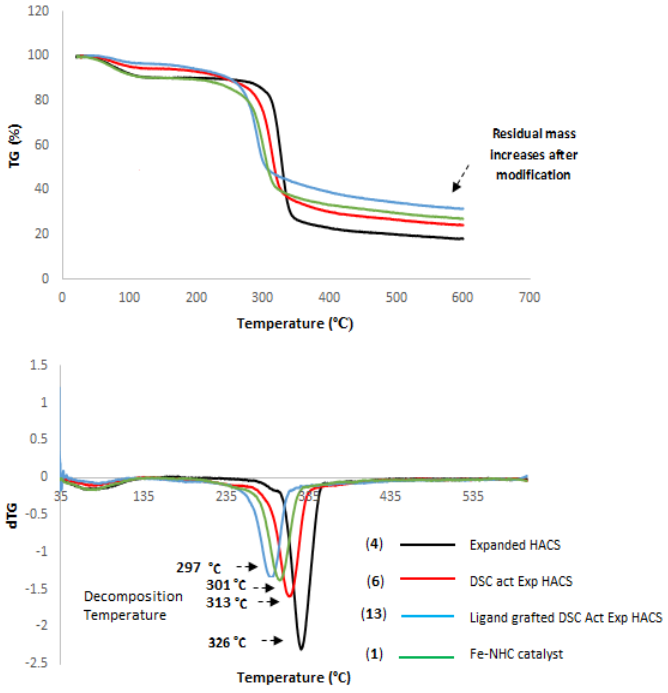

FIGURE 3.15: STA for expanded HACS (**4**), succinimidyl carbonate activated HACS (**6**), ligand grafted DSC activated HACS (**13**) and Fe-NHC catalyst (**1**).

Similarly, the greatest residual mass is observed for decomposition of (**13**) which has the greatest proportion of carbon with respect compounds (**4**) and (**6**), which also has the lowest decomposition temperature (T_d, 297 °C) due to greatest structural and chemical modification. The thermogram for the Fe-NHC catalyst (**1**) shows slight enhancement in thermal stability (T_d, 301 °C) with respect to its precursor ((**13**), T_d 297 °C) which may be related to additional

energy associate with iron-carbene complexation, i.e., Fe-NHC. Interestingly, slightly less residual mass was observed at 600 °C for (**1**) than for ((**13**) probably due to iron itself triggering or catalyzing decomposition of starch. However, this is to be further investigated. Elemental analysis of the residue showed 27% of iron.

3.2.3 Porosimetry and Scanning Electron Microscopy

The BET surface area, pore width and pore volume of expanded HACS (**4**) and its subsequent compounds (**6**), (**13**) and, (**1**) were determined using nitrogen adsorption porosimetry (see Table 3.1 and Figure 3.16). As shown in Figure 3.16, all isotherms exhibit classical hysteresis loops indicative of mesoporosity. On modification of expanded HACS (**4**) through to the desired Fe-NHC (**1**) the BET surface area decreased: 186.7 m^2/g (**4**); 189.5 m^2/g (**6**); 186.0 m^2/g (**13**), and; 135.5 m^2/g (**1**). The subsequent decrease in surface area and pore volume may be explained by possible blocking and filling of the porous structure both by the ligand and importantly iron.

Table 3.1: Porosimitry data for expanded HACS (**4**) and its subsequent compounds (**6**), (**13**) and, (**1**).

	BET surface area (m^2/g)	Desorption pore volume (cm^3/g)	Desorption average pore width (nm)
Expanded HACS (**4**)	186.7	0.91	18.4
DSC activated HACS (**6**)	189.5	0.83	16.9
Ligand grafted starch (**13**)	186.0	0.81	16.1
Fe-NHC catalyst (**1**)	135.5	0.60	16.3

The pore size distribution shows a broad peak within the mesoporous region (2-50 nm). [70] These data prove that activation of the expanded HACS, grafting of the ligand and coordination of iron maintains porosity with significant retention of mesopores.

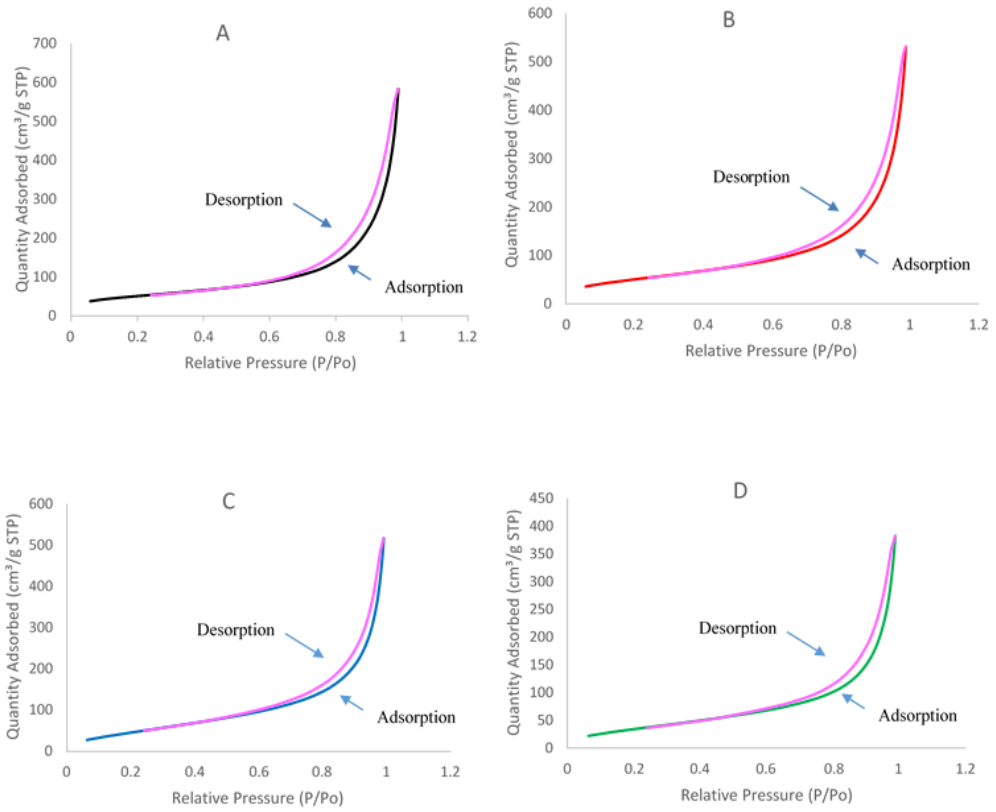

FIGURE 3.16: Adsorption-desorption isotherms plot for (A) expanded HACS (**4**) (B) succinimidyl carbonate activated HACS (**6**) (C) ligand immobilized starch (**13**) and (D) Fe-NHC catalyst (**1**).

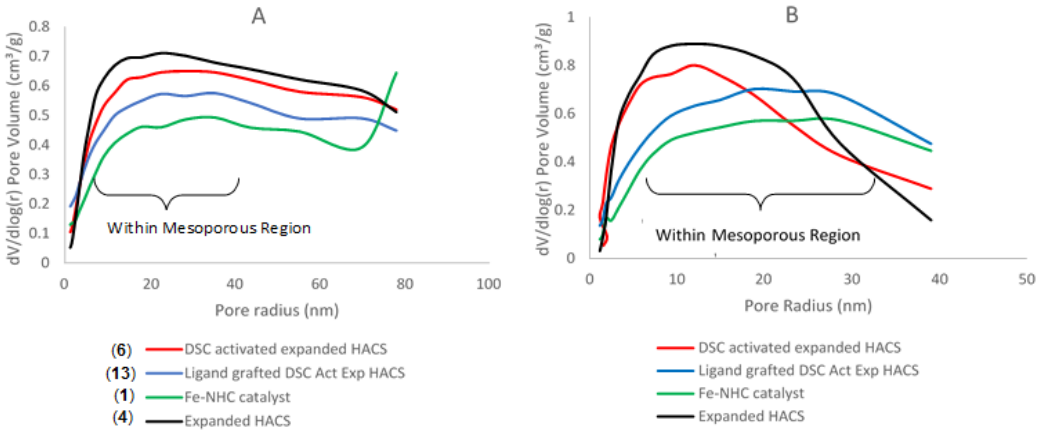

FIGURE 3.17: BJH of expanded HACS (**4**), (**6**), (**13**) and, (**1**).

Scanning Electron Microscopy (SEM)

To further investigate changes in surface structure (topography) and porosity, SEM (see Figure 3.18) was performed on expanded HACS (**4**), succinimidyl carbonate activated HACS (**6**), ligand immobilized starch (**13**) and Fe-NHC catalyst (**1**). Although, the images reveal limited information it can be seen that the extent of pitting and mesh-like network (surrogate for porosity) decreases on the surface from (**4**) to (**6**) to (**13**) to (**1**) which may also be related to the corresponding decrease in BET surface area discussed earlier.

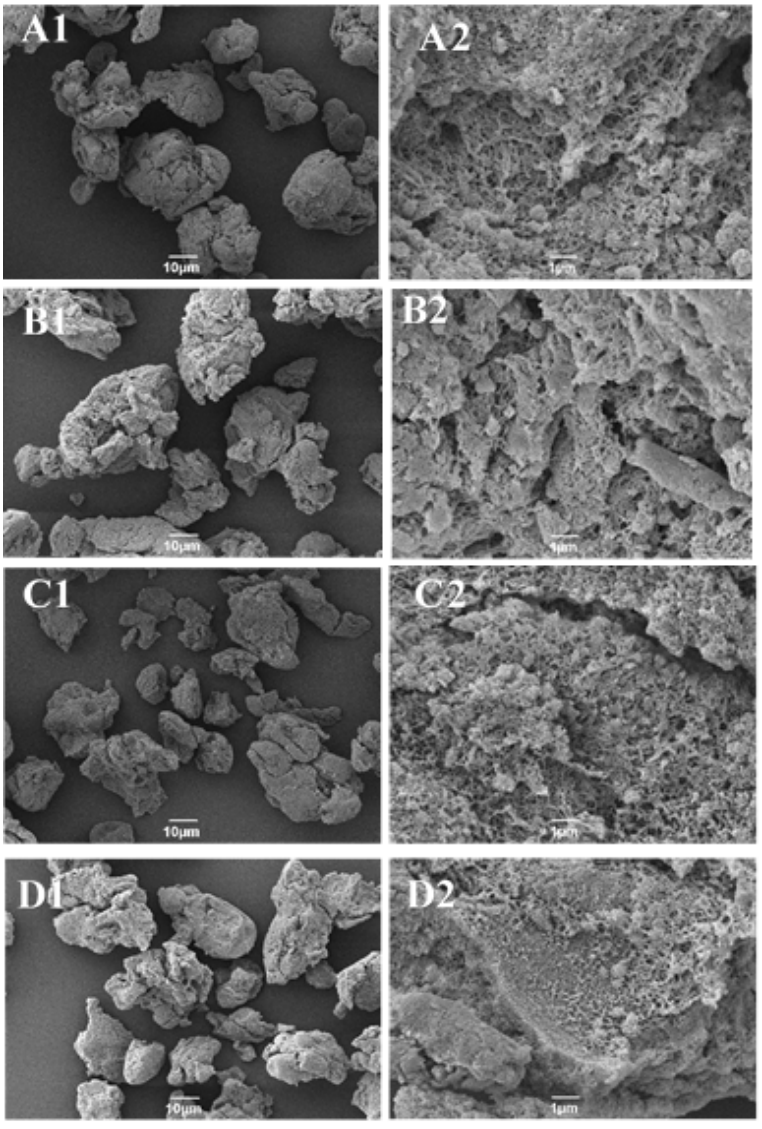

FIGURE 3.18: SEM micrographs of (A) expanded HACS (**4**) (B) succinimidyl carbonate activated HACS (**6**) (C) ligand immobilized starch (**13**) and (D) Fe-NHC catalyst (**1**) (1 (x1000) and 2 (x10000) resolution).

3.2.4 X-ray Photoelectron Spectroscopy (XPS)

Photoelectron spectroscopy is a technique that studies the electronic state and composition of the sample's surface region. It uses photo-ionization and the emitted photoelectron's kinetic energy distribution analysis. In X-Ray Photoelectron Spectroscopy (XPS), X-rays (photon energy = 200-2000 eV) are used to observe core-levels. [71] and [72]

XPS was used to characterize expanded HACS (**4**) and Fe-NHC (**1**) catalyst as shown in Figure 3.19 . The spectrum of expanded HACS (**4**) has two main absorption bands typically at 283.45 and 530.87 eV corresponding to C1s and O1s energy levels, respectively. However, the Fe-NHC catalyst (**1**) has four absorption peaks at about 283.45, 399.88, 533.78 and 711.34 eV corresponding to C1s, N1s, O1s and Fe2p, respectively, providing clear evidence for the presence of iron and nitrogen in addition to the expected carbon and oxygen.

The binding energy and detailed chemical states of C, O, N and Fe are listed in Table 3.2 and the correlated spectra are shown in Figures 3.20 and 3.21. As can be seen, the binding energy at 283.29, 284.81, 286.22 and 288.49 eV are assigned to corresponding chemical states C-C, C-O-H and C-O-C respectively. Analyzing the states of oxygen showed that the binding energy at around 531.26, 534.58 eV corresponding chemical state were C-O and O-H, respectively.

For Fe-NHC catalyst (**1**), the binding energy at 283.41, 284.90, 286.19 and 287.70 eV are related to chemical states C-C, C-O-H C-O-C and C-N respectively. Studying the states of oxygen revealed that the binding energy at around 531.35 and 533.39 eV corresponding chemical state were C=O and O-H respectively. For nitrogen , binding energy at 388.55 and 400.34 eV were assigned to C=N and C-N chemical states, respectively, whereas for Fe, binding energy at 710.59 and 723 eV were related to Fe(III)$2p_{3/2}$ and Fe(III)$2p_{1/2}$ chemical states, respectively.

TABLE 3.2: XPS data analysis for expanded starch **(4)** and Fe-NHC catalyst **(1)**

Sample	Element	Binding Energy / eV	Chemical state
Expanded starch (**4**)	C 1s	283.29	C-C
		284.81	C-O-H
		286.22	C-O-C
	O 1s	531.26	C-O
		534.58	O-H
Fe-NHC catalyst (**1**)	C 1s	283.41	C-C
		284.90	C-O-H
		286.19	C-O-C
		287.70	C-N
	O 1s	531.35	C=O
		533.39	O-H
	N 1s	388.55	C=N
		400.34	C-N
	Fe 2p	710.59	Fe(III)$2p_{3/2}$
		723.00	Fe(III)$2p_{1/2}$

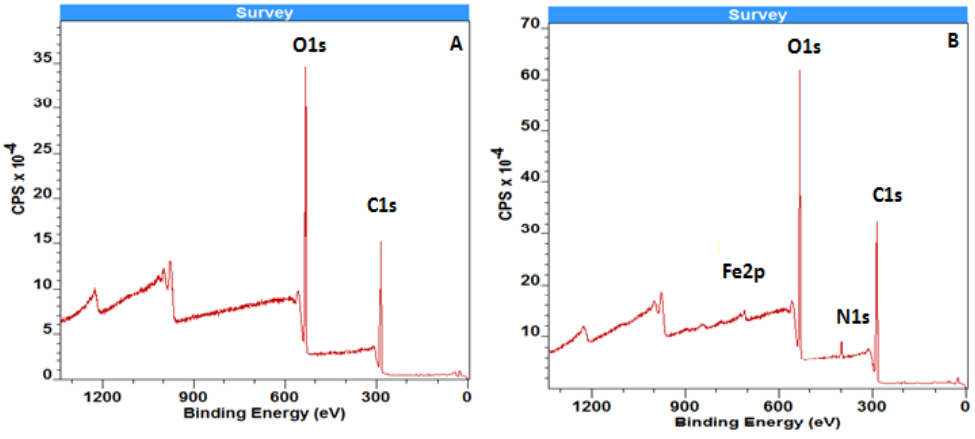

FIGURE 3.19: XPS survey data of (A) expanded HACS (**4**) (B) Fe-NHC catalyst (**1**)).

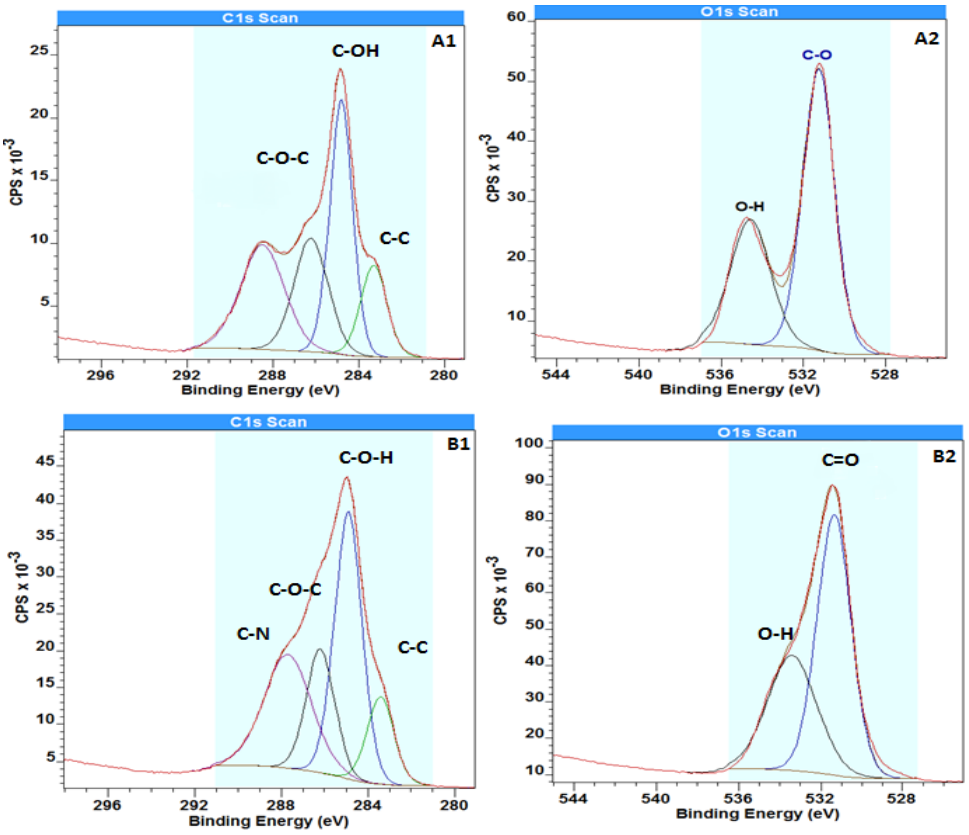

FIGURE 3.20: XPS data of (A1) C1s expanded HACS (**4**) (A2) O1s expanded HACS (**4**) (B1) C1s Fe-NHC catalyst (**1**) (B2) O1s Fe-NHC catalyst (**1**).

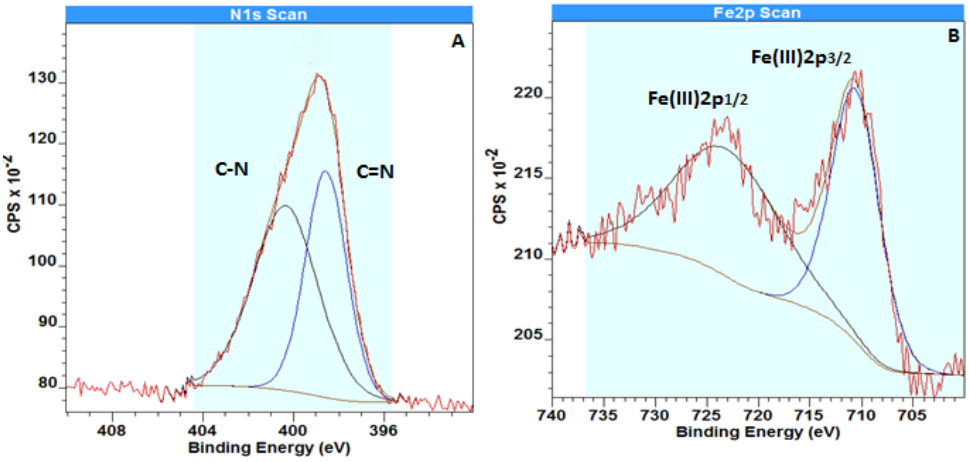

FIGURE 3.21: XPS survey data of (A) N1s Fe-NHC catalyst (**1**) (B) Fe2p Fe-NHC catalyst (**1**)).

3.3 Fructose (2) conversion to HMF (3) conversion

Initially, a series of control experiments were undertaken in the absence of fructose (**2**), i.e., DMSO-d_6 and Fe-NHC catalyst (**1**), in order to confirm the carbohydrate (starch) support was itself not acting as a sacrificial or competing substrate with respect to fructose and to investigate iron leaching. At a simplistic level, DMSO-d_6 (2 ml) was added to Fe-NHC catalyst (**1**) (10 mg) and heated to 100 °C for 0.5 h, 1 h, 3 h and 6 h. The mixture was filtered and analysed by NMR spectroscopy (Figures 3.22 and 3.23). Both ^{1}H and ^{13}C NMR spectroscopy showed no significant spectral change. The standard ^{1}H NMR signal for the non-deuterated CH_3-group in DMSO-d_6 was observed at 2.4 ppm with no other clearly discernible signals even after 6 h at 100 °C. Similarly, the ^{13}C NMR spectrum (Figure 3.23) showed a characteristic signal for the CH_3 carbon in DMSO-d_6 at 39.55 ppm. Thus, with the proviso that a very low concentration of catalyst (**1**) (0.5 mg/ml DMSO) no breakdown of substrate (starch) observed. The starch support is tolerant to attack by the iron-NHC tether. However, it may be that the substrate is being attacked but the concentration of species formed is beyond the detection limits of the instrument. A higher concentration of catalyst to DMSO-d_6 should be explored.

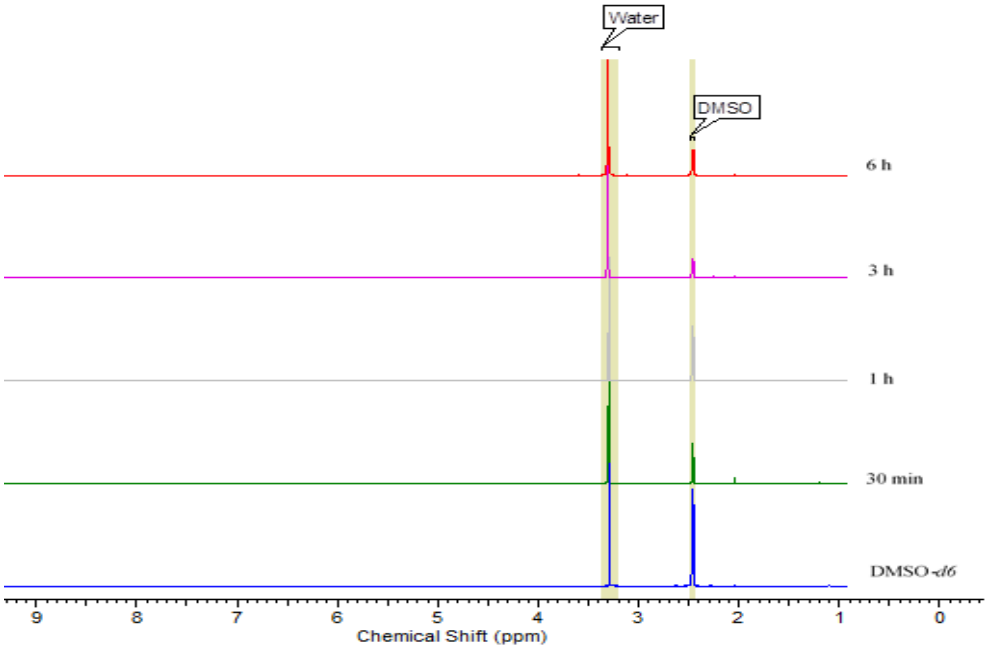

FIGURE 3.22: Stacked ^{1}H NMR spectra of Fe-NHC catalyst (**1**) + DMSO-d_6.

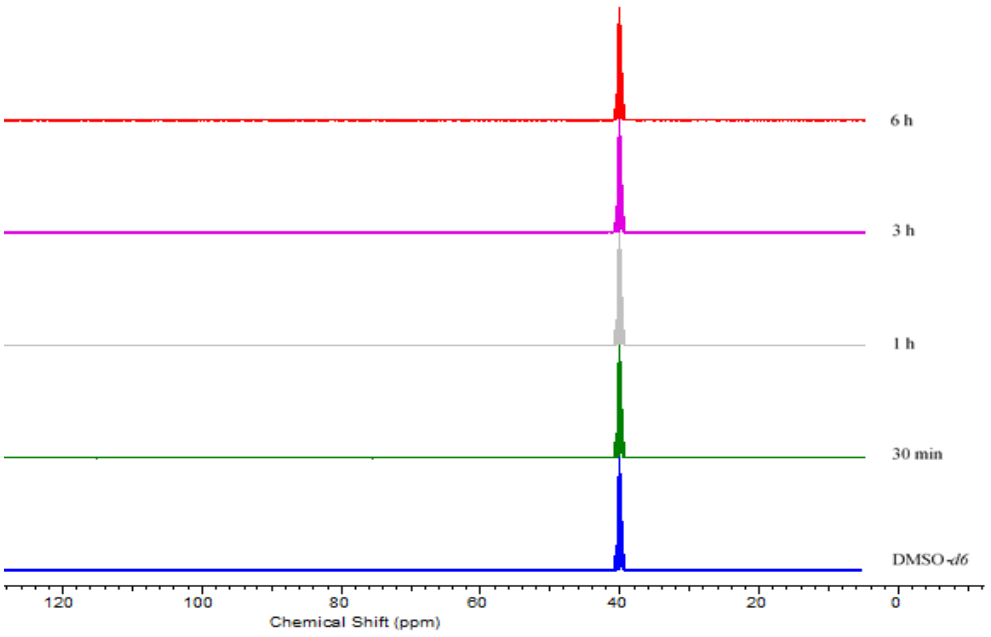

FIGURE 3.23: Stacked ^{13}C NMR spectra of Fe-NHC catalyst (**1**) + DMSO-d_6.

In addition, a control reaction between fructose and DMSO in the absence of catalyst has conducted. The HPLC results shown in Table 3.3 reveal very low conversion (14%) and yield (12%) even after 6 h at 100 °C.

TABLE 3.3: HPLC results for fructose and DMSO reaction in the absence of catalyst.

Time (h)	Conversion (%)	Yield (%)	Selectivity(%)
0.5	0	0	0
1	1	1	1
3	9	7	78
6	14	12	84

To investigate iron leaching from Fe-NHC catalyst (**1**), then Fe-NHC catalyst (20 mg) was added to DMSO-d_6 (4 ml). The mixture was heated for 6 h at 100 °C with constant stirring, cooled and filtered. The filtrate was analysed by ICP-MS to reveal negligible trace of iron in solution (3.5 x 10^{-7} mmol Fe) which may due to surface trapping of residual iron(III) chloride and/or iron oxide. Nevertheless, it can be assumed that the Fe-NHC catalyst (**1**) is neither being sacrificed nor does it leach any complexed iron. Thus, its application as a catalyst for fructose (**2**) to HMF (**3**) conversion is discussed in the following sections.

3.3.1 *Insitu* NMR study: Influence of temperature and time

In order to investigate the effect of temperature (and time) with respect to fructose dehydration, an *insitu* NMR experiment was undertaken. The desired catalyst (**1**), DMSO-d_6 with the appropriate amount of fructose (**2**) were placed inside a standard NMR tube and subjected to variable temperature NMR spectroscopy from 25 °C to 100 °C. ^{1}H and ^{13}C NMR spectra were recorded at regular intervals and are stacked in Figures 3.24 and 3.25.

At 25 °C the NMR shows signals corresponding to fructose and its tautomers (3.0 ppm - 4.5 ppm). It is not until about 70 °C that new signals begin to appear (8.13 ppm; may be due to formic acid [73] and at 9.65 ppm; possibly aldehydic group of furfural). At 80 °C and beyond the intensity of the signal at 3.1 ppm increases and is associated with water [74] and [75] but also, importantly, signals in the aromatic (furanic) region now are more prevalent. The signal at 6.17 ppm is tentatively attributed to C-3 alkene hydrogen in the intermediate
(4R,5R)-4-hydroxy-5-hydroxymethyl-4,5-dihydrofuran-2-carbaldehyde (**3b**) (see Figure 3.29) coupled with the signal at 9.50 ppm corresponding to the aldehydic group. [46] At 100 °C (0 t) the intensity of signals at 8.13 ppm and 9.65 ppm corresponding to formic acid and furfural, respectively and the formation of HMF (**3**) was detected by the presence of the signal at 5.61 ppm (CH_2OH).

At 100 °C with increasing time (3 h) characteristic signals for HMF were clearly evident. Similarly, the ^{13}C NMR spectra (Figure 3.25) clearly shows the tautomeric behaviour of fructose with a range of complex signals from 60 ppm to 104 ppm. The appearance of HMF and or furanic compounds was far less evident most likely due to very low concentrations, i.e., beyond scope of detection.

The *insitu* NMR study clearly revealed a temperature dependence for fructose to HMF conversion. No conversion was detected below 80 °C. The best temperature that gave clearly discernable ^{1}H NMR signals for HMF (**3**) was 100 °C. When held at this temperature then increasing time shows a corresponding increase in signals for HMF. Thus, armed with this knowledge the dehydration reaction was further investigated at 100 °C as discussed as follows.

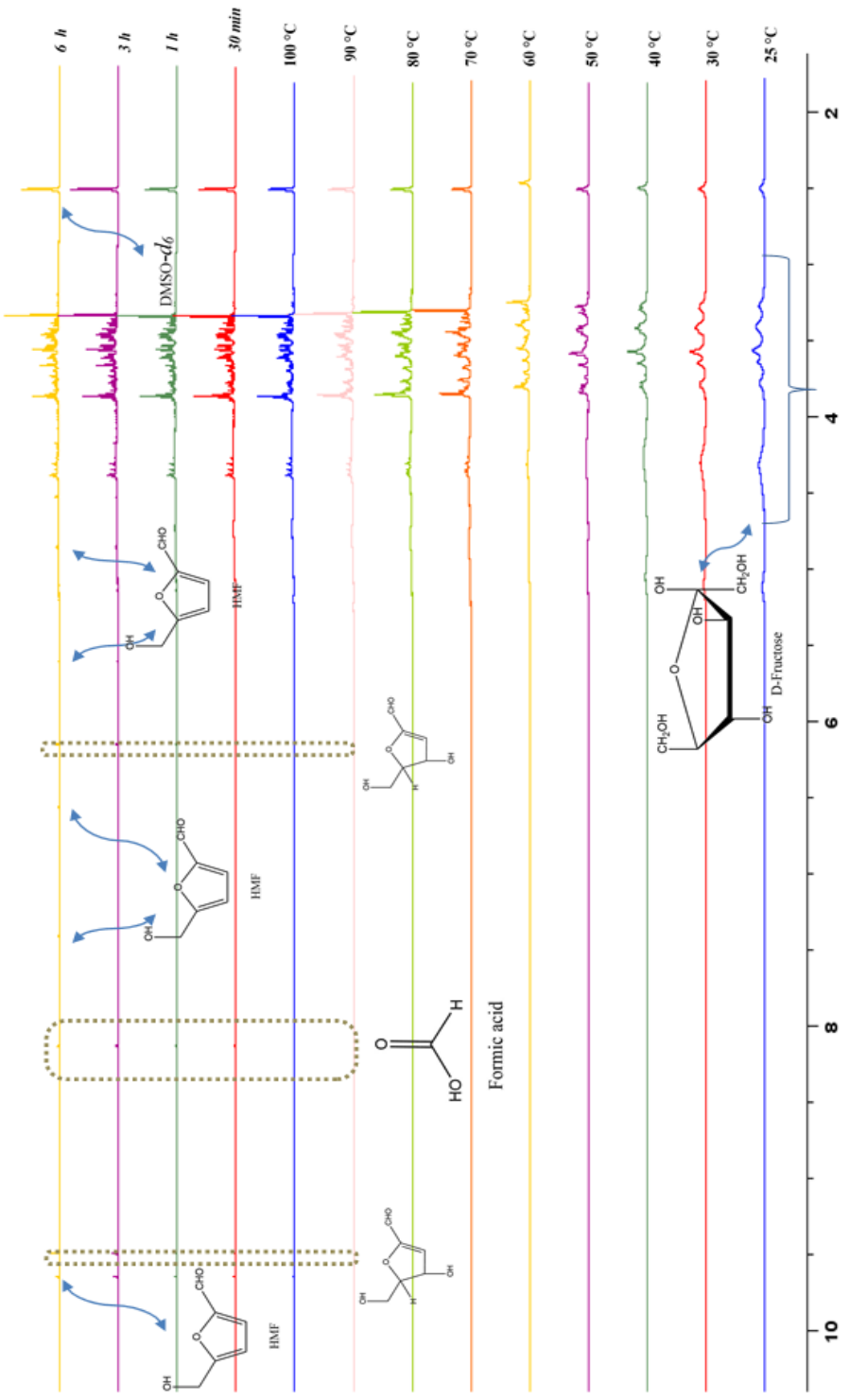

FIGURE 3.24: Stacked ^{1}H NMR spectra for the dehydration of fructose (**2**) to HMF (**3**) over Fe-NHC catalyst (**1**) with changed temperature and time.

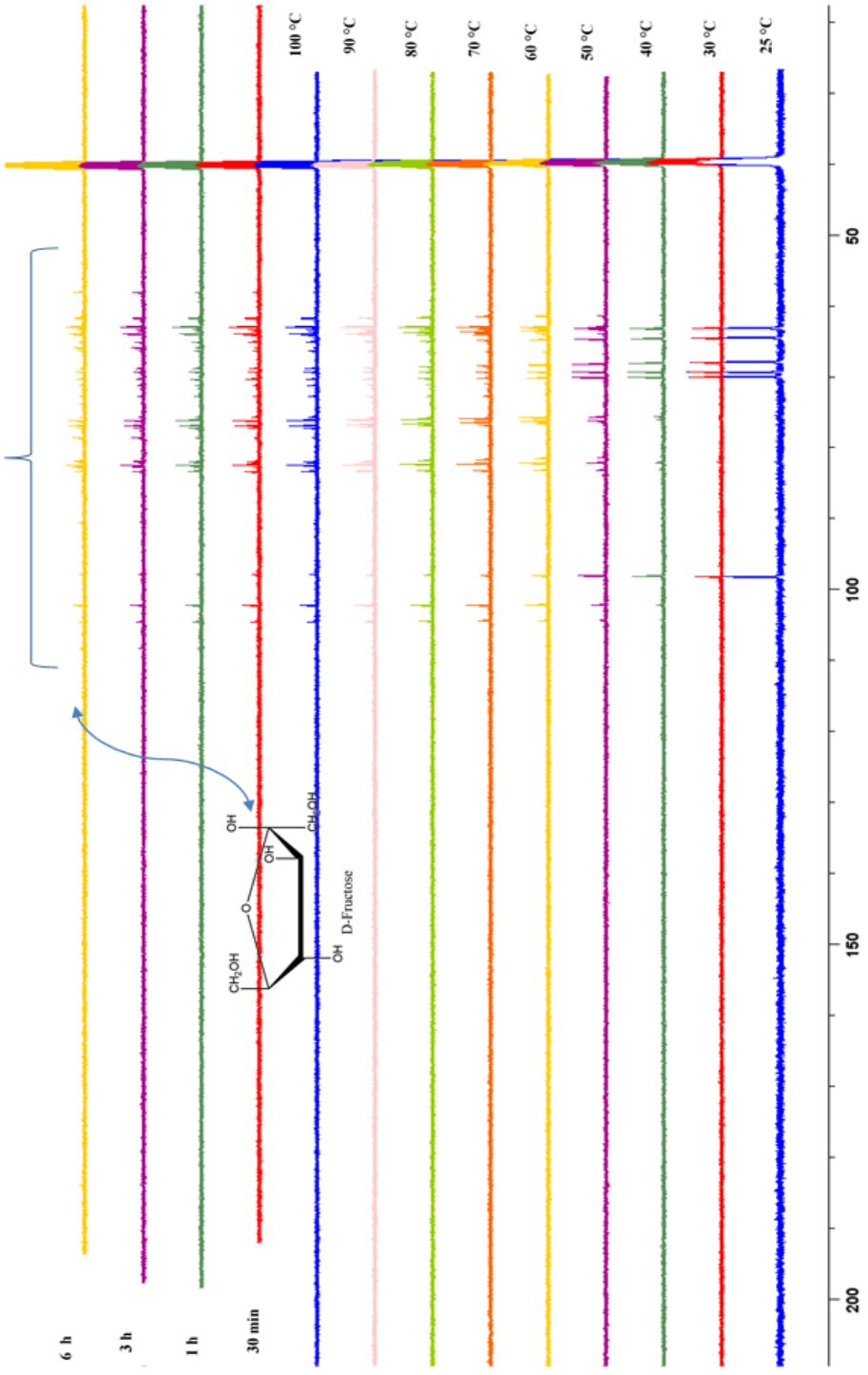

FIGURE 3.25: Stacked ^{13}C NMR spectra for the dehydration of fructose (**2**) to HMF (**3**) over Fe-NHC catalyst (**1**) with changed temperature and time.

3.3.2 In an atmosphere of air (^{1}H and ^{13}C NMR study)

The results and discussion introduced in this section represent the dehydration of D-fructose (**2**) catalyzed by Fe-NHC (**1**) at 100 °C in DMSO-d_6 for 0.5 h, 1 h, 3 h and 6 h in an air atmosphere. At a purely qualitative level the dehydration of fructose (**2**) is characterized by a darkening of the reaction color from clear pale yellow (0.5 h) to light brown (1 h to 3 h) to dark brown (6 h) over time as shown in Figure 3.26. The onset of the dark brown colour is characteristic of HMF decomposition to levulinic acid and humins (see later) as discussed earlier. [76]

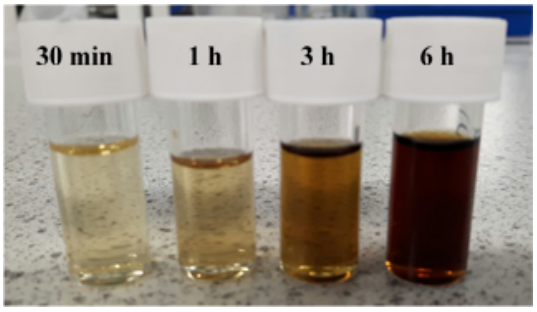

FIGURE 3.26: Color change as the reaction of fructose proceeds with time.

The progress of the dehydration reaction was monitored by nmr spectroscopy (^{1}H and ^{13}C) both *insitu* and batch. Figure 3.27 shows the stacked ^{1}H NMR spectra at 100 °C for the dehydration of fructose (**2**) in the presence of Fe-NHC catalyst (**1**) at t= 0.5 h, 1 h, 3 h and 6 h. The signal at 2.45 ppm is assigned to DMSO-d_6 [75] whilst complex multiplets for fructose are in the region 3-5 ppm. [77] As can be seen from figure 3.27, two, new, weak signals appear at 9.5 ppm and 8.1 ppm in the spectrum after 0.5 h. On closer inspection of the t= 0.5 h spectrum also shows very weak signals at 7.45 ppm, 6.55 ppm and 4.45 ppm which develop in intensity as the reaction proceeds over time. HMF (**3**) is clearly evident after 3 h ((1 H, **H**-C=O, 9.49 ppm), (1H, O=C-C=C**H**, 7.45 ppm), (1H, H_2C-C=C**H**-, 6.55 ppm) and (2H, HO-C$\mathbf{H}_2$ -C=CH, 4.45 ppm)) coupled with significant reduction in the signals for fructose. The signal at 8.08 ppm was assigned to formic acid which is formed due to the addition of two water molecules as a consequence of the reverse hydrolysis reaction that is considered as one of the side reactions of fructose conversion to HMF. [78], [79], [80] and [81] Interestingly, the intensity of HMF signals declined slightly after 6 h reaction time which may be due to the re-hydration side reaction to formic acid and levulinic acid. This observation is

confirmed by HPLC results given later in which the HMF yield calculated after 6 h reaction time is less than that at t = 3 h.

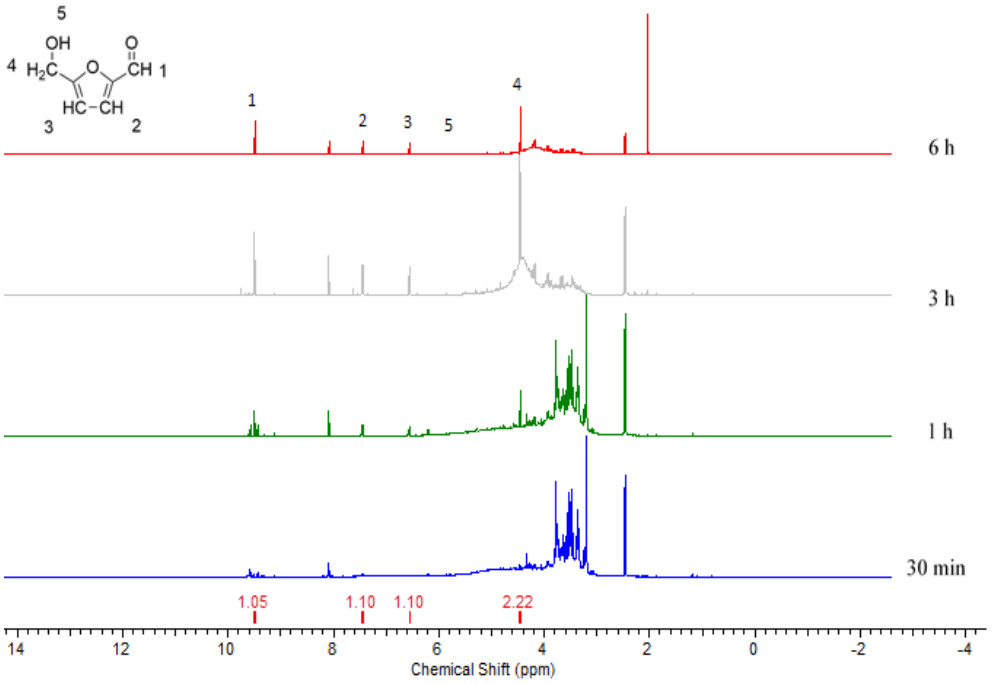

FIGURE 3.27: ^{1}H NMR spectra for the dehydration of fructose (**2**) to HMF (**3**) over Fe-NHC catalyst (**1**).

Although, our control experiment showed no detectable conversion of fructose (**2**) to HMF (**3**) at 100 °C in absence of any Fe-NHC catalyst (**1**) (see Table 3.3), A. Amarasekara *et al* [46] have investigated the mechanism of fructose dehydration in DMSO at 150 °C via NMR. As well as noting changes in the anomeric and tautomeric forms of fructose, e.g., -furanose, -pyranose, -pyranose, they proposed the following mechanism (Figure 3.28) based in the elimination of three water molecules from the two furanose forms as a dehydration reaction leading to HMF. [46]

In our situation conversion occurs at 100 °C in the presence of Fe-NHC catalyst (**1**). Based on the work of J. Guan *et al* [82] we propose the following mechanism (Figure 3.29) for conversion of fructose (**2**) to HMF (**3**). The iron (Fe^{3+}) co-ordinates with the carbonyl and adjacent OH within fructose to form a metal-fructofuranose complex. A series of three dehydrations (-3 H_2O) induced by the catalyst attaching and detaching the fructose ring structure affords the desired HMF (**3**).

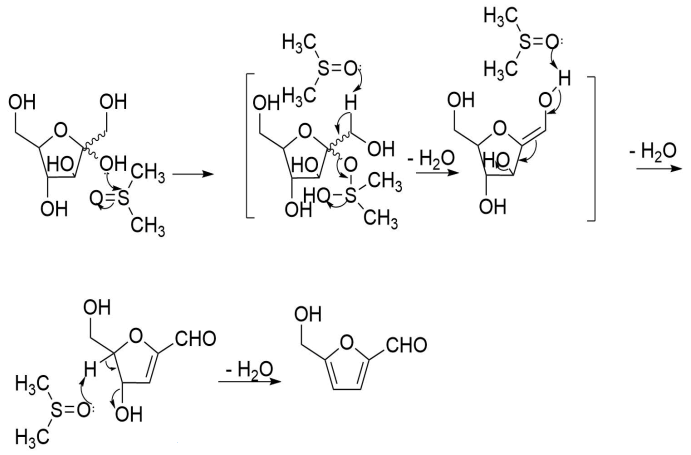

FIGURE 3.28: Proposed mechanism for the dehydration of D-fructose furanose form (αf/β f) to 5-hydroxymethylfurfural in dimethyl sulfoxide at 150 °C. [46]

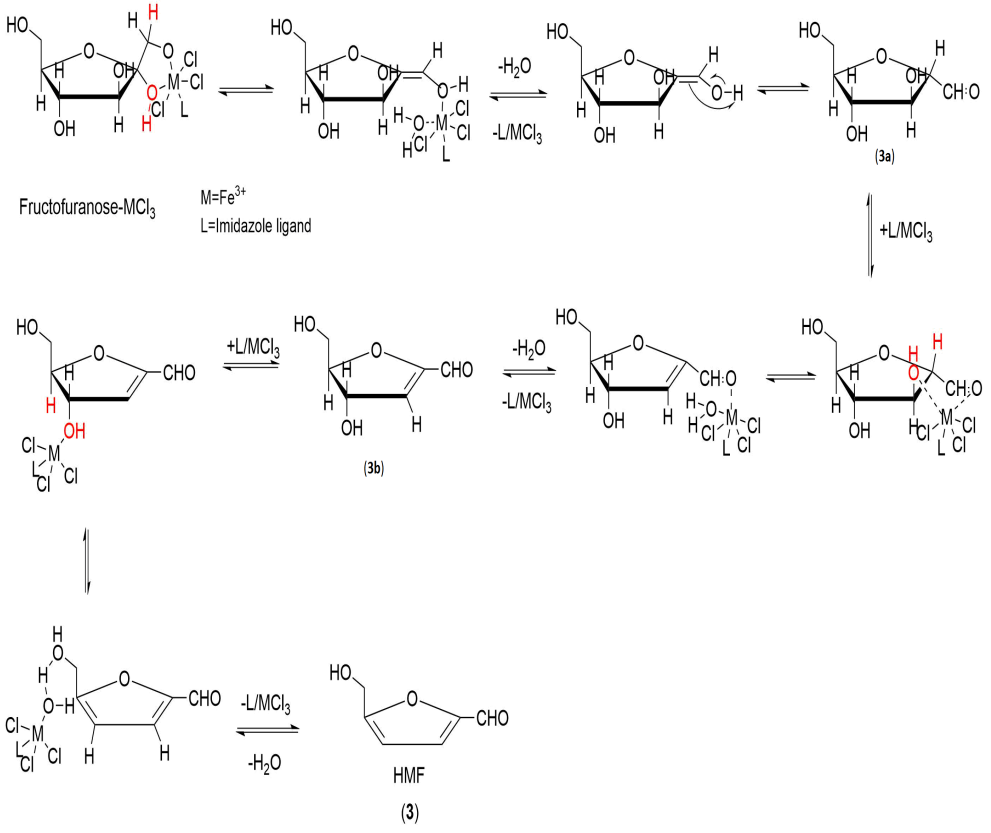

FIGURE 3.29: Proposed mechanism for the dehydration of fructose (**2**) to HMF (**3**) in dimethyl sulfoxide over Fe-NHC catalyst (**1**).

The complementary ^{13}C NMR investigation (see Figure 3.30) also revealed a decrease in signals of fructose coupled with an increase in signals for HMF with respect to time. The signals for DMSO-d_6 are present at 39.5 ppm whilst those for fructose are in the range 60 - 105 ppm. [80] The spectrum after 6 h begins to show carbon signals characteristic of HMF ((56.43 ppm, HO-**C**H_2-C=CH-), (110.24 ppm, HO-CH_2-C=**C**H-), (152.25 ppm, O=HC-**C**H=C-), (162.66 ppm, HO-CH_2-**C**=CH_2-) and 178.53 ppm, O=**C**H-C=CH)). [83] The signals at 31.19 ppm and 204.9 ppm are attributed to a carbonyl containing species yet to be fully determined. The signal at 163.45 ppm most likely corresponds to formic acid which agrees with its ^{1}H NMR peak observed.

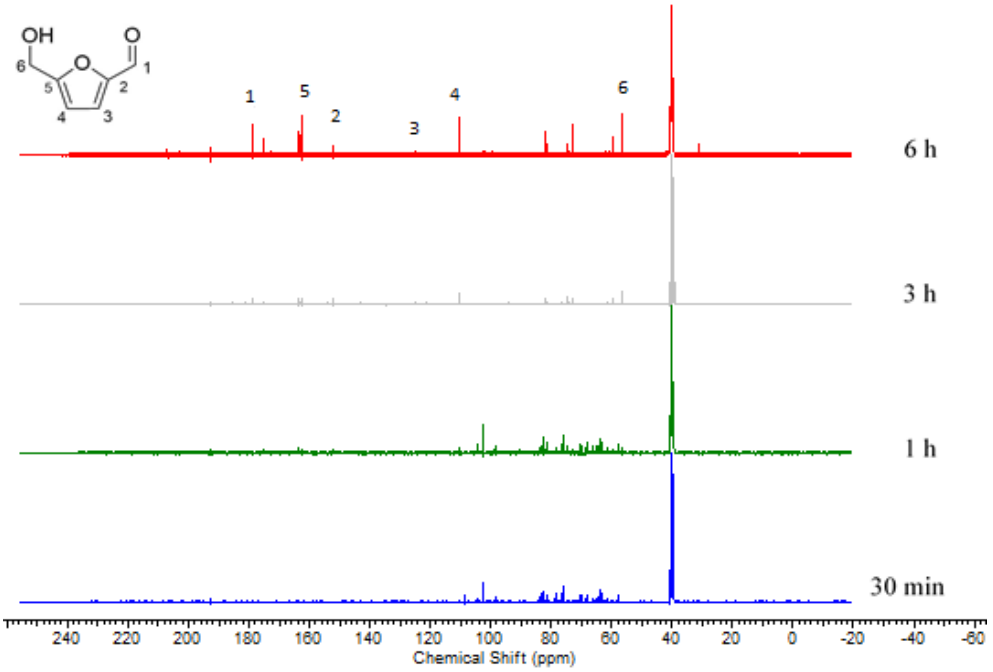

FIGURE 3.30: ^{13}C NMR spectra for the dehydration of fructose (**2**) to HMF (**3**) over Fe-NHC catalyst (**1**).

3.3.3 In an atmosphere of air (Quantification via HPLC)

The progress of the reaction was also monitored by HPLC in order to better investigate yield and selectivity. The results are represented graphically in Figure 3.31 and raw HPLC data is given in the AppendixA . After 0.5 h, high selectivity (86.43%) with moderate HMF yield (50.62%) was obtained thus indicating effectiveness of our novel Fe-NHC (**1**) as a catalyst for fructose (**2**) dehydration to HMF (**3**). The high selectivity at this time could be explained

by the low probability of re-hydration at this point compared to proceeding times. The best HMF yield was obtained at t= 1 h with 63.54%. Whereas for fructose conversion to HMF is 75.83% and 83.79% for HMF selectivity. Three hours reaction time appears to give best fructose conversion (85.09%), selectivity (74.05%) and HMF yield (63.45%). Thereafter, although fructose conversion is the highest (88.64%) for 6 h reaction time both HMF yield and selectivity drop significantly. As proposed earlier this may be due to re-hydration to levulinic acid that has reported a percentage area of 9.90% at 4.74 min retention time which is supported by the NMR analysis discussed before. Some other side products are recorded at different retention times. Among them, 3-furoic acid is identified at 7.88 min with 4.24% area.

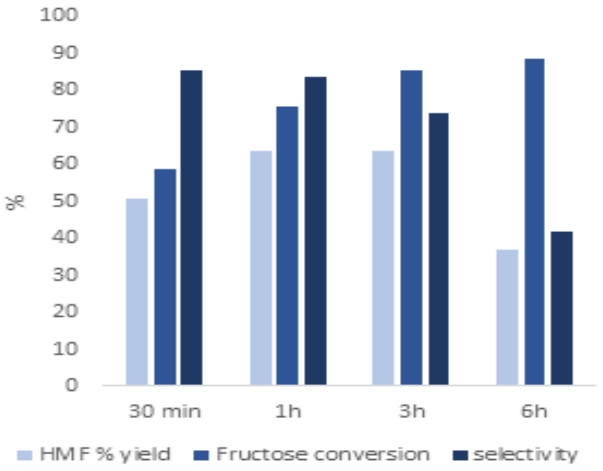

FIGURE 3.31: HMF yields, fructose conversion and selectivity in % for dehydration of fructose (**2**) to HMF (**3**) over Fe-NHC catalyst (**1**).

3.3.4 Catalyst recycling and reuse

Catalyst recycling and re-use was investigated in DMSO-d_6 at 100 °C with each experiment being monitored by NMR (qualitative) and HPLC (quantitative). As shown by the quantitative data in Figure 3.34, the desired Fe-NHC catalyst (**1**) can be re-used up to four times (4x) without significant loss in performance; HPLC results reported 73.77%, 66.82%, 71.85%, 72.37% and 46.76% HMF yields with lowest fructose conversion of 88.03% for the second run and lowest selectivity of 52.81% for the last cycle. The NMR spectra reported (Figure 3.32 and 3.33) show the existence of HMF signals in all 5 cycles of use.

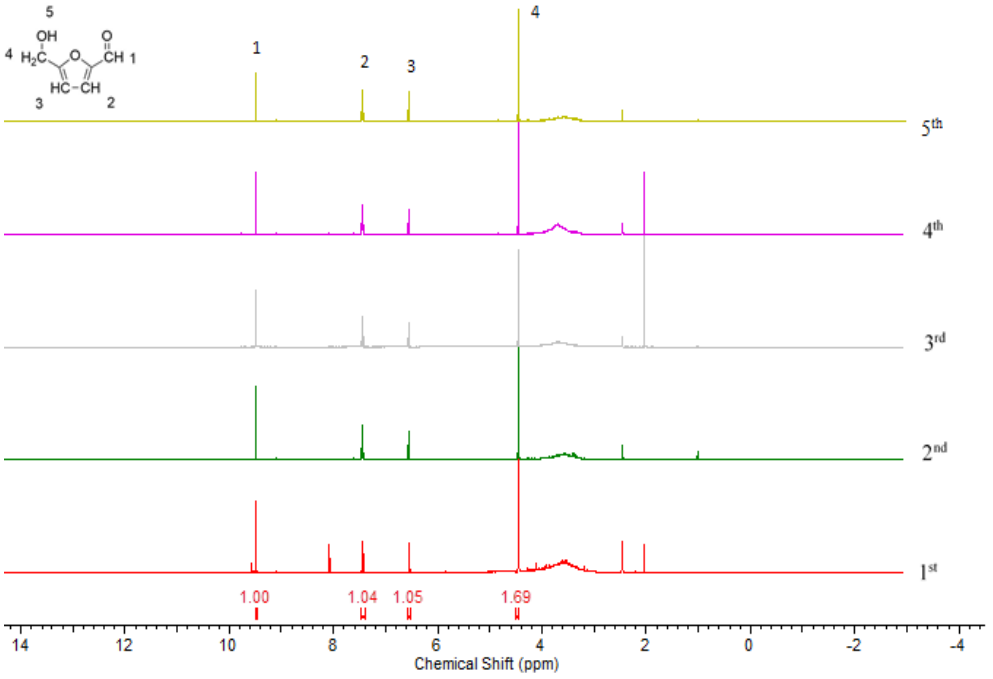

FIGURE 3.32: Stacked ^{1}H NMR spectra of Fe-NHC catalyst (**1**) recycling experiments.

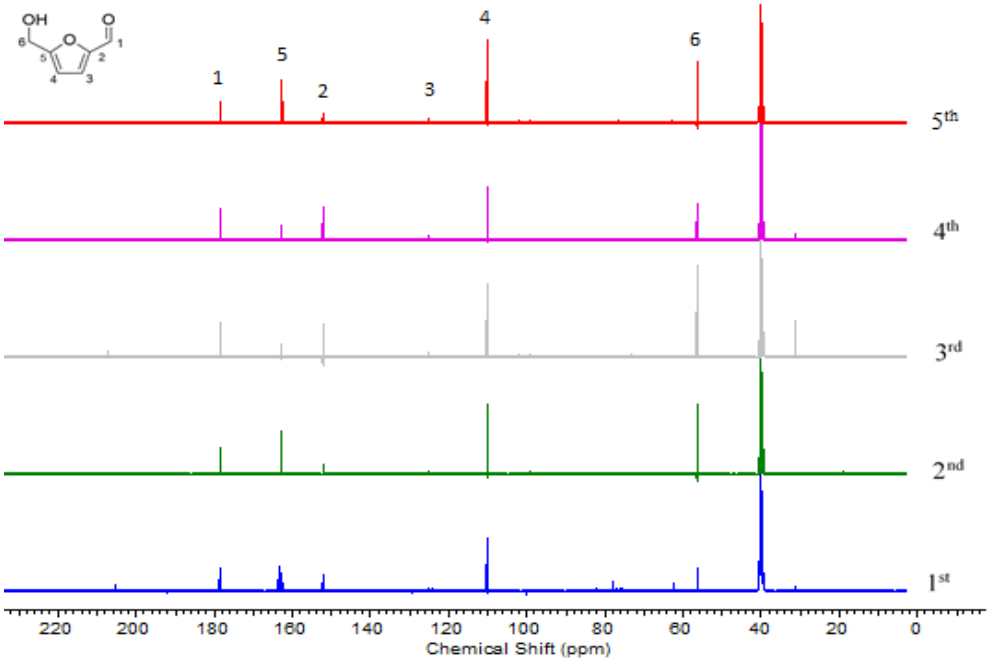

FIGURE 3.33: Stacked ^{13}C NMR spectra of Fe-NHC catalyst (**1**) recycling experiments.

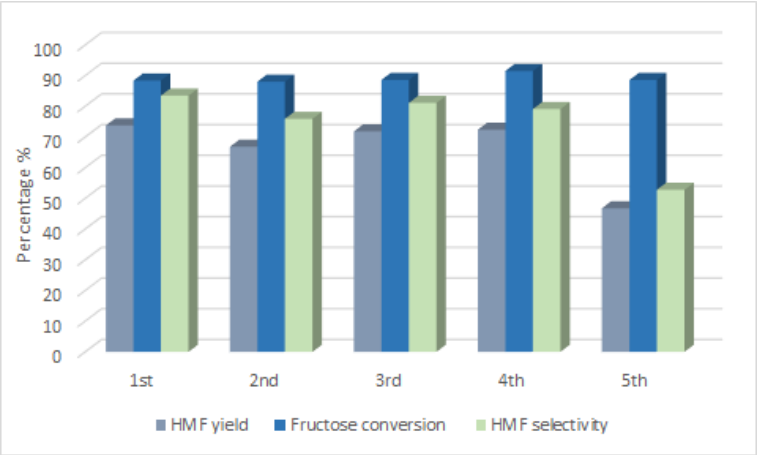

FIGURE 3.34: HPLC results (HMF yield, fructose conversion and HMF selectivity) of Fe-NHC (**1**) catalyst recycling experiments.

3.3.5 Fe-NHC catalyst (1) comparison with other heterogeneous catalysts (Amberlyst-15, Montmorillonite K-10 and ZSM-30)

The acid-catalysed dehydration of fructose (**2**) to HMF (**3**) has been well investigated using a variety of heterogeneous catalysts, namely: Amberlyst-15, Montmorillonite K-10 and ZSM-30. Thus, in order to compare activity between these catalysts and our catalyst (**1**) a series of standard reactions were undertaken using the same amount of fructose and DMSO at 100 °C with the appropriate catalyst. Literature data was not used because lack of knowledge of exactly how the study was performed would add huge uncertainty when trying to compare data. Our methodology removes variables and introduces consistency of approach. The reactions were monitored by NMR and the resultant spectra are shown in Figures 3.35 3.36, 3.37, 3.38, 3.39 and 3.40 while the HPLC results are given in Figures 3.41 and 3.42 .

Over Amberlyst-15, HMF yield increased with time with a maximum value at t =6 h. The behaviour of Montmorillonite K-10 and ZSM-30 catalysts is similar to Fe-NHC catalyst in which the HMF yield had its highest value at t= 3 h.

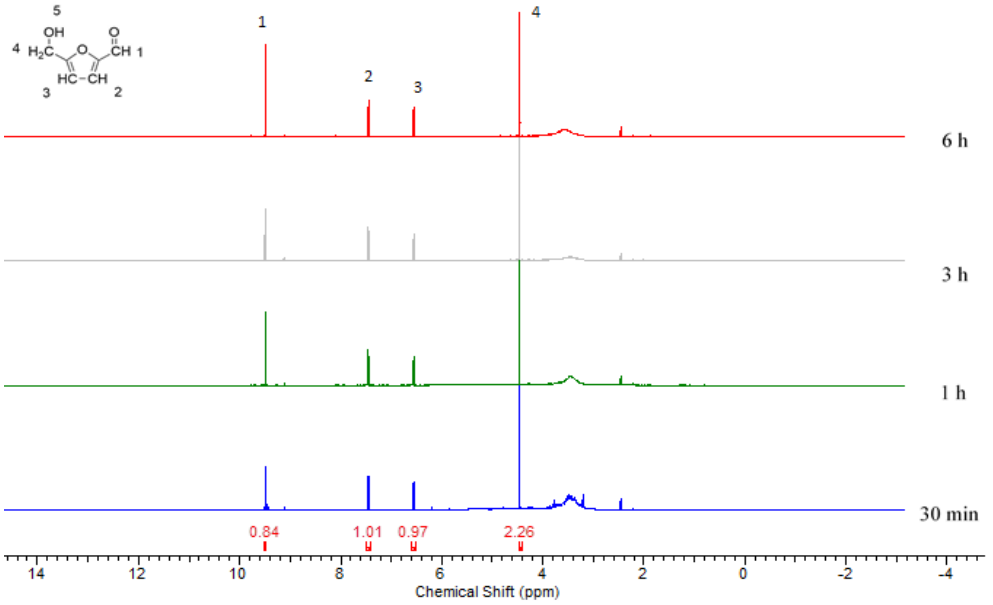

FIGURE 3.35: ^{1}H NMR spectra of fructose conversion to HMF reaction when using Amberlyst-15 catalyst.

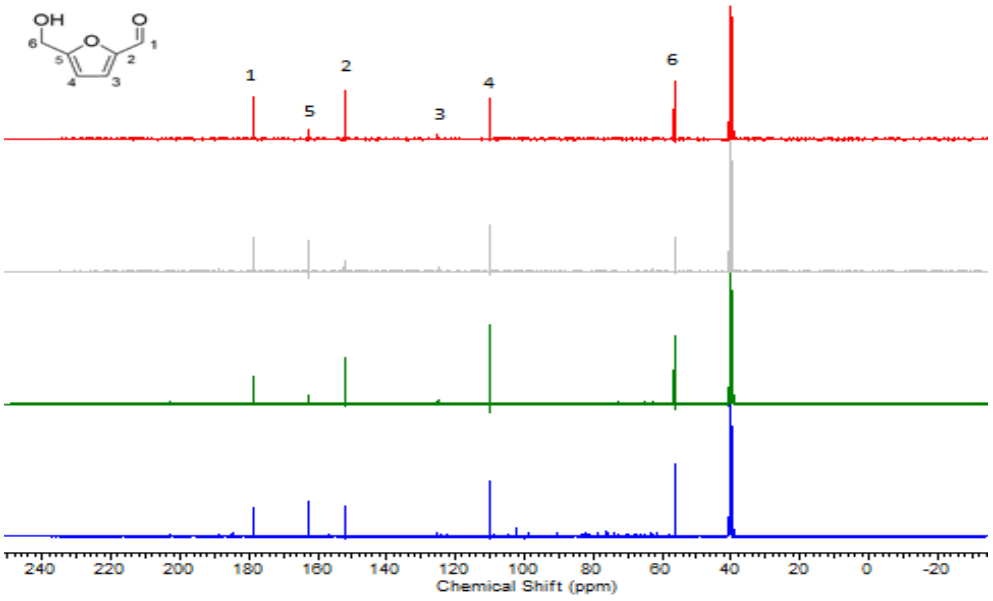

FIGURE 3.36: ^{13}C NMR spectra of fructose conversion to HMF reaction when using Amberlyst-15 catalyst.

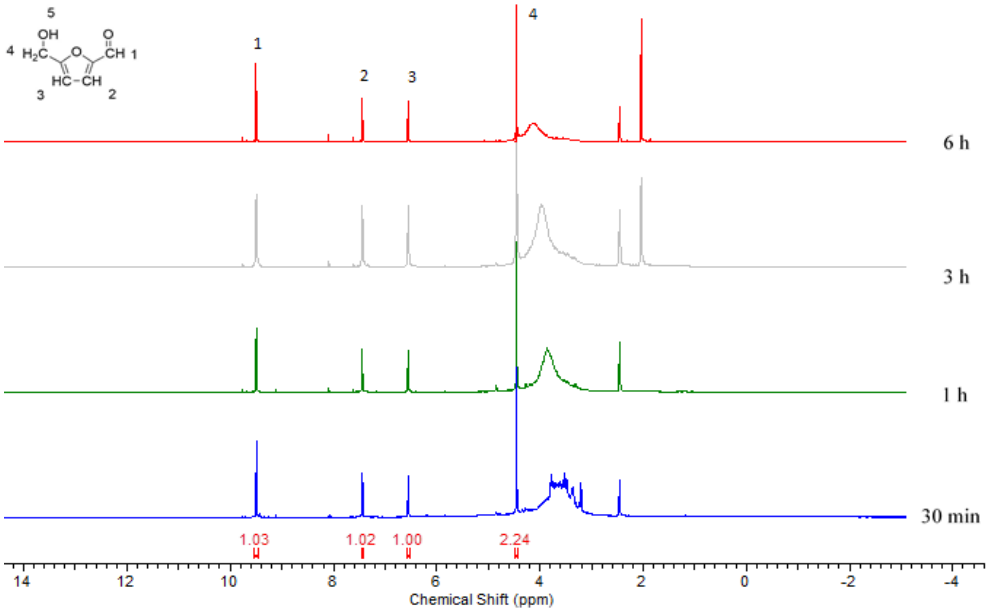

FIGURE 3.37: ^{1}H NMR spectra of fructose conversion to HMF reaction when using Montmorillonite K-10 clay catalyst.

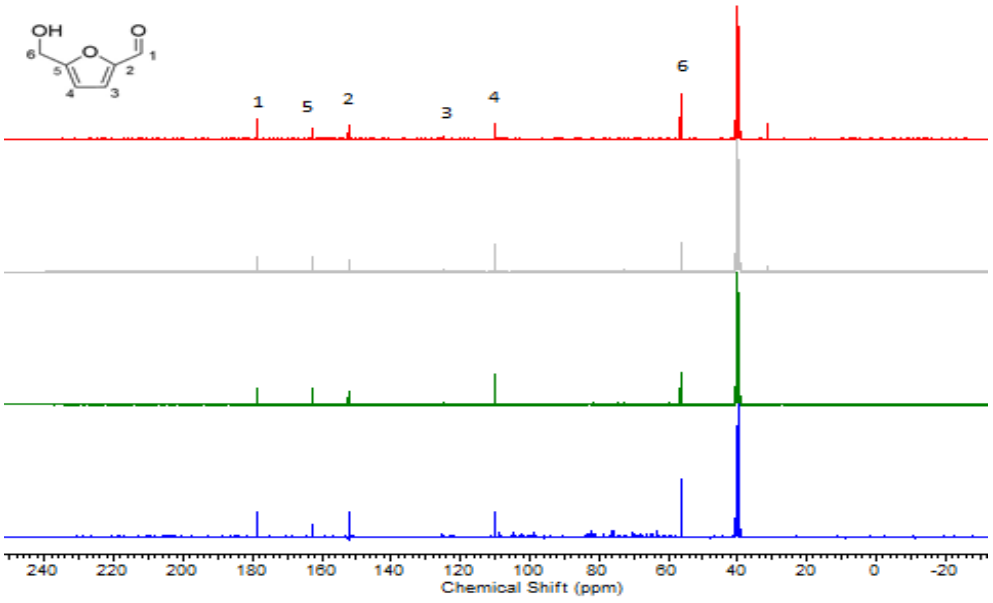

FIGURE 3.38: ^{13}C NMR spectra of fructose conversion to HMF reaction when using Montmorillonite K-10 clay catalyst.

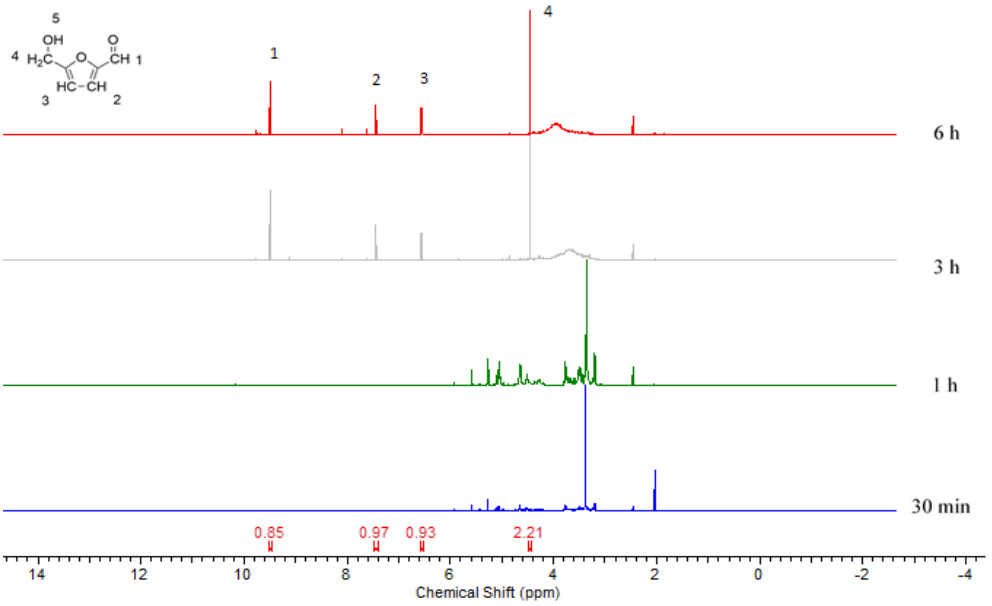

FIGURE 3.39: ^{1}H NMR spectra of fructose conversion to HMF reaction when using ZSM-30.

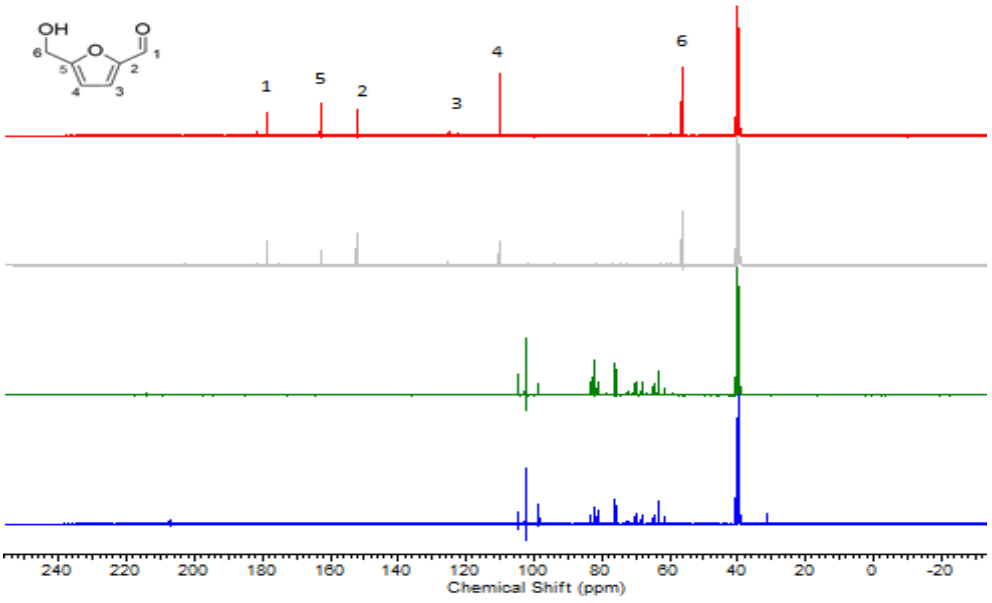

FIGURE 3.40: ^{13}C NMR spectra of fructose conversion to HMF reaction when using ZSM-30.

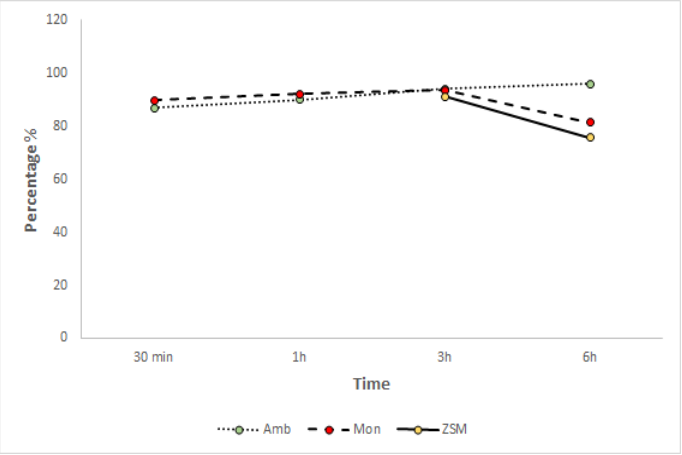

FIGURE 3.41: HMF % yield of fructose conversion to HMF reaction when using Amberlyst-15, Montmorillonite K-10 and ZSM-30.

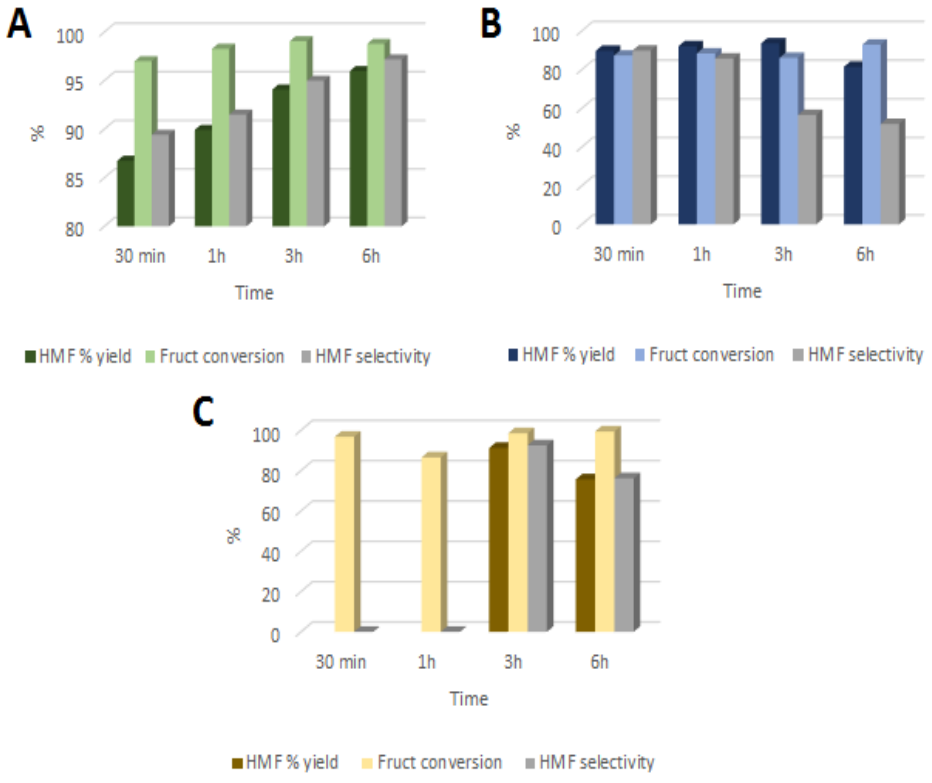

FIGURE 3.42: HPLC results calculations (HMF % yield, fructose conversion to HMF and HMF selectivity) of fructose conversion to HMF reaction when using (A) Amberlyst-15 (B) Montmorillonite K-10 and (C) ZSM-30.

3.3.6 Fructose dehydration in inert atmosphere (N_2): an unusual concept

The reaction of fructose was attempted in an inert atmosphere of nitrogen. The product was analyzed and characterized in the same way as the reaction without nitrogen flow and using the same amounts of reagents as mentioned in section 2.7.

The ^{1}H NMR spectrum of the reaction under nitrogen flow (displayed in Figure 3.47) with Fe-NHC catalyst (**1**) reveals the absence of any HMF signals within all the reaction times. However, the spectra demonstrate the presence of new signals. The signal at 1.2 ppm is believed to be linked to humic acids and the one at 9.6 ppm to intermediate (**3b**) (see Figure 3.29). [54], [84] and [85]

The stacked ^{13}C NMR spectra of this reaction shown in Figure 3.48, also show no dehydration occurred to form HMF, thus complementing the ^{1}H NMR (Figure 3.47). The carbon signal at 33 ppm is believed to be attributed to humic acid too. [54], [84] and [85] Although both ^{1}H and ^{13}C NMR showed no clear evidence of HMF, the latter was detected by HPLC as shown in Figure 3.43 albeit in small amounts.

It can be noticed from the HPLC results that there is a relatively good conversion of fructose reaction (Figure 3.43). However, the HMF yield obtained from these reactions and the HMF selectivity is quite low which means that fructose is converted to other products with higher percentage areas rather than to HMF. This was found clearly in the results and the expected products are tentatively thought to be formic acid (RT: 4.2 min), levulinic acid (RT: 4.8 min), furfural (RT: 8.5 min), 2-furoic acid (RT: 6.5 min), 3-furoic acid (RT: 7.5 min).

Figures 3.46, 3.45 and 3.46 provide a more close comparison between the HPLC results obtained in both air and N_2 atmosphere. With respect to HMF % yield and selectivity, it is clear from the graphs that in air atmosphere, the catalyst performance is better. As mentioned earlier, a relatively good conversion of fructose was reported but not to HMF.

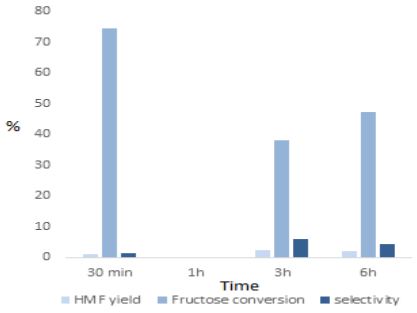

FIGURE 3.43: HMF yields, fructose conversion and selectivity in % for dehydration of fructose (**2**) to HMF (**3**) over Fe-NHC catalyst (**1**) (N_2 flow).

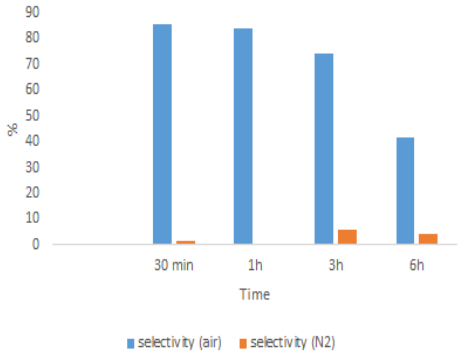

FIGURE 3.44: Comparison of fructose selectivity obtained from conversion of fructose (**2**) to HMF (**3**) over Fe-NHC catalyst (**1**) (air atmosphere and N_2 flow).

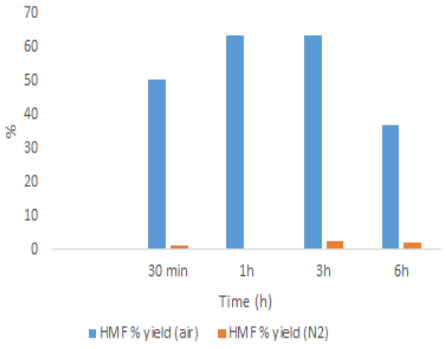

FIGURE 3.45: Comparison of HMF yields obtained from conversion of fructose (**2**) to HMF (**3**) over Fe-NHC catalyst (**1**) (air atmosphere and N_2 flow).

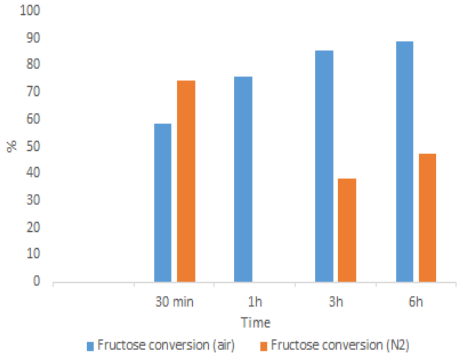

FIGURE 3.46: Comparison of fructose conversion obtained from conversion of fructose (**2**) to HMF (**3**) over Fe-NHC catalyst (**1**) (air atmosphere and N_2 flow).

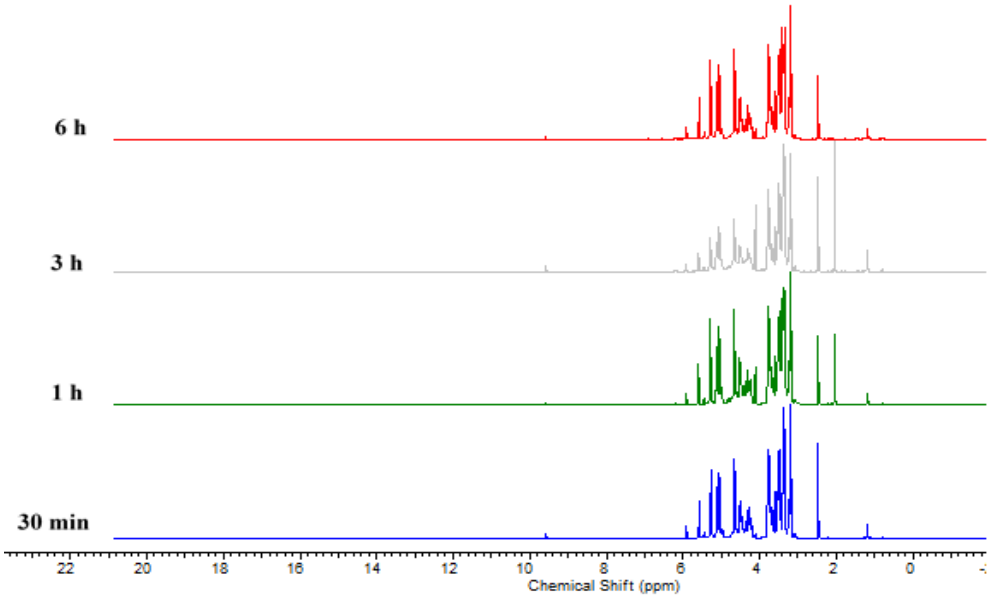

FIGURE 3.47: Stacked ^{1}H NMR spectrum of fructose conversion to HMF with Fe-NHC (**1**) under N_2 flow.

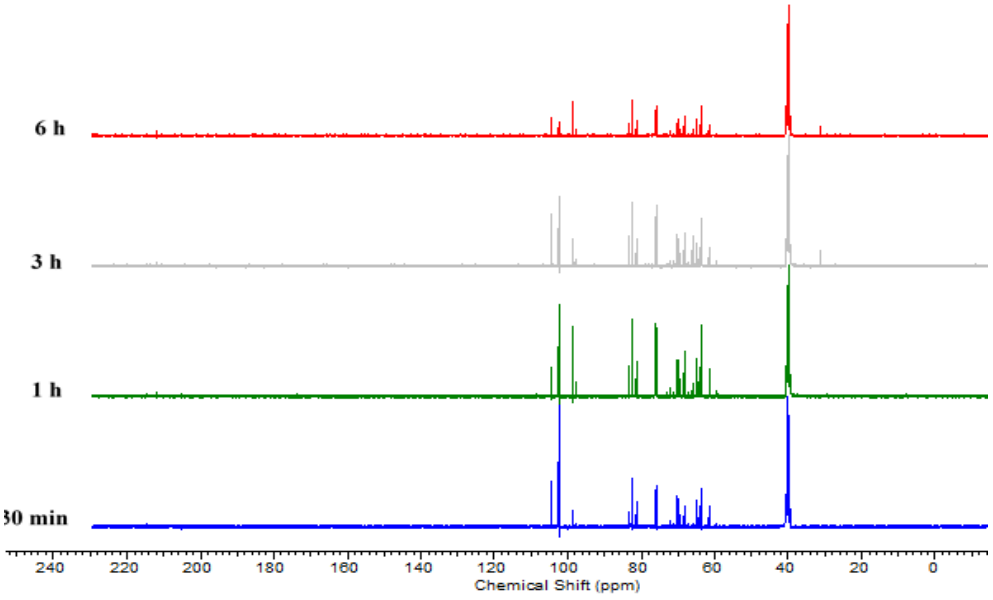

FIGURE 3.48: Stacked ^{13}C NMR spectrum of fructose conversion to HMF with Fe-NHC (**1**) under N_2 flow.

Chapter 4

Conclusions and Future Work

i. The synthesis of Fe-NHC tethered to expanded high amylose corn starch (HACS) can be successfully accomplished using a convergent strategy that adopts *green(er)* solvents such as propylene carbonate and CPME in preference of DMF and CH_2Cl_2 where appropriate. The degree of substitution (DS) is difficult to exceed beyond 0.33±0.11% even under forcing conditions. Further work needs to be undertaken as the synthesis of (**1**) currently still uses an excess of reagents and solvents. Protection and deprotection strategy is used which is incommensurate with the principles of green chemistry. First Pass Metrics need to be considered in more detail. [86] For the purpose of increasing the awareness of chemists about the importance of using more efficient chemical synthesis procedures, many metrics have been suggested in the recent years. One of them is E-Factor, which can be calculated by the following equation:

$$E - Factor = \frac{Total\ waste\ (kg)}{kg\ product} \tag{4.1}$$

It focuses on the waste amount which is formed for a particular amount of product. It is efficient to use this by industry to help decreasing the quantity of waste produced. Mass intensity is another metric and it is found as following:

$$Mass\ Intensity\ (MI) = \frac{Total\ amount\ used\ in\ aprocess/step\ (kg)}{Product\ amount\ (kg)} \tag{4.2}$$

Mass Intensity pays consideration to the stoichiometry, the yield, the reagent and the solvent used in the reaction mixture represented in weight rather than in percentage. [87], [88] and [89]

ii. Fe can be successfully complexed to NHC with a loading of 0.26 mmol/g based on a DS of 0.33±0.11%. The presence and amount of Fe can be characterized both qualitatively (colour) and quantitatively (ICP). XPS provides clear evidence for iron species whereas TEM provides evidence for iron clusters. Care needs to be taken as it is assumed that all iron present is co-ordinated to the NHC and not trapped within the mesoporous structure of the starch support. The effect of stirring rate needs to be considered to investigate diffusion in and out of the mesopores.

Further work needs to be done to improve DS. This may be reviewing the chemistry to activate starch as very high DS can be achieved for reactions such as acetylation. A high DS may lead to a higher iron-loading but as shown in this thesis 0.26 mmol/g Fe serves as an excellent catalyst for fructose dehydration. Thus, it may be that a lower loading may work equally well this is to be investigated.

iii. The Fe-NHC catalyst (**1**) appears to be heterogeneous as no discernible iron leaching was observed. Catalyst (**1**) is novel and converts fructose to HMF above 80 °C in DMSO in air at best after 1 h. Poor conversion is noted when the reaction is carried out under a flow of nitrogen. Further work needs to be undertaken to investigate atmosphere dependency. An inert atmosphere of nitrogen, which is also oxygen and moisture free, inhibits HMF formation whereas in an open atmosphere the conversion proceeds well. Moisture in the air may be catalyzing the conversion of fructose to HMF.

iv. Catalyst (**1**) can be re-used up to 4 x without any adverse drop in conversion or selectivity and is comparable with other heterogeneous catalysts, e.g. Amberlyst-15, Montmorillonite K-10 and ZSM-30.

v. Mesoporosity remains despite a series of chemical conversions but BET surface drops especially when iron is included. Finally, although this thesis looks at fructose to HMF conversion, catalyst (**1**) should be investigated in other heavily used synthetic transformations, for example, oxidations [90], amidations reliant on stoichiometric reagents [91] and carbon-carbon bond forming reactions that currently use palladium catalysts. [92]

Appendices

Appendix A

The V_n values, % of DSC groups and D.S are summarized in Tables A.1 and A.2 (V_0 = 16.7 ml) .

TABLE A.1: V_n recorded values for DS determination.

	V_n1	V_n2	V_n3
3.16 molar equivalent of DSC	15.3	15.4	14.6
6.22 molar equivalent of DSC	15.5	15.1	15.2

TABLE A.2: DSC percentage and D.S of disuccinimidyl carbonate activated expanded HACS (**6**).

	% DSC	D.S
3.16 molar equinelant of DSC	20.27±5.21	0.33±0.11
6.22 molar equinelant of DSC	18.13±2.59	0.28±0.05

Calculation of Fe loading on Fe-NHC catalyst (1) from ICP-AES data

The concentration of Fe in the Fe-NHC catalyst (**1**) is 14287863.09 ppb which is equal to 14289 ppm. Therefore the Fe loading of the catalyst was calculated as below.

Mass of Fe = 14289 ppm x 0.05 g (mass of sample) = 714.45 g

Number of moles of Fe (mol) = mass of Fe / Molar mass of Fe = 714.45 g / 55.845 g/mol = 12.79 mol

Number of moles of Fe (mmol) = 12.79 mol / 1000 = 0.01279 mmol

So the loading level of Fe = 0.01279 mmol / 0.05 g (mass of sample) = 0.2559 mmol/g.

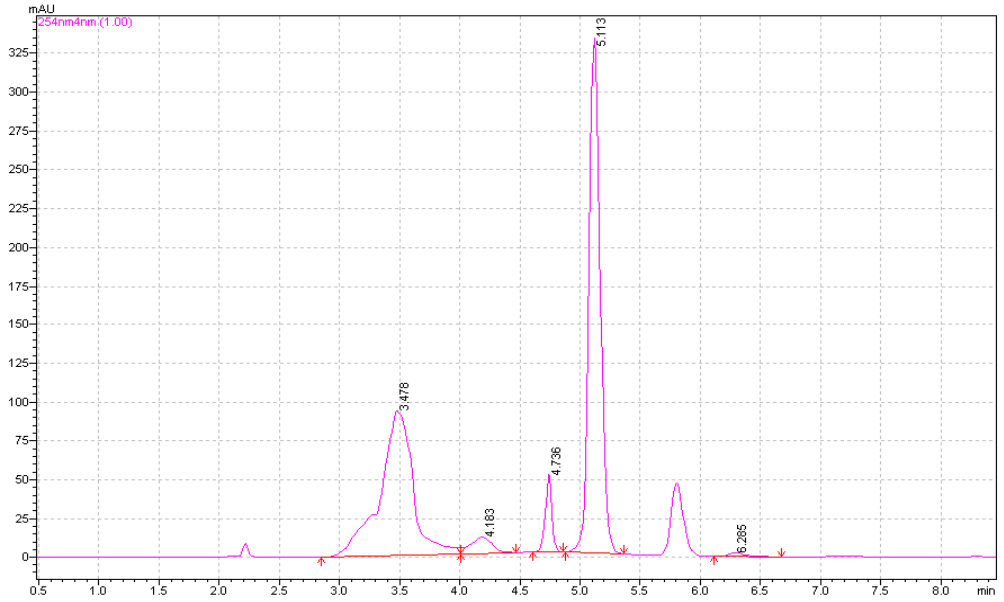

FIGURE A.1: HPLC chromatogram for fructose (**2**) conversion to HMF (**3**) using Fe-NHC catalyst (**1**) (air) (30 min).

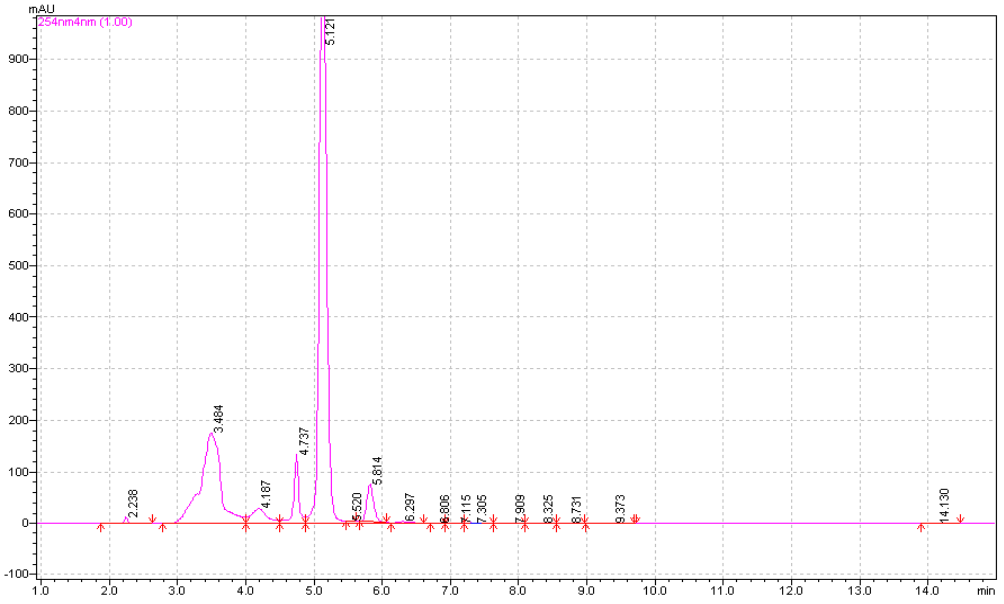

FIGURE A.2: HPLC chromatogram for fructose (**2**) conversion to HMF (**3**) using Fe-NHC catalyst (**1**) (air) (1 h).

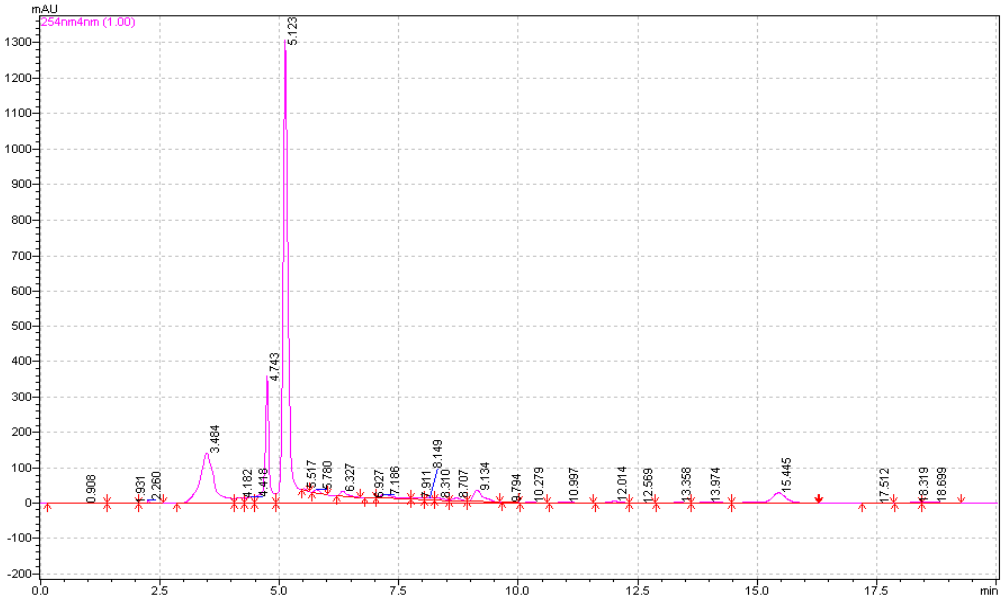

FIGURE A.3: HPLC chromatogram for fructose (**2**) conversion to HMF (**3**) using Fe-NHC catalyst (**1**) (air) (3 h).

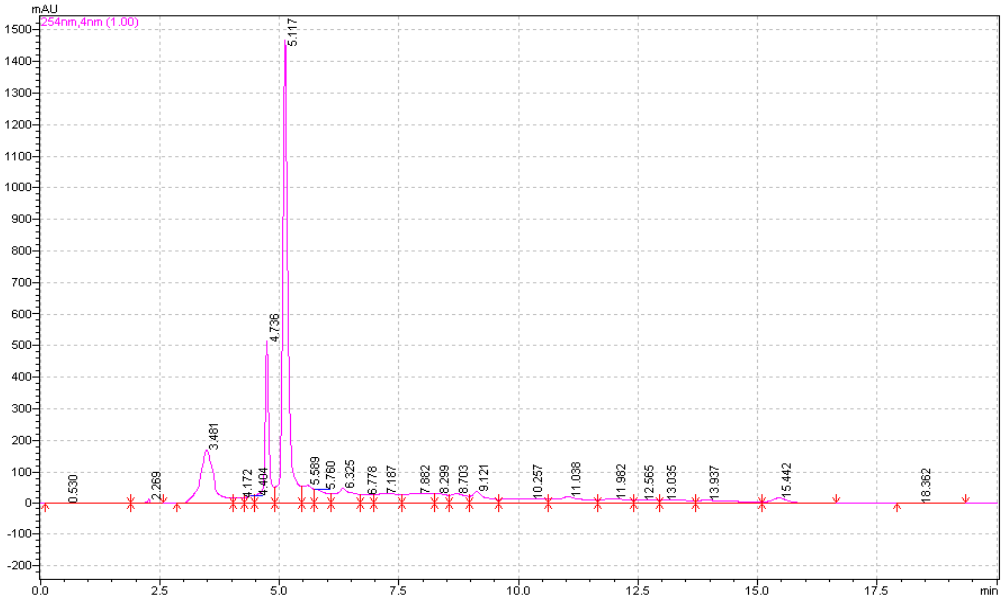

FIGURE A.4: HPLC chromatogram for fructose (**2**) conversion to HMF (**3**) using Fe-NHC catalyst (**1**) (air) (6 h).

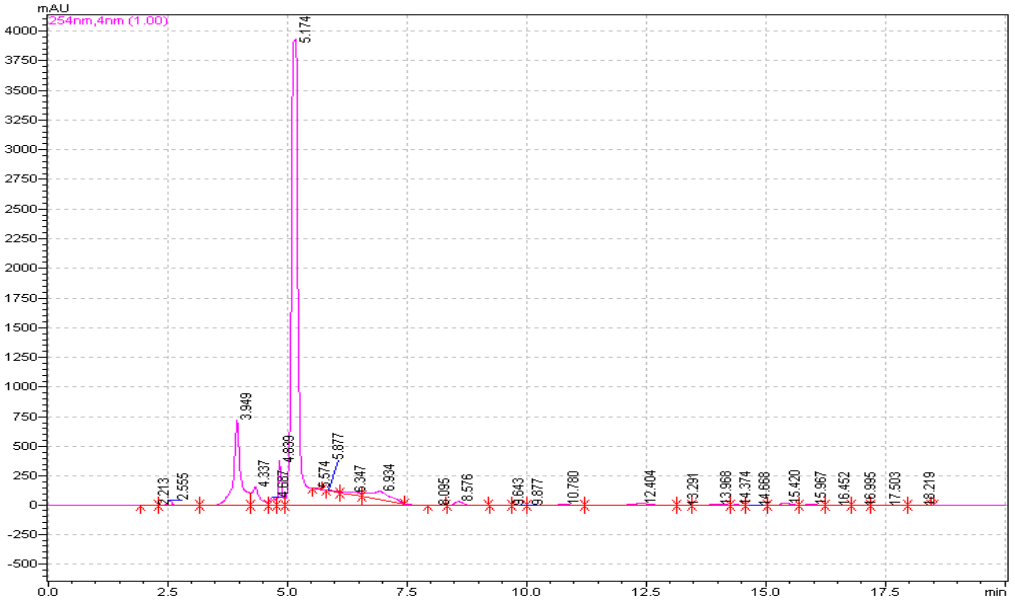

FIGURE A.5: HPLC chromatogram for catalyst reusability test (first).

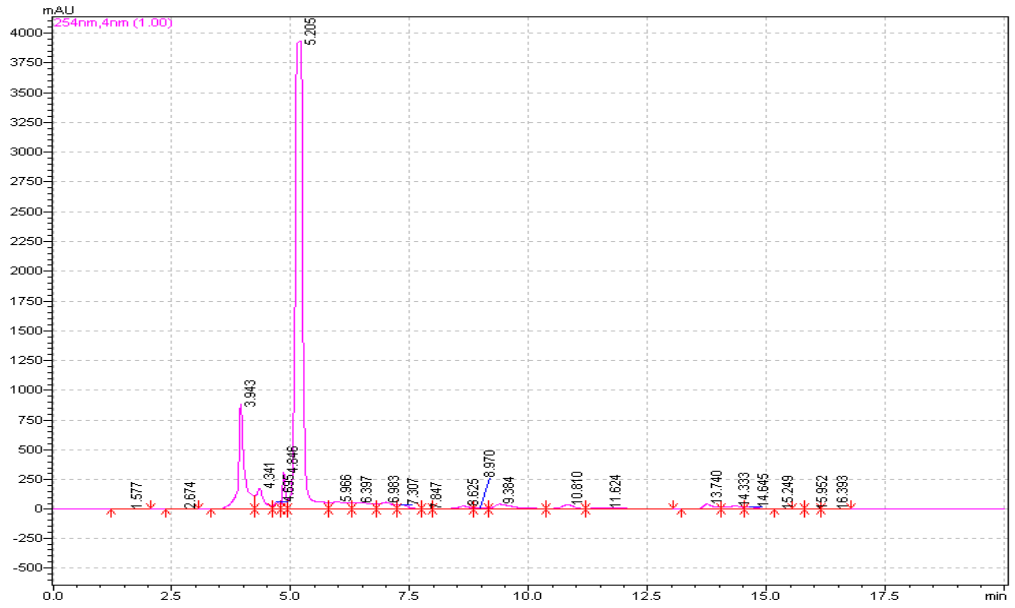

FIGURE A.6: HPLC chromatogram for catalyst reusability test (second).

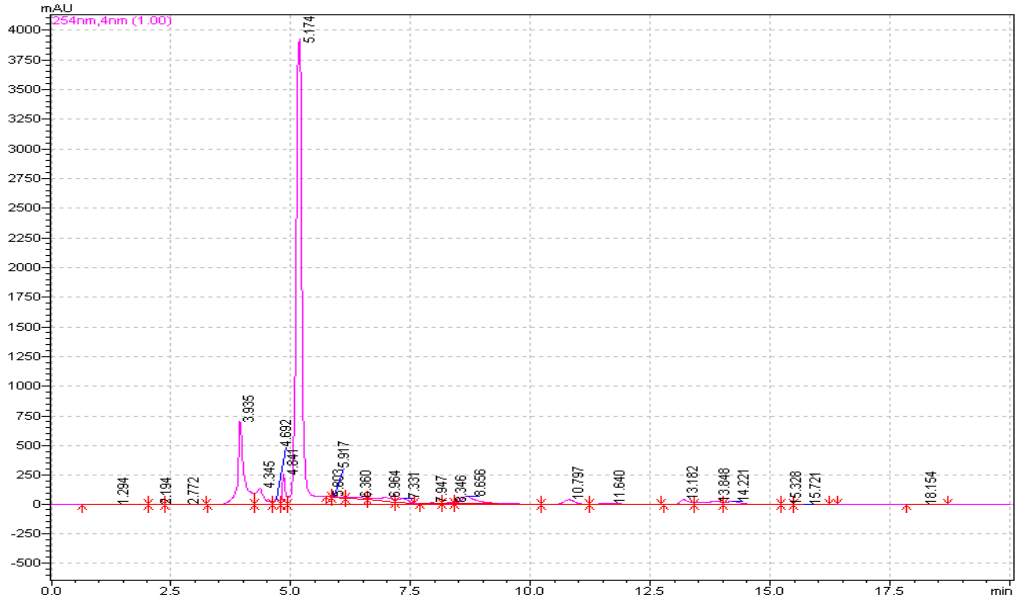

FIGURE A.7: HPLC chromatogram for catalyst reusability test (third).

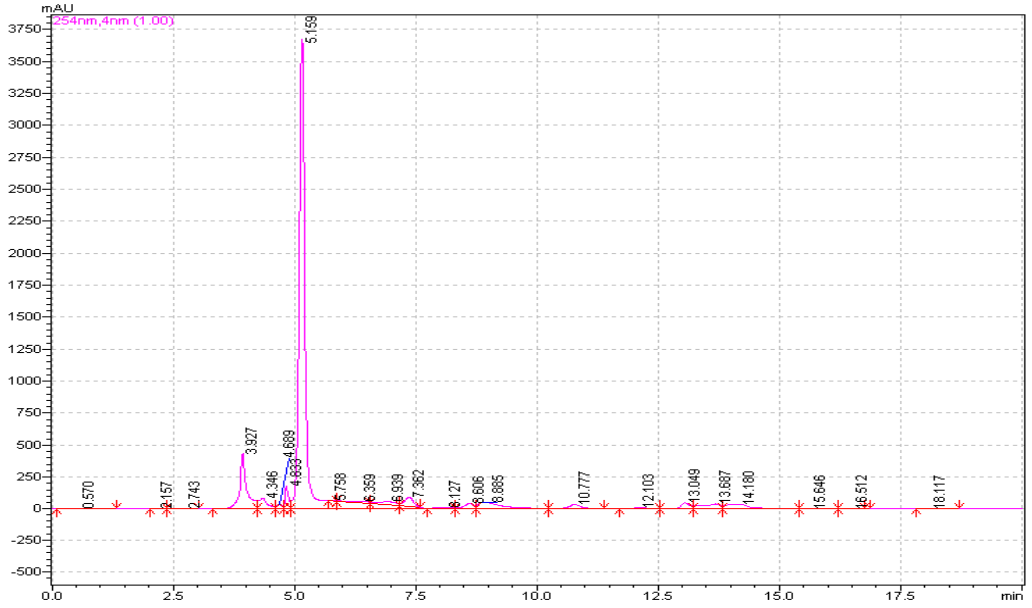

FIGURE A.8: HPLC chromatogram for catalyst reusability test (fourth).

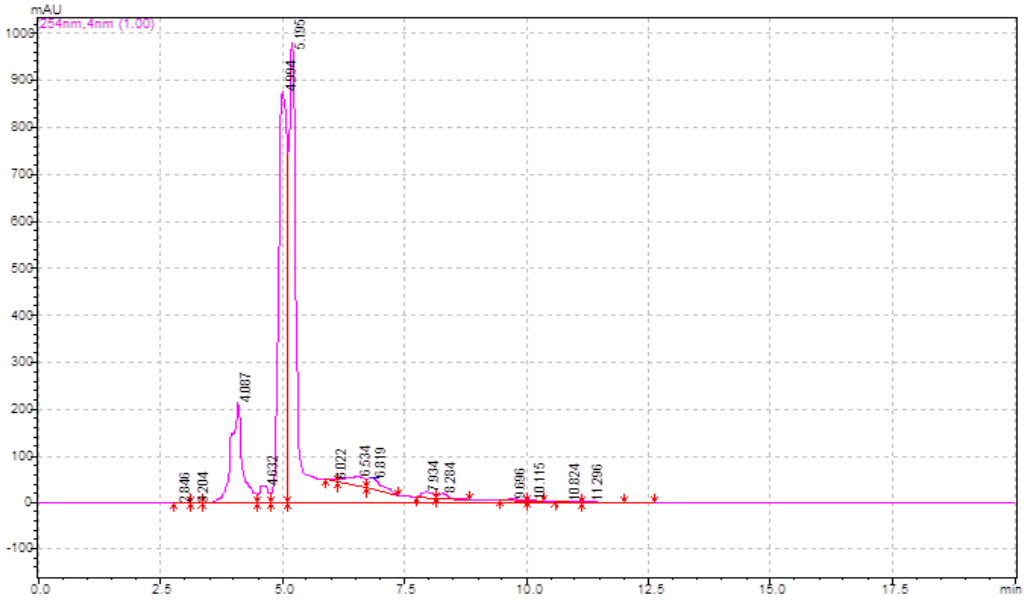

FIGURE A.9: HPLC chromatogram for catalyst reusability test (fifth).

Abbreviations

ATR-IR	Attenuated total reflection
BET	Brunauer Emmett Teller
BJH	Barrett Joyner and Halenda
CHyM	Centre of Hyperpolarisation in Magnetic resonance
CMF	Chloromethyl furfural
CPME	Cyclopentyl methyl ether
DFF	Diformyl furan
DMAP	Dimethyl aminopyridine
DMF	Dimethylformamide
DMSO	Dimethyl sulfoxide
DS	Degree of substitution
DSC	Disuccinimidyl carbonate
Fe-NHC	Iron-nitrogen heterocyclic carbene
FIR	Far infrared
HACS	High amylose corn starch
HMF	Hydroxymethyl furfural
HPLC	High performance liquid chromatography
ICP-MS	Inductively coupled plasma-mass spectroscopy
IR	Infrar red spectroscopy
MAS NMR	Magic angle spinning nuclear magnetic resonance
NHCs	Nitrogen heterocyclic carbenes
NMR	Nuclear magnetic resonance
PC	Propylene carbonate
PMI	Process mass intensity

ppb	part per billion
ppm	part per million
rpm	revolution per minute
SDGs	Sustainable development goals
SEM	scanning electron microscopy
STA	Simultaneous thermal analysis
***t*-Boc**	*tert*-Butyloxycarbonyl
TEA	Triethylamine
TEM	Transmission electron microscopy
TFA	Trifluoroacetic acid
TMS	Tetramethylsilane
XPS	X-Ray Photoelectron Spectroscopy
ZSM	Zeolite Socony Mobil

References

[1] Sustainable Development Knowledge Platform;. Accessed: 2016-10-25. https://sustainabledevelopment.un.org/sdgs. Available from: https://sustainabledevelopment.un.org/sdgs.

[2] Anastas PT, Warner JC. *Principles of green chemistry Green chemistry: Theory and practice*. Oxford university press New York. 1998;p. 11–56.

[3] Doi S, Clark JH, Macquarrie DJ, Milkowski K. New materials based on renewable resources: chemically modified expanded corn starches as catalysts for liquid phase organic reactions. *Chem Commun*. 2002;(22):2632–2633.

[4] Cioc RC, Ruijter E, Orru RV. Multicomponent reactions: advanced tools for sustainable organic synthesis. *Green Chem*. 2014;16(6):2958–2975.

[5] Matlin SA, Mehta G, Hopf H, Krief A. The role of chemistry in inventing a sustainable future. *Nat Chem*. 2015;7(12):941–943.

[6] Rodriguez-Reinoso F. The role of carbon materials in heterogeneous catalysis. *Carbon*. 1998;36(3):159–175.

[7] Lancaster M. *Green chemistry: an introductory text*. Royal Society of Chemistry; 2010;p.86-88.

[8] Lam E, Luong JH. Carbon materials as catalyst supports and catalysts in the transformation of biomass to fuels and chemicals. *ACS Catal*. 2014;4(10):3393–3410.

[9] Yang Y, Hu Cw, Abu-Omar MM. Conversion of carbohydrates and lignocellulosic biomass into 5-hydroxymethylfurfural using $AlCl_3.6H_2O$ catalyst in a biphasic solvent system. *Green Chem.* 2012;14(2):509–513.

[10] Climent MJ, Corma A, Iborra S. Conversion of biomass platform molecules into fuel additives and liquid hydrocarbon fuels. *Green Chem.* 2014;16(2):516–547.

[11] Auer E, Freund A, Pietsch J, Tacke T. Carbons as supports for industrial precious metal catalysts. *Appl Catal.* 1998;173(2):259–271.

[12] de Frémont P, Marion N, Nolan SP. Carbenes: Synthesis, properties, and organometallic chemistry. *Coord Chem Rev.* 2009;253(7):862–892.

[13] Arduengo AJ, Harlow RL, Kline M. A stable crystalline carbene. *J Am Chem Soc.* 1991;113(1):361–363.

[14] Hopkinson MN, Richter C, Schedler M, Glorius F. An overview of *N*-heterocyclic carbenes. *Nature.* 2014;510(7506):485–496.

[15] Ranganath KVS, Onitsuka S, Kiran Kumar A, Inanaga J. Recent progress of *N*-heterocyclic carbenes in heterogeneous catalysis. *Catal Sci Tech.* 2013;3(9):2161–2181.

[16] Yong G, Zhang Y, Ying JY. Efficient Catalytic System for the Selective Production of 5-Hydroxymethylfurfural from Glucose and Fructose. *Angew Chem Int Ed.* 2008;47(48):9345–9348.

[17] Kim YH, Shin S, Yoon HJ, Kim JW, Cho JK, Lee YS. Polymer-supported *N*-heterocyclic carbene-iron(III) catalyst and its application to dehydration of fructose into 5-hydroxymethyl-2-furfural. *Catal Commun.* 2013;40:18–22.

[18] Jenkins PJ, Donald AM. The influence of amylose on starch granule structure. *Int J Biol Macromolec.* 1995;17(6):315–321.

[19] Shi YC, Capitani T, Trzasko P, Jeffcoat R. Molecular Structure of a Low-Amylopectin Starch and Other High-Amylose Maize Starches. *J Cereal Sci.* 1998;27(3):289–299.

[20] Buléon A, Colonna P, Planchot V, Ball S. Starch granules: structure and biosynthesis. *Int J Biol Macromol*. 1998;23(2):85–112.

[21] Xu Y, Miladinov V, Hanna MA. Synthesis and Characterization of Starch Acetates with High Substitution. *Cereal Chem*. 2004;81(6):735–740.

[22] A Korma S. Chemically Modified Starch and Utilization in Food Stuffs. *Int J Food Sci Nutr*. 2016;5(4):264.

[23] Hunt AJ, Matharu AS, King AH, Clark JH. The importance of elemental sustainability and critical element recovery. *Green Chem*. 2015;17(4):1949–1950.

[24] Hunt AJ, Clark JH. *Element Recovery and Sustainability*. RSC green chemistry series. Royal Society of Chemistry; 2013;p.1-28.

[25] Lillo V, Mas-Marzá E, Segarra AM, Carbó JJ, Bo C, Peris E. Palladium–NHC complexes do catalyse the diboration of alkenes : mechanistic insights. *Chem Commun*. 2007;0(32):3380–3382.

[26] Marion N, Nolan SP. N-heterocyclic carbenes in gold catalysis. *Chem Soc Rev*. 2008;37(9):1776–1782.

[27] Riener K, Haslinger S, Raba A, Högerl MP, Cokoja M, Herrmann WA. Chemistry of iron *N*-heterocyclic carbene complexes: syntheses, structures, reactivities, and catalytic applications. *Chem Rev*. 2014;114(10):5215–5272.

[28] Kernbach U, Ramm M, Luger P, Fehlhammer WP. A Chelating Triscarbene Ligand and Its Hexacarbene Iron Complex. *Angew Chemie*. 1996;35(3):310–312.

[29] Hahn FE, Jahnke MC. Heterocyclic carbenes: synthesis and coordination chemistry. *Angew Chemie*. 2008;47(17):3122–3172.

[30] Ohki Y, Hoshino R, Tatsumi K. N-Heterocyclic Carbene Complexes of Three- and Four-Coordinate Fe(I). *Organometallics*. 2016;35(10):1368–1375.

[31] Gallezot P. Conversion of biomass to selected chemical products. *Chem Soc Rev.* 2012;41(4):1538–1558.

[32] Qin YZ, Zong MH, Lou WY, Li N. Biocatalytic Upgrading of 5-Hydroxymethylfurfural (HMF) with Levulinic Acid to HMF Levulinate in Biomass-Derived Solvents. *ACS Sustainable Chem Eng.* 2016;4(7):4050–4054.

[33] Rosatella AA, Simeonov SP, Frade RF, Afonso CA. 5-Hydroxymethylfurfural (HMF) as a building block platform: Biological properties, synthesis and synthetic applications. *Green Chem.* 2011;13(4):754–793.

[34] Climent MJ, Corma A, Iborra S. Conversion of biomass platform molecules into fuel additives and liquid hydrocarbon fuels. *Green Chem.* 2013;16(2):516–547.

[35] Zhang J, Das A, Assary RS, Curtiss LA, Weitz E. A combined experimental and computational study of the mechanism of fructose dehydration to 5-hydroxymethylfurfural in dimethylsulfoxide using Amberlyst 70, PO_4^{3-}/niobic acid, or sulfuric acid catalysts. *Appl Catal B.* 2016;181:874–887.

[36] Qiao Y, Theyssen N, Hou Z. Acid-Catalyzed Dehydration of Fructose to 5-(Hydroxymethyl)furfural. *Recycl Catal.* 2014;2(1):36–60.

[37] Zhao J, Zhou C, He C, Dai Y, Jia X, Yang Y. Efficient dehydration of fructose to 5-hydroxymethyl furfural over sulfonated carbon sphere solid acid catalysts. *Catal Today.* 2016;264:123–130.

[38] Chen J, Li K, Chen L, Liu R, Huang X, Ye D. Conversion of fructose into 5-hydroxymethylfurfural catalyzed by recyclable sulfonic acid-functionalized metal–organic frameworks. *Green Chem.* 2014;16(5):2490–2499.

[39] Xue Z, Cao B, Zhao W, Wang J, Yu T, Mu T. Heterogeneous Nb-containing catalyst/*N*,*N*-dimethylacetamide–salt mixtures: novel and efficient catalytic systems for the dehydration of fructose. *RSC Adv.* 2016;6(69):64338–64343.

[40] Dibenedetto A, Aresta M, Pastore C, di Bitonto L, Angelini A, Quaranta E. Conversion of fructose into 5-HMF: a study on the behaviour of heterogeneous cerium-based catalysts and their stability in aqueous media under mild conditions. *RSC Adv.* 2015;5(34):26941–26948.

[41] Pierre Y D, Cecilia M, Javier PR. Biobased Chemicals from Conception toward Industrial Reality: Lessons Learned and To Be Learned. *ACS Catal.* 2012;2(7):1487–1499.

[42] Bozell JJ, Petersen GR. Technology development for the production of biobased products from biorefinery carbohydrates. *Green Chem.* 2010;12(4):539–554.

[43] Wang J, Qu T, Liang M, Zhao Z. Microwave assisted rapid conversion of fructose into 5-HMF over solid acid catalysts. *RSC Adv.* 2015;5(128):106053–106060.

[44] Tong X, Wang Y, Nie G, Yan Y. Selective dehydration of fructose and sucrose to 5-hydroxymethyl-2-furfural with heterogeneous Ge(IV) catalysts. *Environ Prog Sustain Energy.* 2015;34(1):207–210.

[45] Antal MJ, Mok WSL, Richards GN. Mechanism of formation of 5-(hydroxymethyl)-2-furaldehyde from D-fructose and sucrose. *Carbohydr Res.* 1990;199(1):91–109.

[46] Amarasekara AS, Williams LD, Ebede CC. Mechanism of the dehydration of d-fructose to 5-hydroxymethylfurfural in dimethyl sulfoxide at 150 °C: an NMR study. *Carbohydr Res.* 2008;343(18):3021–3024.

[47] Román-Leshkov Y, Chheda JN, Dumesic JA. Phase modifiers promote efficient production of hydroxymethylfurfural from fructose. *Science.* 2006;312(5782):1933–1937.

[48] Barclay T, Ginic-Markovic M, Johnston MR, Cooper P, Petrovsky N. Observation of the keto tautomer of D-fructose in D_2O using ^1H NMR spectroscopy. *Carbohydr Res.* 2012;347(1):136–141.

[49] Akien GR, Qi L, Horvath IT. Molecular mapping of the acid catalysed dehydration of fructose. *Chem Commun.* 2012;48(47):5850–5852.

[50] Shimizu Ki, Uozumi R, Satsuma A. Enhanced production of hydroxymethylfurfural from fructose with solid acid catalysts by simple water removal methods. *Catal Commun.* 2009;10(14):1849–1853.

[51] Guo X, Zhu C, Guo F. Direct Transformation of Fructose and Glucose to 5-Hydroxymethylfurfural in Ionic Liquids under Mild Conditions. *BioResources.* 2016;11(1):2457–2469.

[52] Chheda JN, Román-Leshkov Y, Dumesic JA. Production of 5-hydroxymethylfurfural and furfural by dehydration of biomass-derived mono- and poly-saccharides. *Green Chem.* 2007;9(4):342–350.

[53] Gomes F, Pereira L, Ribeiro N, Souza M. Poduction of 5-hydroxymethylfurfural (HMF) via fructose dehydration: effect of solvent and salting-out. *Braz J Chem Eng.* 2015;32(1):119–126.

[54] Lewkowski J. Synthesis, chemistry and applications of 5-hydroxymethylfurfural and its derivatives. *Arkivoc.* 2001;2001:17–54.

[55] Brunauer S, Emmett PH, Teller E. Adsorption of gases in multimolecular layers. *JACS.* 1938;60(2):309–319.

[56] Elomaa M, Asplund T, Soininen P, Laatikainen R, Peltonen S, Hyvärinen S, et al. Determination of the degree of substitution of acetylated starch by hydrolysis, ^{1}H NMR and TGA/IR. *Carbohydr Polym.* 2004;57(3):261–267.

[57] Stojanović v, Jeremić K, Jovanović S, Lechner MD. A Comparison of Some Methods for the Determination of the Degree of Substitution of Carboxymethyl Starch. *Starch.* 2005;57(2):79–83.

[58] Diamanti S, Arifuzzaman S, Elsen A, Genzer J, Vaia RA. Reactive patterning via post-functionalization of polymer brushes utilizing disuccinimidyl carbonate activation to couple primary amines. *Polymer.* 2008;49(17):3770–3779.

[59] Zhang Z, Macquarrie DJ, Clark JH, Matharu AS. Chemical modification of starch and the application of expanded starch and its esters in hot melt adhesive. *RSC Advances*. 2014;4(79):41947–41955.

[60] Dawson DM, Jamieson LE, Mohideen MIH, McKinlay AC, Smellie IA, Cadou R, et al. High-resolution solid-state ^{13}C NMR spectroscopy of the paramagnetic metal–organic frameworks, STAM-1 and HKUST-1. *Phys Chem Chem Phys*. 2013;15(3):919–929.

[61] Shin JY, Lee BS, Jung Y, Kim SJ, Lee SG. Palladium nanoparticles captured onto spherical silica particles using a urea cross-linked imidazolium molecular band. *Chem Commun*. 2007;(48):5238–5240.

[62] Narayanaswamy N, Avinash MB, Govindaraju T. Exploring hydrogen bonding and weak aromatic interactions induced assembly of adenine and thymine functionalised naphthalenediimides. *New J Chem*. 2013;37(5):1302–1306.

[63] Raju M, Mäeorg S, Tšubrik O, Mäeorg U. Efficient solventless technique for Boc-protection of hydrazines and amines. *Arkivoc*. 2009;6:291–297.

[64] Wah HLK, Postel M, Tomi F. The iron-nitrato/iron-nitrosyl couple in the presence of hexamethylphosphoric triamide and its relevance to oxygen activation and transfer. X-ray structure of $Fe(NO_3)(Cl)_2$ $(HMPA)_2$. *Inorg Chem*. 1989;28(2):233–238.

[65] Reimer L, Kohl H. *Transmission Electron Microscopy: Physics of Image Formation*. Springer Series in Optical Sciences. Springer New York; 2008.

[66] Gunter PLJ, Niemantsverdriet JWh, Ribeiro FH, Somorjai GA. Surface Science Approach to Modeling Supported Catalysts. *Catal Rev*. 1997;39(1-2):77–168.

[67] Bell AT. The impact of nanoscience on heterogeneous catalysis. *Science*. 2003;299(5613):1688–1691.

[68] Widmann G, Schubnell M, Riesen R, Schawe J, Darribére C, Jörimann U. Interpreting TGA curves. 2001;1:1–20.

[69] Kaith BS, Jindal R, Jana AK, Maiti M. Development of corn starch based green composites reinforced with Saccharum spontaneum L fiber and graft copolymers – Evaluation of thermal, physico-chemical and mechanical properties. *Bioresource Technol.* 2010;101(17):6843–6851.

[70] Groen JC, Peffer LAA, Pérez-Ramırez J. Pore size determination in modified micro- and mesoporous materials. Pitfalls and limitations in gas adsorption data analysis. *Micropor Mesopor Mat.* 2003;60(1–3):1–17.

[71] Siegbahn K. Electron spectroscopy - an outlook. *J Electron Spectrosc Relat Phenom.* 1974;5(1):3–97.

[72] Ge Y. *Chemical and Electronic Properties of Semiconducting Oligomer and Thiol Monolayer Interfaces.* University of Massachusetts Lowell; 2008.

[73] Welton T. Solvents and sustainable chemistry. *Proc Math Phys Eng Sci.* 2015;471(2183):20150502.

[74] Zhang J, Weitz E. An in Situ NMR Study of the Mechanism for the Catalytic Conversion of Fructose to 5-Hydroxymethylfurfural and then to Levulinic Acid Using ^{13}C Labeled D-Fructose. *ACS Catal.* 2012;2(6):1211–1218.

[75] Gottlieb HE, Kotlyar V, Nudelman A. NMR Chemical Shifts of Common Laboratory Solvents as Trace Impurities. *J Org Chem.* 1997;62(21):7512–7515.

[76] Qi X, Watanabe M, Aida TM, Smith RL Jr. Efficient process for conversion of fructose to 5-hydroxymethylfurfural with ionic liquids. *Green Chem.* 2009;11(9):1327–1331.

[77] De Bruyn A, Anteunis M, Verhegge G. A ^{1}H-NMR. study of D-fructose in D_2O. *Carbohydr Res.* 1975;41(1):295–297.

[78] Gottlieb HE, Graczyk-Millbrandt G, Inglis GGA, Nudelman A, Perez D, Qian Y, et al. Development of GSK's NMR guides – a tool to encourage the use of more sustainable solvents. *Green Chem.* 2016;18(13):3867–3878.

[79] Babij NR, McCusker EO, Whiteker GT, Canturk B, Choy N, Creemer LC, et al. NMR Chemical Shifts of Trace Impurities: Industrially Preferred Solvents Used in Process and Green Chemistry. *Org Process Res Dev.* 2016;20(3):661–667.

[80] Melo FCd, Souza RFd, Coutinho PLA, Souza MOd. Synthesis of 5-Hydroxymethylfurfural from Dehydration of Fructose And Glucose Using Ionic Liquids. *J Braz Chem Soc.* 2014;25(12):2378–2384.

[81] Carniti P, Gervasini A, Marzo M. Absence of expected side-reactions in the dehydration reaction of fructose to HMF in water over niobic acid catalyst. *Catal Commun.* 2011;12(12):1122–1126.

[82] Guan J, Cao Q, Guo X, Mu X. The mechanism of glucose conversion to 5-hydroxymethylfurfural catalyzed by metal chlorides in ionic liquid: A theoretical study. *Comp Theor Chem.* 2011;963(2–3):453–462.

[83] Wei Z, Liu Y, Thushara D, Ren Q. Entrainer-intensified vacuum reactive distillation process for the separation of 5-hydroxylmethylfurfural from the dehydration of carbohydrates catalyzed by a metal salt–ionic liquid. *Green Chem.* 2012;14(4):1220–1226.

[84] Trubetskoj OA, Hatcher PG, Trubetskaya OE. ^{1}H-NMR and ^{13}C-NMR spectroscopy of chernozem soil humic acid fractionated by combined size-exclusion chromatography and electrophoresis. *Chem Ecol.* 2010;26(4):315–325.

[85] Amir S, Hafidi M, Merlina G, Hamdi H, Revel JC. Elemental analysis, FTIR and ^{13}C-NMR of humic acids from sewage sludge composting. *Agronomie.* 2004;24(1):13–18.

[86] McElroy C, Constantinou A, Jones LC, Summerton L, Clark JH. Towards a holistic approach to metrics for the 21st century pharmaceutical industry. *Green Chem.* 2015;17(5):3111–3121.

[87] Constable DJC, Curzons AD, Cunningham VL. Metrics to green chemistry—which are the best? *Green Chem.* 2002 17 Oct;4(6):521–527.

[88] Augé J. A new rationale of reaction metrics for green chemistry. Mathematical expression of the environmental impact factor of chemical processes. *Green Chem.* 2007;10(2):225–231.

[89] Andraos J. Unification of Reaction Metrics for Green Chemistry: Applications to Reaction Analysis. *Org Process Res Dev.* 2005;9(2):149–163.

[90] Marr AC. Organometallic hydrogen transfer and dehydrogenation catalysts for the conversion of bio-renewable alcohols. *Catal Sci Technol.* 2012;2(2):279–287.

[91] Bode JW, Sohn SS. *N*-Heterocyclic Carbene-Catalyzed Redox Amidations of α-Functionalized Aldehydes with Amines. *J Am Chem Soc.* 2007;129(45):13798–13799.

[92] Bedford RB. How low does iron go? Chasing the active species in fe-catalyzed cross-coupling reactions. *Acc Chem Res.* 2015;48(5):1485–1493.